MISSOURI S&T

CENTER FOR TRANSPORTATION INFRASTRUCTURE AND SAFETY

Polyurethane Foam Infill for Fiber-Reinforced Polymer (FRP) Bridge Deck Panels

by

Jeffery S. Volz, PhD, SE, PE
Benjamin Gliha

NUTC R295 / R302

A National University Transportation Center at Missouri University of Science and Technology

Disclaimer

The contents of this report reflect the views of the author(s), who are responsible for the facts and the accuracy of information presented herein. This document is disseminated under the sponsorship of the Department of Transportation, University Transportation Centers Program and the Center for Transportation Infrastructure and Safety NUTC program at the Missouri University of Science and Technology, in the interest of information exchange. The U.S. Government and Center for Transportation Infrastructure and Safety assumes no liability for the contents or use thereof.

Technical Report Documentation Page

1. Report No.	2. Government Accession No.	3. Recipient's Catalog No.
NUTC R295 / R302		

4. Title and Subtitle	5. Report Date
Polyurethane Foam Infill for Fiber-Reinforced Polymer (FRP) Bridge Deck Panels	May 2014
	6. Performing Organization Code

7. Author/s	8. Performing Organization Report No.
Jeffery S. Volz, PhD, SE, PE	Project # 00037417 / 00039445

9. Performing Organization Name and Address	10. Work Unit No. (TRAIS)
Center for Transportation Infrastructure and Safety/NUTC program Missouri University of Science and Technology 220 Engineering Research Lab Rolla, MO 65409	11. Contract or Grant No. DTRT06-G-0014

12. Sponsoring Organization Name and Address	13. Type of Report and Period Covered
U.S. Department of Transportation Research and Innovative Technology Administration 1200 New Jersey Avenue, SE Washington, DC 20590	Final
	14. Sponsoring Agency Code

15. Supplementary Notes

16. Abstract

The objective of the proposed research is to develop, test, and evaluate fiber-reinforced, polyurethane foams to replace the costly honeycomb construction currently used to manufacture FRP bridge deck panels. The effort will focus on developing an FRP sandwich panel to replace the precast, stay-in-place forms currently used to construct reinforced concrete bridge decks.

17. Key Words	18. Distribution Statement
Cost effective, corrosion-resistant bridge decks	No restrictions. This document is available to the public through the National Technical Information Service, Springfield, Virginia 22161.

19. Security Classification (of this report)	20. Security Classification (of this page)	21. No. Of Pages	22. Price
unclassified	unclassified	123	

Form DOT F 1700.7 (8-72)

FINAL Report

Polyurethane Foam Infill for Fiber-Reinforced Polymer (FRP) Bridge Deck Panels

By

Jeffery S. Volz, SE, PE, PhD (Principal Investigator)
K. Chandrashekhara (Co-Principal Investigator)
Victor Birman (Co-Principal Investigator)
Stephen Hawkins
Matthew Hopkins
Zhen Huo
Mohaned Mohamed
Hesham Tuwair

Missouri University of Science and Technology, Rolla, Missouri

May 2014

EXECUTIVE SUMMARY

On behalf of the Missouri Department of Transportation (MoDOT), Missouri University of Science and Technology completed a research study on a novel fiber-reinforced polymer (FRP) bridge deck panel that incorporates a polyurethane foam infill. The ***objective*** of the research was to develop, test, and evaluate fiber-reinforced, polyurethane (PU) foams to replace the costly honeycomb construction currently used to manufacture FRP bridge deck panels. Initially, the effort focused on developing an FRP sandwich panel to replace the precast, stay-in-place forms currently used to construct reinforced concrete bridge decks. However, during the course of the project, the research effort expanded to include full-depth bridge deck panels as well. This report documents the results of this study.

The report is composed of eight chapters. Chapter 1 gives a brief introduction to the subject area, explains the necessity of this research, and also presents the objectives and scope of work of the investigation. Chapter 2 explains the PU foams selected for component testing and decisions made concerning which materials to move forward for further testing and evaluation. Chapter 3 details the small-scale sandwich panel testing program and results. Chapter 4 contains the stiffness and strength analysis of the small-scale panel test results, including recommendations on which FRP/PU foam combination to advance to the next phase. Chapter 5 presents the mid-scale sandwich panel testing program and results, which includes static, fatigue, and durability testing of the prototype FRP/PU foam sandwich panel. Chapter 6 details construction and testing of a prototype full-scale FRP/PU foam deck panel. Chapter 7 contains a summary of the research investigation as well as recommendations on moving forward. Finally, Chapter 8 contains supplementary information on many unique aspects of FRP bridge decks.

Based on the results of this study, the research team recommends proceeding with the Type 3 (PRISMA FOAM) sandwich panel as a cost-effective, full-depth alternative to reinforced concrete bridge decks or as a partial-depth, stay-in-place form to replace the current precast panels used to construct reinforced concrete bridge decks. To facilitate this implementation, additional work is required in order to develop the design methodology and construction details necessary to implement FRP deck panels on an actual bridge, addressing issues such as panel-to-panel connections, panel-to-girder connections, bridge skew, roadway crown, bridge rail attachment, and deck drainage.

ACKNOWLEDGEMENTS

The authors would like to acknowledge the many individuals and organizations that made this research project possible. First and foremost, the authors wish to extend a very sincere thank you to the Missouri Department of Transportation (MoDOT). In addition to their financial support, the authors appreciate MoDOT's vision and commitment to innovative concepts and pushing the boundaries of current practice. In particular, the success of this project would not have been possible without the support, encouragement, and patience of Mr. Andrew Hanks. The authors also wish to extend a sincere thank you to MoDOT's Technical Advisory Group for their thorough review of the draft final report and many insightful comments, namely William Dunn, Andrew Hanks, Bryan Hartnagel, Dennis Heckman, Gregory Sanders, and Scott Stotlemeyer. Special thanks also to Mr. Bill Stone for his flexibility, insight, and continued support of the project.

The authors would also like to thank the National University Transportation Center (NUTC): Center for Transportation Infrastructure and Safety (CTIS) housed at Missouri University of Science and Technology (Missouri S&T), which provided valuable match funding from the United States Department of Transportation through RITA and the UTC Program. This match funding allowed for more extensive testing and research on the many factors critical to success of the project.

The authors would also like to thank the companies that provided material and equipment contributions necessary for the successful completion of this project, including Atlas Iron Works, Bayer MaterScience, Owens Corning, and VectorPly.

Finally, the authors would like to thank Missouri S&T for their valuable contributions to the research. The university awarded a Chancellor's Fellowships to one of the graduate students working on this project. The authors also appreciate the tireless staff of the Department of Civil, Architectural, and Environmental Engineering and the Center for Infrastructure Engineering Studies. Their assistance both inside and out of the various laboratories was invaluable to the successful completion of this project.

TABLE OF CONTENTS

Page

TABLE OF CONTENTS (cont'd)

TABLE OF CONTENTS (cont'd)

LIST OF ILLUSTRATIONS

Page

LIST OF ILLUSTRATIONS (cont'd)

Page

LIST OF ILLUSTRATIONS (cont'd)

Page

LIST OF TABLES

Page

1. INTRODUCTION

1.1. PROBLEM STATEMENT AND JUSTIFICATION

The deterioration of our nation's infrastructure is an almost daily news item that attracts passionate political, economic, and socio-economic discussions. One of the leading causes of this deterioration is the "bare roads policy" adopted by the majority of state highway agencies during the 1960's. This policy involves the application of deicing salts on state roads during winter months to reduce traffic accidents, injuries, and fatalities. An unfortunate side effect of this policy is that deicing salts attack the steel embedded in reinforced concrete bridges, leading to premature deterioration. In 2002, a study sponsored by the Federal Highway Administration (Koch, et al., 2002) predicted that the U.S. will spend an estimated 8.3 billion dollars annually over the next twenty years in an effort to repair or replace bridges exhibiting corrosion-related damage, with indirect costs exceeding 10 times that amount.

Although still in their infancy, fiber-reinforced polymer (FRP) bridges have shown great promise in eliminating corrosion concerns and meeting (or exceeding) FHWA's goal of 100-year life spans for bridges. While FRP bridges are cost-effective in terms of life cycle analyses, the combination of higher first costs and limited state DOT budgets has restricted their use. One area that has shown some headway is the use of FRP for bridge decks, focusing on the location where the majority of corrosion-related damage normally occurs. However, first costs still hamper widespread use of this approach.

FRP bridge deck panels offer superior corrosion resistance, at one-fifth the weight of reinforced concrete. However, current FRP bridge deck panels typically rely on an intricate geometric honeycomb system between the top and bottom layers of the sandwich panel. This labor-intensive honeycomb construction doubles the cost of FRP panels compared to reinforced concrete. Although cost-effective in terms of longevity of the bridge and overall reductions in weight, the lower first cost of reinforced concrete precludes the use of FRP bridge decks in the majority of situations.

Closed-cell, high-density polyurethane foams lower first cost, offering a cost-effective alternative to the complex honeycomb construction. Structural sandwich panels with a polyurethane foam infill are well established in other commercial applications, such as automobiles, aircraft, and prefabricated buildings. Several recent advances in polyurethane foam formulations have resulted in a material that can resist the localized compressive stresses and fatigue loading beneath a truck wheel, making this type of sandwich panel construction a viable alternative for bridge decks. Once these panels can compete against reinforced concrete on a first-cost basis, their significantly longer life expectancies will save considerable money for MoDOT and the residents of Missouri.

1.2. OBJECTIVE AND RESEARCH PLAN

The ***objective*** of the research was to develop, test, and evaluate fiber-reinforced, polyurethane (PU) foams to replace the costly honeycomb construction currently used to manufacture FRP bridge deck panels. Initially, the effort focused on developing an FRP sandwich panel to replace the precast, stay-in-place forms currently used to construct reinforced concrete bridge decks. However, during the course of the project, the research effort expanded to include full-depth bridge deck panels as well.

The ***research plan*** involved investigating alternative PU foam formulations and configurations; performing component testing to evaluate the different PU foam alternatives; and manufacturing, testing, and evaluating small-scale, mid-scale, and full-scale FRP/PU foam sandwich panels. Initially, the research team investigated four different types of PU foam. From those, three were selected to move forward to the next phase of the research – manufacturing, testing, and evaluating small-scale FRP/PU foam sandwich panels. The results of the small-scale testing and analysis phase lead to selection of a single FRP/PU foam sandwich panel to move forward to the next phase – manufacturing, testing, and evaluating mid-scale sandwich panels. Finally, as a proof-of-concept, the researchers manufactured and tested a full-scale deck panel. This report documents the results of this study.

1.3. TECHNICAL REPORT ORGANIZATION

This report documents a research project on FRP bridge decks with PU foam infill performed by Missouri University of Science and Technology (Missouri S&T) on behalf of the Missouri Department of Transportation (MoDOT). The report is composed of eight chapters. Chapter 1 gives a brief introduction to the subject area, explains the necessity of this research, and also presents the objectives and scope of work of the investigation. Chapter 2 explains the PU foams selected for component testing and decisions made concerning which materials to move forward for further testing and evaluation. Chapter 3 details the small-scale sandwich panel testing program and results. Chapter 4 contains the stiffness and strength analysis of the small-scale panel test results, including recommendations on which FRP/PU foam combination to advance to the next phase. Chapter 5 presents the mid-scale sandwich panel testing program and results, which includes static, fatigue, and durability testing of the prototype FRP/PU foam sandwich panel. Chapter 6 details construction and testing of a prototype full-scale FRP/PU foam deck panel. Chapter 7 contains a summary of the research investigation as well as recommendations on moving forward. Finally, Chapter 8 contains supplementary information on many unique aspects of FRP bridge decks.

2. EVALUATION OF POLYURETHANE FOAM ALTERNATIVES

The following section presents the different polyurethane (PU) foam types selected as potential candidates for the sandwich panel construction. Each foam type is then subjected to flatwise compression and tension testing, which entails placing a compressive or tensile load perpendicular to the longitudinal axis of the panel. These tests were used to evaluate the resistance of the PU foam infill to localized stresses, either direct compressive stresses caused by wheel loads or secondary stresses caused by wrinkling or buckling of the FRP facesheets (tension and compression).

2.1. POLYURETHANE FOAM TYPES SELECTIED FOR TESTING

The four PU foams selected as potential candidates for the core of the FRP sandwich panel represent the full range of infill material types currently available. The four types selected include the following:

- Type 1: High density foam (PU RIGID)
- Type 2: Low density foam with FRP webs (WEB-CORE)
- Type 3: Trapezoidal, low-density foam with mat reinforcement (PRISMA FOAM)
- Type 4: Low density stitched foam (PU STITCHED)

The Type 1 (PU RIGID), shown in Fig. 2.1, consists of a relatively high density polyurethane foam (6 pcf) without any special provisions or configuration. The advantage of the Type 1 material is that the manufacturing process is relatively simple as it only entails bonding of a top and bottom facesheet to the foam to form the sandwich panel. The disadvantage is that horizontal shear transfer between the facesheets relies solely on the shear strength and stiffness of the PU foam. The other disadvantage is that as the density of the PU foam increases, which increases horizontal shear transfer strength and stiffness, the cost increases.

Figure 2.1: Type 1 Polyurethane Foam (PU RIGID)

The Type 2 (WEB-CORE), shown in Fig. 2.2, consists of thin, interconnecting, glass mat/resin webs that form a bi-directional FRP gridwork that is infilled with a low density polyurethane foam (2 pcf). The advantage of the Type 2 material is that the FRP webs provide enhanced horizontal and vertical shear strength and stiffness, increasing the effectiveness of the sandwich panel. This type of panel is also relatively simple to manufacture, although the FRP webs require more care to ensure proper infusion of the resin. The disadvantage is that the FRP gridwork increases the cost of the foam compared to the Type 1.

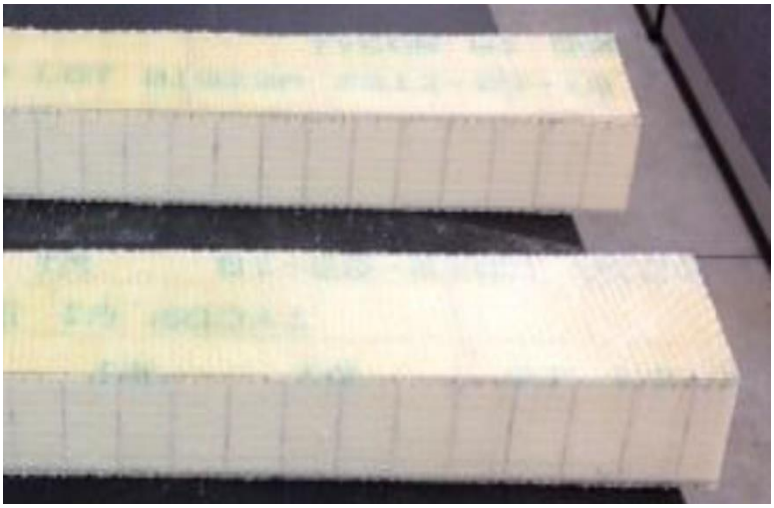

Figure 2.2: Type 2 Polyurethane Foam (WEB-CORE)

The Type 3 (PRISMA FOAM), shown in Fig. 2.3, consists of a low density, trapezoidal-shaped PU foam (2 pcf) with a combination of two plies of a knitted, E-glass, biaxial, matted reinforcement that encompasses each cell. The advantage of the Type 3 material is the significantly enhanced horizontal and vertical shear strength and stiffness that result from the diagonal FRP webs. This truss-type of gridwork also enhances lateral distribution of localized loads, such as those that result from truck tires acting on the bridge deck panel. The disadvantage is the increased manufacturing time and complexity, and thus cost, to form the diagonal FRP webs.

The Type 4 (PU STITCHED), shown in Fig. 2.4, consists of vertical, intermittent, fiberglass bridging strands that stitch the two facesheets together through the low density PU foam (2 pcf). The advantage of the Type 4 material is the enhanced horizontal shear transfer between the facesheets, increasing the effectiveness of the sandwich panel. This type of panel is also relatively simple to manufacture as it doesn't require the same level of care to ensure proper infusion of the stitches as with the Type 2 core. The disadvantage is that the intermittent nature of the stitching is not as effective as the Type 2 or Type 3 web configurations, and the stitching increases the cost of the foam compared to the Type 1 material.

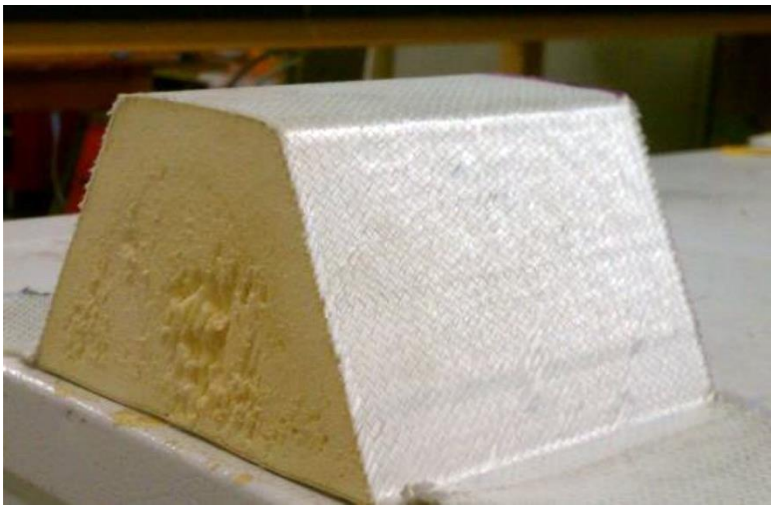

Figure 2.3: Type 3 Polyurethane Foam (PRISMA FOAM)

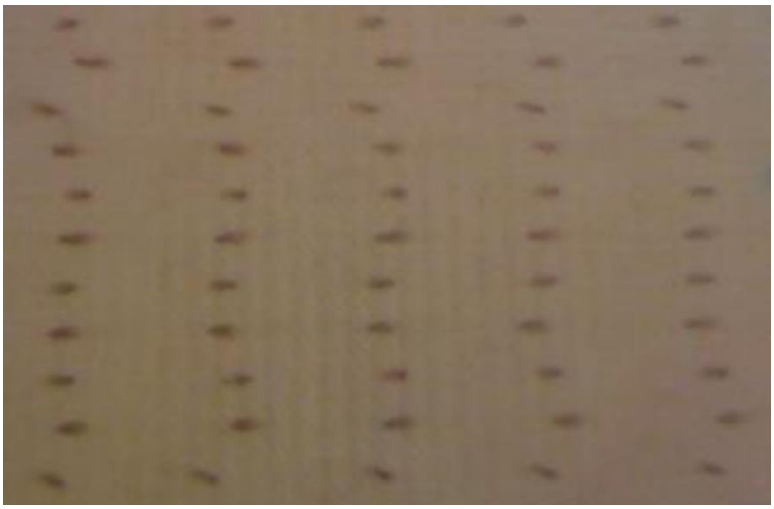

Figure 2.4: Type 4 Polyurethane Foam (PU STITCHED)

2.2. FLATWISE COMPRESSION TESTING

Flatwise compression testing is a very simple small scale experiment for sandwich constructions that has many attractive qualities. The specimens for this test can easily be produced from a larger panel or beam, the test setup does not require any specialized equipment, and the results can be used to estimate the compressive strength and stiffness of the core material while using very little material. These properties make it ideal for quality control and comparative studies. The only downside to this kind of testing is that the properties are only measured in the direction perpendicular to the facings, so it is not completely representative of

anisotropic or orthotropic core materials. Also, the specimens need to have relatively constant rectangular or circular cross-section in the direction of the load.

2.2.1. Test Methodology. There is a standard method for flatwise compression testing that is detailed in ASTM C365/C365M: Standard Test Method for Flatwise Compressive Properties of Sandwich Cores (ASTM, 2011). This standard served as a guideline for the tests, however not all the details of the standard were strictly followed. Therefore, a detailed description of the specimen preparation, the test setup, and the test procedure is provided.

2.2.1.1. Specimen Preparation. The specimens for this experiment were produced by cutting small square pieces from a larger beam segment using a fine toothed band saw. The specimens were laid out at random using a ruler and a square. Then, after sectioning, a coarse grit belt sander was used to lightly sand away any imperfections and ensure the sides were adequately straight and orthogonal to the adjacent sides. Initially, three specimens each were cut for each type of PU foam. These specimens were approximately 3.5 in. x 3.5 in. in cross section perpendicular to the flatwise direction and had a depth equal to that of the associated sandwich construction. After testing the initial specimens, one additional specimen for each core type was fabricated to alleviate some issues that occurred in the initial tests. These extra specimens were cut in the same manner and had the same approximate dimensions as the initial specimens.

2.2.1.2. Test Setup. The test setup used for this experiment consisted of two compression platens, one fixed and one free to pivot, that imparted the load onto the specimen via a displacement controlled drive mechanism. The MTS-880 Universal Testing Machine (UTM) in the structural engineering lab was used to accomplish the testing. The upper platen consisted of a 4 in. x 4 in. x ½ in. A36 steel plate welded at a right angle to a 2 in. x ½ in. A36 steel strip that was installed into the pneumatic grips of the moveable upper crosshead. The lower platen was a round loading platen with a 12 in. diameter. It consisted of two machined steel pieces that allowed the top to pivot relative to the bottom through a hemispherical interface between the two pieces. This attachment sat on the lower crosshead and, during the test, was essentially stationary but able to rotate. A photograph of the setup is presented in Fig. 2.5.

2.2.1.3. Test Procedure. Specimens were tested on multiple days at about the same time of day under similar temperature and humidity conditions. Before testing, the length, width, and depth of each specimen was measured using digital or dial calipers to the nearest 0.001 in. A minimum of three measurements were taken for each dimension and the average was recorded. The specimen was placed on the lower platen, and the platens were moved until there was a narrow gap above the specimen. The lower platen was locked into place and adjusted to be parallel with the top platen, and the load was zeroed. The specimen was centered using the concentric rings of the lower platen and the edges of the upper platen as a reference. For specimens with slight wrinkles in the facings, a thin ⅛-in.-thick rubber pad, Shore A hardness of 60, was placed between each platen to avoid any stress concentrations. The upper head was lowered until a small load was registered (10-50 lb.), then the displacement was zeroed. The test was displacement-controlled at a rate of 0.1 in./min. Displacement and load were recorded simultaneously at a rate of 10 Hz. The test was stopped once the displacement reached 50-80% of the depth of the specimen, which took 10-15 minutes, and the specimen was then unloaded.

Figure 2.5: Flatwise Compression Test Setup

2.2.2. Test Results. The load and displacement were the primary results for this experiment, and before they could be normalized the data needed to be refined. The load versus displacement plots displayed Hookean (linear elastic) behavior before failure, but there were false nonlinearities and discrepancies in the initial readings. The nonlinearity was caused by small gaps in the system. Also, during testing the displacement was set to zero at a non-zero load. Both of these issues lead to a false offset in the displacement. In order to correct this issue, regression analysis of the linear region of the load versus displacement plot was used to correct this offset. Different ranges of the data were explored, and the range with the best correlation factor was chosen to be representative of the linear elastic region of the sample. Then, using the regression equation, the genuine part of the load versus displacement curve was offset by the x-axis intercept of the regression equation. Then, the false data at the beginning of the test was replaced by a projection of the linear region that intersected the origin. A graphical representation of this procedure is presented in Fig. 2.6.

After the data was corrected, the concepts of engineering stress and strain could be used to normalize the load and deflection values for comparison between specimens and core types. The engineering stress and strain in the axial direction can be found using Eqns. 2.1 and 2.2, respectively.

$$\sigma = {}^{F}/_{A_o} \tag{2.1}$$

$$\varepsilon = {}^{\Delta L}/_{L_o} \tag{2.2}$$

In Eqn. 2.1, σ is the engineering stress in the axial direction measured in pounds per square inch (psi), F is the applied load in pounds, and A_o is the initial cross-sectional area of the specimen measured perpendicular to the load in square inches. In Eqn. 2.2, ε is the engineering

strain in the axial direction measure in inches per inch (in./in.), ΔL is the displacement parallel to the load measured in inches, and L_o is the initial length of the specimen parallel to the load measured in inches. Using the axial stress and strain from the load-displacement plot, the axial strength and stiffness of the material in compression can be determined.

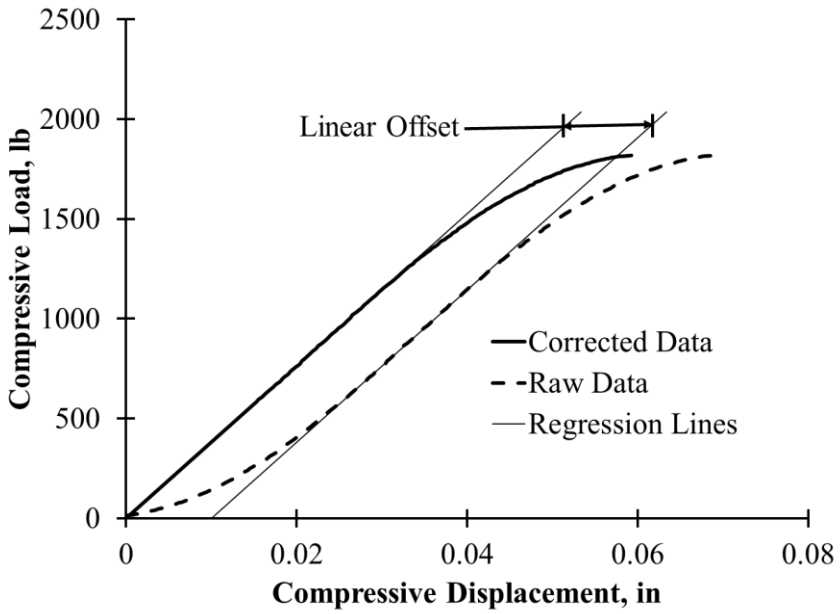

Figure 2.6: Load vs. Displacement Correction using Linear Regression

These concepts can be applied to the core materials using the load and displacement results for the experiment by making some observations. The engineering stress and strain are average values over the cross-section, so they are not completely representative of the stresses and strains in individual parts of the core. However, they are a reasonable global approximation that can be representative of the system as a whole. Also, the stress and strain are oriented in the flatwise direction, which is perpendicular to the facing, therefore the properties that are estimated in this experiment are not necessarily representative of the properties in the other orthogonal directions.

Special considerations must also be made when using the equations. The height of the core is not the same as the total height of the specimen because the facings contribute to the total height, so the initial length that must be used in Eqn. 2.2 is equal to the height of the specimen minus twice the thickness of the facings. Next, the displacement recorded in the test can be considered the same as the displacement in Eqn. 2.2 as long as the facing material is several orders of magnitude stiffer than the core material. This means the facings compress very little during the test and do not contribute significantly to the measured displacement.

If these assumptions are made, the stress and strain in the core material can be calculated for each test. Then, the stress at failure can be considered the compressive strength of the core

because the failure will occur inside the core of the specimen. This will be denoted as the flatwise compressive strength because it is measured in the flatwise direction. Then, linear regression can be performed on the plot of stress versus strain to calculate the axial stiffness of the core in compression. This stiffness is the slope of the line made by a regression of the stress versus strain plot, which will be performed over the range of stress and strain that directly corresponds to the range of load and displacement that was formerly used to correct the offset in the load-displacement plot. This axial stiffness in compression will be denoted as the flatwise compressive modulus.

2.2.2.1. Results for Type 1. Three specimens were originally prepared and tested for the Type 1 core. However, during the testing of the original Specimen 1-1-C, the lower crosshead of the machine was not locked properly and the results were unusable. A fourth specimen was prepared and successfully tested, and the results of this test were used to replace the original 1-1-C data. Once the initial false nonlinearities and discrepancies in the load versus displacement response were corrected, the stress and strain were calculated for each specimen. The plot of stress and strain for each specimen is shown in Fig. 2.7. The stress versus strain response can be divided into three distinct regions, as shown in Fig. 2.8. The Type 1 core is constructed of rigid polyurethane foam that typically displays this type of response, and each region can be explained in physical terms.

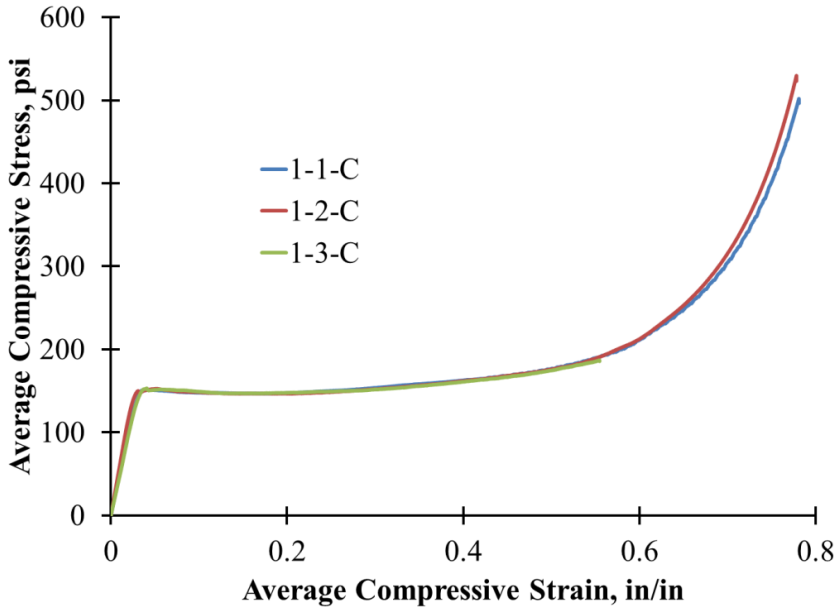

Figure 2.7: Stress-Strain Results for Type 1 Flatwise Compression Test

In the first region, the cells of the foam are compressing uniformly. The cells are distributed relatively evenly in size and location, and the polyurethane plastic that the foam is manufactured from behaves approximately linear elastically to a point. As a result, the foam has a global response that is apparently linear elastic, and the stress versus strain plot in this region is

linear. Eventually, some of the cell walls and struts reach their strength or stability limit, and the specimen transitions into the second region.

In the second region, the specimen starts to fail as some of the cells collapse due to excessive buckling, yielding, and/or fracturing of the cell wall and struts. This begins at a critical location, which sets off a chain reaction that spreads throughout the cross-section, eventually encompassing the entire specimen. The material has an apparent yield point at the beginning of this region as stress temporarily peaks then fluctuates slightly as it remains nearly constant.

Finally, in the third region, the majority of the cells of the foam have begun to collapse and are permanently damaged. The damaged cell walls and struts deform to the point that their movement is impeded by the cells and struts near them. Eventually, through a process commonly referred to as densification, the foam becomes denser and more stable on the cellular scale as the voids close up. This response causes the stress to increase in a quasi-exponential manor as the foam becomes apparently stronger.

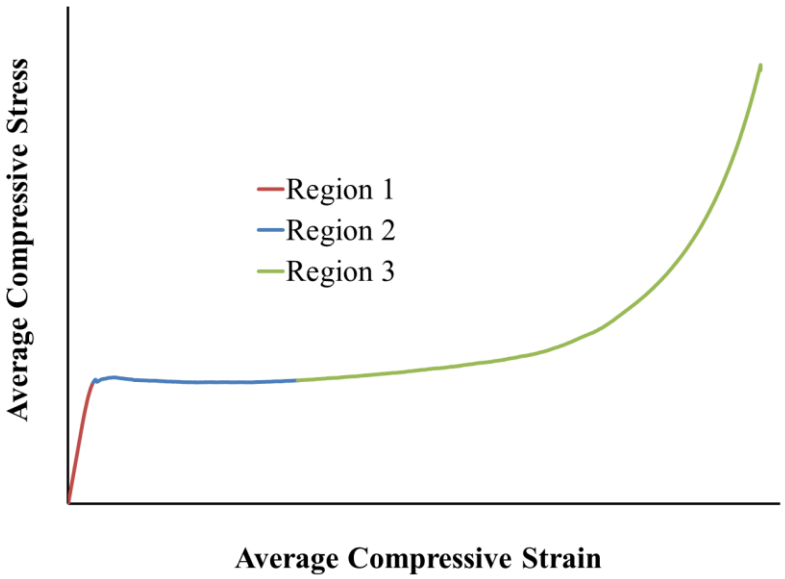

Figure 2.8: Generalized Stress-Strain Response for Type 1 Compression Test

The plot of stress versus strain was then used to determine the strength and stiffness of the core material. The strength can be considered as the stress at failure, but first a failure point must be established. The failure occurs in the transition between the first two regions described previously and requires closer examination in order to define that point. Figure 2.9 shows a close up plot of stress versus strain for Specimen 1-2-C before and after failure.

In this plot, the transition between the regions is much more gradual, and the point of failure becomes difficult to define and somewhat subjective. However, there is an apparent yielding point that is located at the first small peak in stress where the specimen likely started to

fail. Also, this yield point is present on the stress versus strain curves for all three specimens, and it is easy to determine the stress and strain at this point. As a result, the flatwise compressive strength will be considered as the stress at this point. A visual representation of what the failure of the specimens actually looked like just after failure and at the end of the test is shown in Figs. 2.10 and 2.11, respectively.

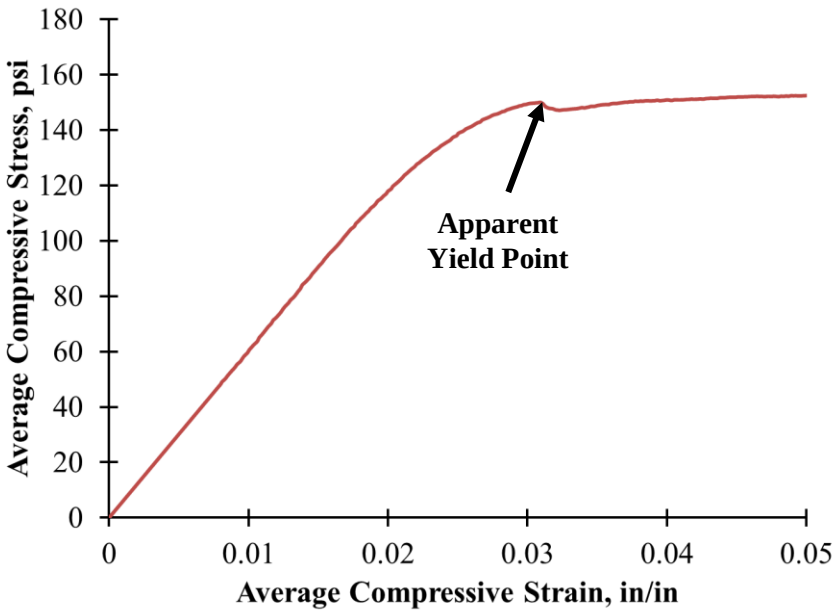

Figure 2.9: Stress-Strain Response at Failure for Specimen 1-2-C Compression Test

Figure 2.10: Damage at Failure for Flatwise Compression Testing of Type 1

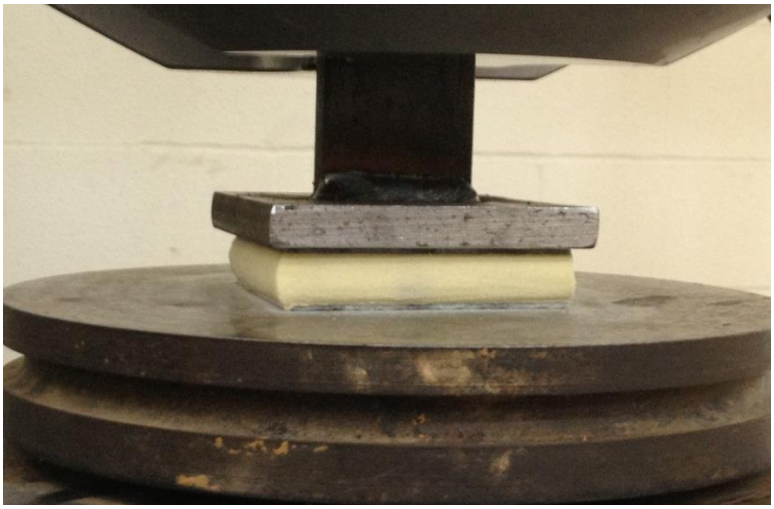

Figure 2.11: Damage at End of Test for Flatwise Compression Testing of Type 1

The axial stiffness is the next item of concern. Linear regression analysis was used to calculate this stiffness by using the range of stress and strain that corresponded to the load and displacement range used to correct the raw data. This range varied between specimens, but on average the regression with the greatest correlation occurred at a strain range of 0.007 to 0.016 in./in. and utilized at least 30 data points. The slope of the regression equation was considered the flatwise compressive modulus with units of pounds per square inch (psi). A summary of the results for flatwise compressive strength and modulus for each Type 1 specimen is presented in Table 2.1.

Table 2.1: Flatwise Compression Testing Results for Type 1

Specimen	Flatwise Compressive Strength (psi)	Flatwise Compressive Modulus (psi)
1-1-C	150	5,150
1-2-C	151	6,030
1-3-C	153	4,770

2.2.2.2. Results for Type 2. Originally, three specimens were also prepared and tested for the Type 2 core. The results for each of these specimens appeared useable, but the results for the first specimen had a significantly higher strength than the other specimens. A fourth specimen was prepared and tested in an attempt to verify any outliers. The results for the fourth specimen showed a noticeably lower stiffness while the strength was similar to the second and third specimens. There were no unusual occurrences during testing that would indicate poor results for any of the specimens, but after examining the amount of web reinforcement in each specimen, it

was found that the first specimen had two complete cells while the other specimens had only one complete cell. Also, it was noted that the fourth specimen was wrinkled on one face and rubber pads were used to distribute the load more evenly in an attempt to prevent any unusual localized failure. It was apparent that the Type 2 specimens had a high degree variability, and the results of the test were highly dependent on the location and quantity of reinforcing webs. Nevertheless, the data is sufficient for a comparison between the core types.

Moving forward with the analysis, the initial false nonlinearities and discrepancies in the load versus displacement response were corrected, and the stress and strain were calculated for each specimen. The plot of stress versus strain is presented in Fig. 2.12. The stress versus strain response has two distinct regions that are apparent in the figure, and each region can be explained based on the Type 2 core construction. The Type 2 core consists of thin, interconnecting, glass mat/resin webs that form a bi-directional FRP gridwork that is infilled with a low density polyurethane foam. This FRP gridwork plays an important role in the stress versus strain response.

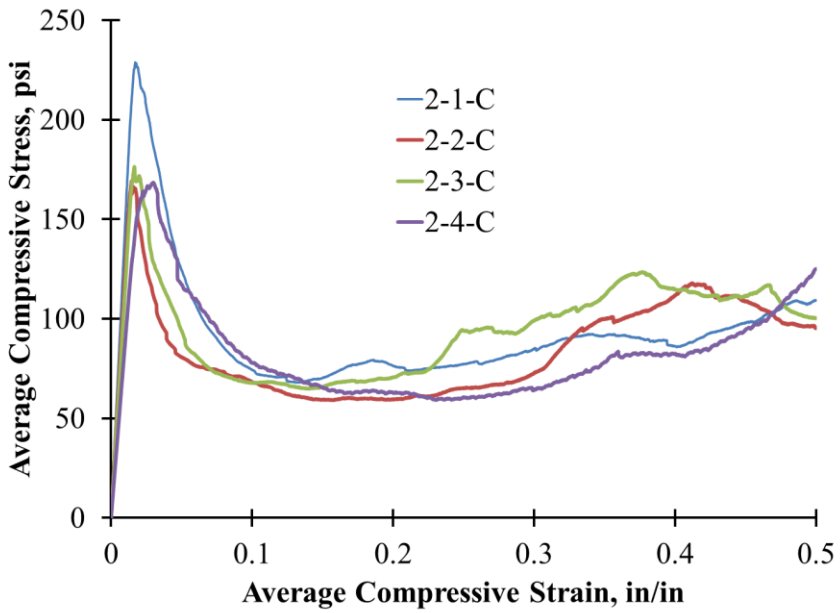

Figure 2.12: Stress-Strain Results for Type 2 Flatwise Compression Test

In the first region, the web reinforcement has an apparent linear elastic behavior because the material consists of resin and fibers that display Hookean behavior to a point. The flexible foam contributes almost nothing to the response directly, but it does provide stability for the webs as they are very thin relative to their length. As a result, the global stress versus strain response in this region is linear, but as the load increases, minor defects in the webs or adjacent foam resulted in portions of the FRP gridwork beginning to buckle, and the behavior transitioned into the second region.

In the second region, immediately following the linear region, the webs that initially buckled began to buckle excessively and started to fracture. The stress redistributed to adjacent webs, but they too buckled and fractured as the stress increased. This non-sequential failure of the FRP gridwork caused the stress to decrease rapidly and erratically. Due to the very low strength and stiffness of the flexible foam, the stress versus strain plots did not display a yielding failure, and the stress did not noticeably increase at high displacements as with the Type 1 specimens.

The compressive strength and stiffness were calculated using the stress versus strain plots. The flatwise compressive strength is more evident for the Type 2 core because failure occurred suddenly and was accompanied by a significant drop in load immediately after the peak value. Therefore, the stress at the maximum load was considered to be the flatwise compressive strength. A visual representation of what the failure of the specimens actually looked like just after failure and at the end of the test is shown in Figs. 2.13 and 2.14, respectively.

Figure 2.13: Damage at Failure for Flatwise Compression Testing of Type 2

The stiffness is again designated as the flatwise compressive modulus with the same definition and units described previously, and it was found using the same type of linear regression analysis. The regression region once more varied between specimens, but on average the regression with the greatest correlation occurred at a strain range of 0.006 to 0.012 in./in. while using at least 20 data points. A summary of the results for flatwise compressive strength and modulus for each specimen is presented in Table 2.2.

2.2.2.3. Results for Type 3. The true value of the Type 3 core is its use as a mold for the FRP layers that form the truss-type panel. However, the foam will provide a slight degree of secondary bracing/stability to the FRP webs and facesheets, and the decision was made to test the foam alone without any of the mat reinforcement. Representative square blocks of the Type 3 material were sectioned for testing, with three random samples chosen from the six available specimens.

Figure 2.14: Damage at End of Test for Flatwise Compression Testing of Type 2

Table 2.2: Flatwise Compression Testing Results for Type 2

Specimen	Flatwise Compressive Strength (psi)	Flatwise Compressive Modulus (psi)
2-1-C	229	14,790
2-2-C	169	13,710
2-3-C	176	12,750
2-4-C	168	9,740

As expected, without the FRP mat reinforcement, the Type 3 foam performed very similar to the Type 1 foam as the only difference between them involved the density – 2 pcf and 6 pcf for the Type 3 and Type 1, respectively. The stress-strain diagrams for the Type 3 core had the same general shape as those shown in Figs. 2.8 and 2.9 for the Type 1 material. As with the Type 1 material, the Type 3 foam experienced an initial linear-elastic region that terminated in a distinct "yield" point. The region that followed was characterized by a relatively constant stress level with increasing strain as the cell walls began to experience progressive buckling and collapse. Finally, as the cells within the foam compressed completely, the third region occurred, which was characterized by the stress increasing in a quasi-exponential manor due to densification of the foam.

Linear regression analysis was again used to calculate the flatwise compression stiffness by using the range of stress and strain that corresponded to the load and displacement range used to correct the raw data. The slope of the regression equation was again considered the flatwise compressive modulus with units of psi. A summary of the results for flatwise compressive strength and modulus for each Type 3 specimen is presented in Table 2.3.

Table 2.3: Flatwise Compression Testing Results for Type 3

Specimen	Flatwise Compressive Strength (psi)	Flatwise Compressive Modulus (psi)
3-1-C	57	2,150
3-2-C	61	2,270
3-3-C	58	2,040

2.2.2.4. Results for Type 4. The response of the Type 4 foam (stitching) was very similar to that for the Type 2 foam (web-core). This result was not unexpected as the stitching used in the Type 4 core is an intermittent version of the continuous FRP gridwork used in the Type 2 foam. However, although the overall behavior was similar, the intermittent nature of the stitching had a fairly pronounced effect on both the stiffness of the foam and the peak strength compared to that for Type 2.

The shape of the stress-strain response for the Type 4 foam followed the same general trend as shown in Fig. 2.12 for the Type 2 material. The initial region was characterized by a linear-elastic response followed by an abrupt decrease in load as all of the stitching buckled and/or fractured nearly simultaneously within the specimen. This behavior provided a very clear peak value, with the stress at the maximum load considered to be the flatwise compressive strength. As with Types 1 through 3, the stiffness was found using a linear regression analysis. A summary of the results for flatwise compressive strength and modulus for each specimen is presented in Table 2.4.

Table 2.4: Flatwise Compression Testing Results for Type 4

Specimen	Flatwise Compressive Strength (psi)	Flatwise Compressive Modulus (psi)
4-1-C	93	3,450
4-2-C	91	3,310
4-3-C	99	3,630

2.3. FLATWISE TENSION TESTING

Another useful small scale test is flatwise tension testing. It has the same benefits as flatwise compression with one exception. The specimens for this test require more preparation, but they can still be produced from a larger panel or beam and modified for testing. The test

setup is also very similar and does not require highly specialized equipment. After the test, the results can be used to estimate the tensile strength of the core or the bond between the core and the facing, depending on where failure occurs first. Also, the tensile stiffness of the core material can be estimated. However, it has the same downsides as flatwise compression testing. The properties are only measured in the direction perpendicular to the facings, and are not necessarily representative of properties in other directions. The specimens also need to have a uniform rectangular or circular cross-section in the direction of the loading.

2.3.1. Test Methodology. There is a standard method for flatwise tension testing that is detailed in ASTM C297/C297M: Standard Test Method for Flatwise Tensile Strength of Sandwich Constructions (ASTM, 2010). This standard served as a guideline for the tests, however not all the details of the standard were strictly followed. Therefore, a detailed description of the specimen preparation, the test setup, and the test procedure is provided.

2.3.1.1. Specimen Preparation. As with the flatwise compression specimens, the flatwise tension specimens were prepared from a larger beam segment using a fine toothed band saw. The specimens were laid out at random using a ruler and a square. Then, after sectioning, a coarse grit belt sander was used to lightly sand away any imperfections and ensure the sides were adequately straight and orthogonal to the adjacent sides. The final dimensions of the specimens were 3.5 in. x 3.5 in. in cross section perpendicular to the flatwise direction and had a depth equal to that of the associated sandwich panel construction. Three specimens were prepared for each core type.

After the specimens were prepared, some special measures were required prior to testing. The specimens could not be properly gripped for a tension test, so plates that could be gripped by the testing machine needed to be adhered to the specimens. These plates were manufactured using A36 steel and consisted of a 6 in. x 6 in. x ¼ in. plate with a 2 in. x ¼ in. bar welded to the center of the plate at a right angle. These plates are far more rigid than the specimens, and they allowed the testing machine to impart tensile stresses on the specimens without significantly influencing the deformation results. Before the plates were adhered to the foam samples, the length and width of each specimen was measured using digital or dial calipers to the nearest 0.001 in., and three measurements were taken for each. The average was recorded. The height and facing thickness of the specimens was measured from the original beams before cutting any specimens. A minimum of 30 measurements were taken and the average was reported.

The procedure for adhering the steel plates to the specimens consisted of the following sequence. The first plate was placed into the center of the pneumatic grips of the lower crosshead of the MTS-880 UTM, and using a bubble level the square face of the plate was positioned perpendicular to the applied load. Once the plate was centered and leveled, the grips were fully engaged to hold it in place. The lower crosshead was then locked into place to ensure it was stationary. Next, two part epoxy was thoroughly mixed and applied to the flat surface of the plate. The epoxy used was 3M 08101 structural adhesive. Immediately afterwards, the specimen was placed onto the epoxy, and the specimen was centered using the edges of the plate as a reference. Then, additional epoxy was mixed and applied to the top face of the specimen, and the upper plate was placed flat side down onto the specimen. Again the edges of the plate were used

to ensure the specimen was centered in the square portion of the plates. The upper pneumatic grips of the test machine were lowered until the bar of the upper plate was sufficiently inside the grips. A bubble level and visual inspection were used to ensure the assembly was properly aligned and centered. The grips were then engaged to lock the upper plate into place, and a small amount of compressive force (10 - 50 lb.) was applied. The procedure up to this point took 5 - 10 minutes to complete. Once pressure was applied, the assembly had to cure for one hour before the epoxy had enough usable strength to be moved.

After the initial curing period, the assembly was marked to ensure it would be tested using the same orientation. It was removed and stored at standard room temperature and humidity conditions until testing was completed a few days later. The epoxy required a minimum 8 hour curing period to achieve full strength. Figure 2.15 shows a photograph of Specimen 2-1-T after it was adhered to the plates.

Figure 2.15: Prepared Specimen for Flatwise Tension Test

2.3.1.2. Test Setup. The test setup used for this experiment was relatively straightforward. After adhering the plates to the specimens and allowing the epoxy to reach full strength, the same pneumatic grip setup on the MTS-880 UTM was used to test the specimens. The assembly was gripped in the same orientation as that used to adhere the plates. The lower crosshead was locked to remain stationary while the upper crosshead served as the moveable head and could be displaced at a specified rate. A photograph of the setup is presented in Fig. 2.16.

2.3.1.3. Test Procedure. All specimens were tested at approximately the same time of day in similar temperature and humidity conditions. During testing, the specimen assembly was placed into the pneumatic grips of the lower crosshead in the same position used for adhering the plates, and a bubble level was used to ensure is was aligned perpendicular to the load before the grips were engaged. The lower crosshead was locked into place and the load was zeroed. The upper crosshead was lowered until the top of the assembly was adequately within the grips, and

the alignment of the system was visually inspected before the grips were engaged. Once the grips were engaged, the displacement was zeroed and the load was allowed to float. Displacement was then added at a constant rate of 0.01-0.02 in./min., and the tensile load was recorded simultaneously. Load and displacement were recorded at a rate of 10 Hz. In general, the tension tests were characterized by a linear-elastic response followed by an abrupt decrease in load at failure, which took 5-20 minutes depending on the particular foam sample.

Figure 2.16: Flatwise Tension Test Setup

2.3.2. Test Results. The primary results to be analyzed were the load and displacement, but as with the flatwise compression testing, the analysis could not be started until the load versus displacement was corrected. The load versus displacement plots displayed linear elastic behavior prior to failure, but there were discrepancies in the initial readings caused by setting the displacement to zero at a non-zero load. In order to fix this problem, the same linear regression analysis of the load versus displacement plot was used. Again, different ranges of the data were explored, and the range with the best correlation factor was chosen. Then, using the regression equation, the linear region of the data was offset to make its projection intersect the origin. Graphically, this is the same as the method already presented in Fig. 2.6 of Section 2.2.2. The only difference is the loads and displacements are in tension, and the nonlinear region caused by slack in the system was not prevalent in the flatwise tension testing. The primary issue was the offset caused by setting the displacement to zero while the load was non-zero.

After the data was corrected, the concepts of engineering stress and strain that were discussed previously in Section 2.2.2 were used to normalize the load and displacement values for comparison between specimens and core types. The equations used to calculate engineering stress and strain in the axial direction along with an explanation of the variables can be found in the aforementioned section as Eqns. 2.1 and 2.2, respectively.

Once more assumptions must be made to apply these concepts of stress and strain to the tension specimens. The engineering stress and strain calculated using the aforementioned

equations are average values over the cross-section, and are not completely representative of the stresses and strains in individual parts of the core. They are however an adequate global approximation. The stress and strain are again oriented in the flatwise direction, perpendicular to the facing, and are not representative of material properties in orthogonal directions. Also, the initial length that must be used in Eqn. 2.2 is equal to the height of the specimen minus twice the thickness of the facings, which is the height of the core. Then, since the stiffnesses of the glue and the facing material are much larger than that of the core material, it is reasonable to assume that deformations within the epoxy layer and the facings are negligible, and the recorded displacement can be input directly into Eqn. 2.2 as the displacement of the core alone.

Using these assumptions, the stress and strain in the core material can be calculated for each test. From these results, the stress at failure can be considered the flatwise tensile strength of the core or the bond between the core and the facings, depending on where the failure initialized. Then, linear regression can once more be performed on the plot of stress versus strain to calculate the axial stiffness of the core in tension. This calculation was done using the same method used in Section 2.2.2 for the flatwise compression tests. The axial stiffness in tension measured in the flatwise direction was denoted as the flatwise tensile modulus.

2.3.2.1. Results for Type 1. Three specimens were prepared from the larger beam segment for the Type 1 core, and they were prepared and tested using the procedures presented previously in this section. However, during testing of the first specimen, the upper crosshead of the machine was rotated from its original position, and when the grips clamped down on the assembly, it applied a torsional force to the specimen causing it to prematurely fail when it was loaded. After the crosshead grips were aligned properly, the other two specimens were successfully tested. Due to a lack of material, no additional specimens could be prepared, so only the results from the two successful tests will be presented.

The initial discrepancies in the load versus displacement response were corrected, and the stress and strain were calculated for each specimen. The plot of stress and strain for each specimen is shown in Fig. 2.17. The stress-strain response was almost completely linear prior to failure. Since cells of the foam are uniform in size and distribution, the behavior is similar to that of solid polyurethane, which in this case is nearly linear elastic in nature. The plot of stress versus strain was then used to determine the tensile strength and stiffness of the core material. The strength can be considered as the stress at failure, which occurred very abruptly at the maximum stress. The stress at this point will be considered the flatwise tensile strength, and failure occurred in the rigid polyurethane foam for both specimens. Figure 2.18 is a photograph of the fracture that occurred at the peak load, while Fig. 2.19 reveals the fracture surface examined after completion of the test.

The axial stiffness is the next item of concern. Linear regression analysis was used to calculate this stiffness by using the range of stress and strain that corresponded to the load and displacement range used to correct the raw data. This range varied between specimens, but on average the regression with the greatest correlation occurred at a strain range of 0.0001 to 0.015 in./in. and utilized at least 800 data points. The slope of the regression equation was considered

the flatwise tensile modulus with units of psi. A summary of the results for flatwise tensile strength and modulus for each Type 1 specimen is presented in Table 2.5.

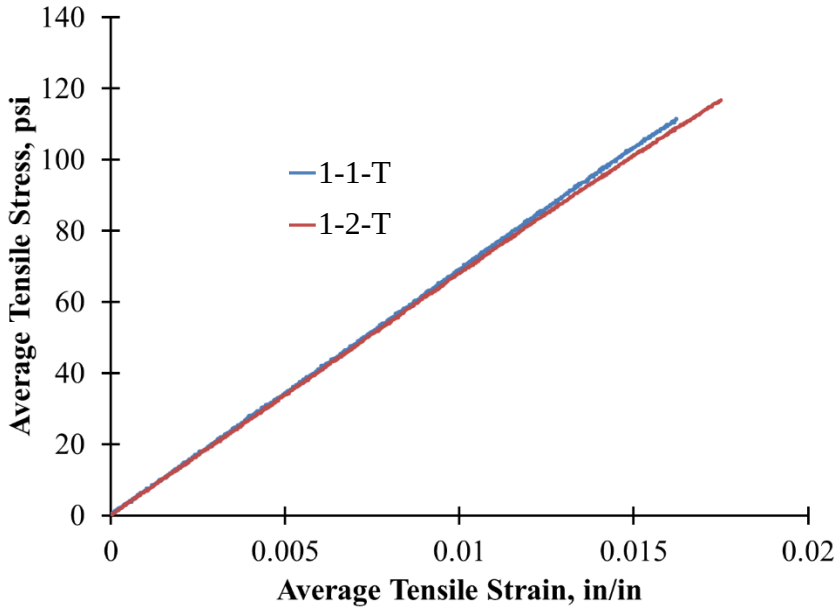

Figure 2.17: Stress-Strain Results for Type 1 Flatwise Tension Test

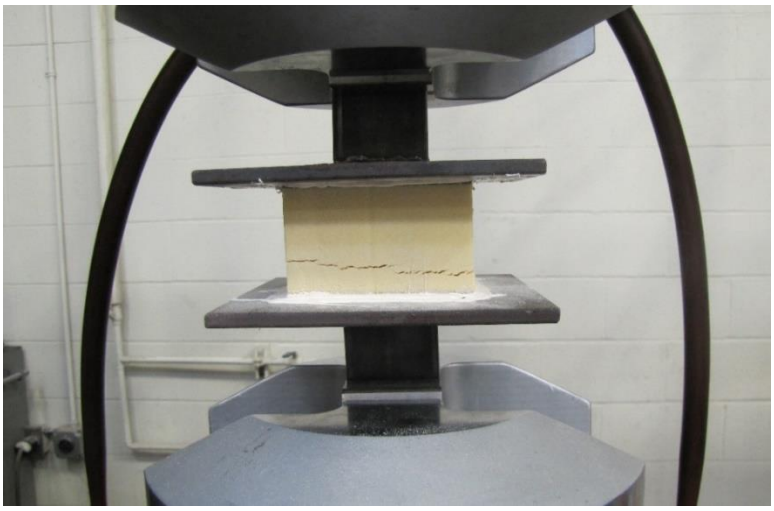

Figure 2.18: Damage at Failure for Flatwise Tension Testing of Type 1

2.3.2.2. Results for Type 2. Three specimens were prepared and tested for the Type 2 core, and there were no difficulties while testing this specimen type. Each specimen had a slightly different plan location of the FRP webs within the foam, but only one complete cell of

web reinforcing was present in each specimen. Consequently, there were noticeable variations in the results between specimens, but there was no physical indication that one of the tests could be a statistical outlier. Following the tests, the initial discrepancies in the load versus displacement response were corrected, and the stress and strain were calculated for each specimen. The stress-strain plot for each specimen is shown in Fig. 2.20. The stress-strain response has two distinct regions visible in the figure that are related to the constituent materials of the Type 2 core.

Figure 2.19: Fracture Surface for Flatwise Tension Testing of Type 1

Table 2.5: Flatwise Tension Testing Results for Type 1

Specimen	Flatwise Tensile Strength (psi)	Flatwise Tensile Modulus (psi)
1-1-T	112	6,900
1-2-T	117	6,800

The first region has an overall linear stress-strain response before the first peak in load. In this region, fiber reinforced polyurethane webs and the flexible polyurethane foam are acting together, but the foam contributes very little to the response. Since the polyurethane and reinforcing webs are approximately linear elastic in nature, the composite core has a relatively linear elastic response. Then, a transition into the second region occurred due to the very low stiffness and strength of the flexible foam, the location and distribution of the reinforcing webs, and the nature of the bond between the core and facing.

The second region began just after the first peak in stress. The stress-strain behavior became erratic as the stress began to decrease in steps in this region. This was caused by asynchronous failures in different parts of the core. In areas of high stress concentrations, the

web reinforcing began to fracture or debond from the facing at the base and the foam started to crack, causing the load to decrease and redistribute to different parts of the core. Failure occurred in the bond between the core and facing for Specimens 2-1-T and 2-3-T, and for Specimen 2-2-T, failure occurred in the core material alone.

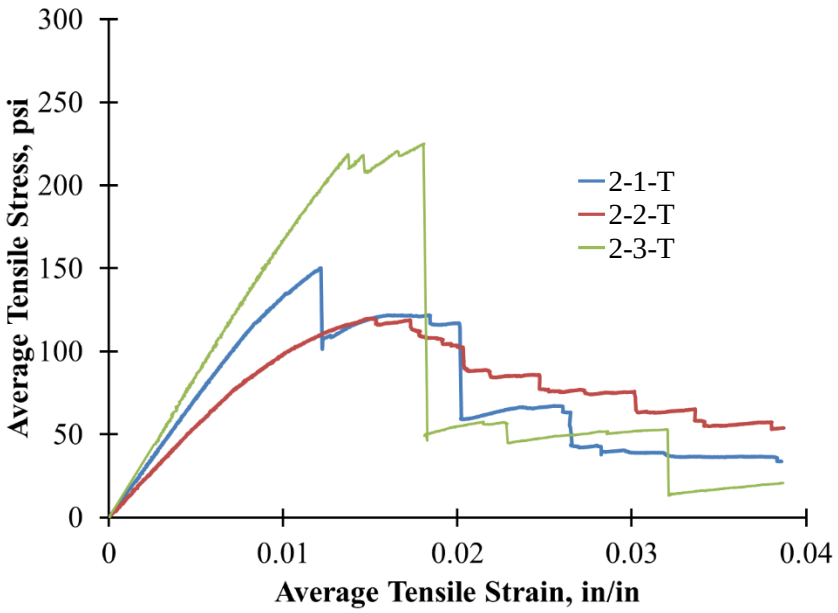

Figure 2.20: Stress-Strain Results for Type 2 Flatwise Tension Test

The stress-strain plot was then used to calculate the tensile strength of the core and/or the bond between the core and the facings. The first peak in stress attained by the specimens was considered the failure point and the stress at this point was considered the flatwise tensile strength. The two failure types are shown in Figs. 2.21 (core) and 2.22 (bond).

The axial stiffness was once again designated as the flatwise tensile modulus with the same definition, units, and regression analysis described previously. The regression region varied between specimens, but on average the regression with the greatest correlation occurred at a strain range of 0.002 to 0.007 in./in. while using at least 300 data points. A summary of the results for flatwise tensile strength and modulus for each Type 2 specimen is presented in Table 2.6.

2.3.2.3. Results for Type 3. As with the flatwise compression testing, the flatwise tension testing for the Type 3 core consisted of testing the foam alone without any mat reinforcement. Representative square blocks of the Type 3 material were sectioned for testing, with three random samples chosen from the five available specimens. The stress-strain response of the Type 3 foam was essentially linear prior to failure, where an abrupt drop in stress occurred when the foam fractured, similar to the response shown in Fig. 2.17 for the Type 1 foam. Figure 2.23 is a photograph of the fracture that occurred at the peak load.

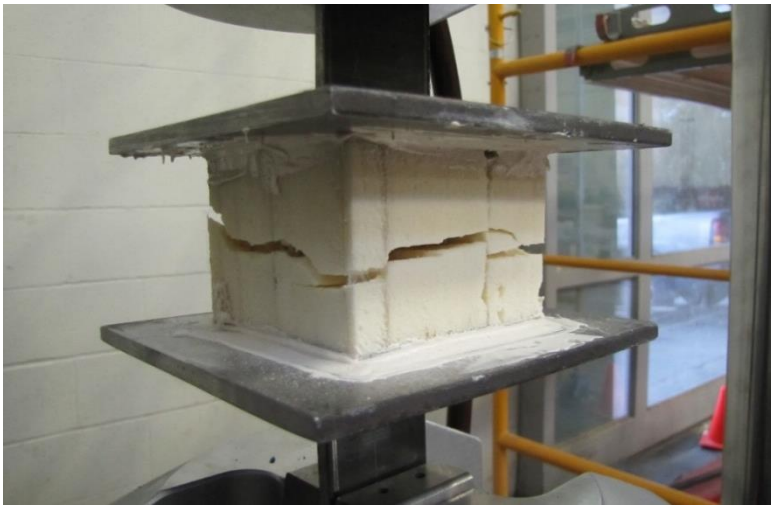

Figure 2.21: Type 2 Core Failure During Flatwise Tension Test

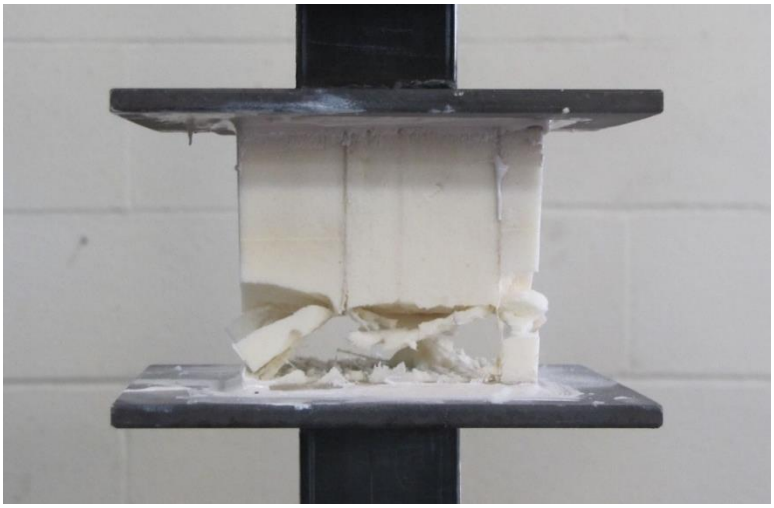

Figure 2.22: Type 2 Bond Failure During Flatwise Tension Test

Table 2.6: Flatwise Tension Testing Results for Type 2

Specimen	Flatwise Tensile Strength (psi)	Flatwise Tensile Modulus (psi)
2-1-T	150	14,270
2-2-T	120	11,050
2-3-T	219	16,800

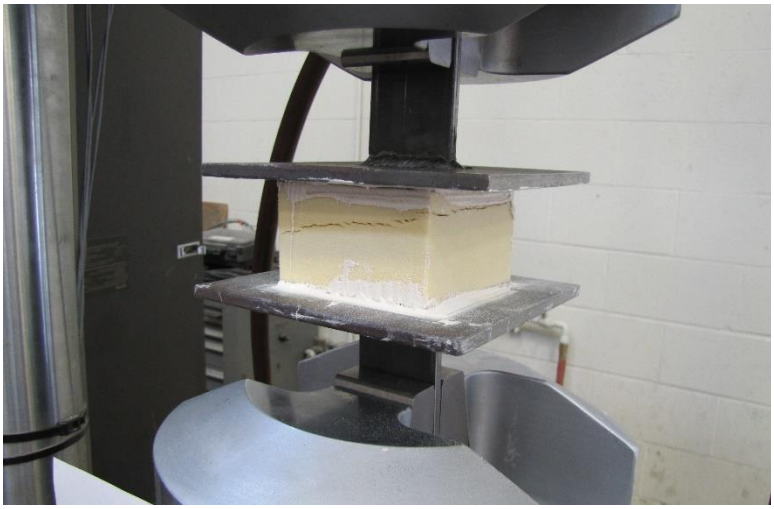

Figure 2.23: Damage at Failure for Flatwise Tension Testing of Type 3

Linear regression analysis was again used to calculate the flatwise tensile stiffness by using the range of stress and strain that corresponded to the load and displacement range used to correct the raw data. The slope of the regression equation was again considered the flatwise tensile modulus with units of psi. A summary of the results for flatwise tensile strength and modulus for each Type 3 specimen is presented in Table 2.7.

Table 2.7: Flatwise Tension Testing Results for Type 3

Specimen	Flatwise Tensile Strength (psi)	Flatwise Tensile Modulus (psi)
3-1-T	48	2,390
3-2-T	43	2,230
3-3-T	51	2,370

2.3.2.4. Results for Type 4. The response of the Type 4 foam (stitching) was again very similar to that for the Type 2 foam (web-core). This result was not unexpected as the stitching used in the Type 4 core is an intermittent version of the continuous FRP gridwork used in the Type 2 foam. However, although the overall behavior was similar, the intermittent nature of the stitching had a fairly pronounced effect on the stiffness of the foam, the peak strength, and the post peak behavior compared to that for Type 2.

The shape of the stress-strain response for the Type 4 foam followed the same general trend as shown in Fig. 2.20 for the Type 2 material and characterized by two distinct regions. The first region displayed a linear stress-strain response with the FRP stitching and flexible polyurethane foam acting together, although the stitching supported the majority of the load.

Once the stress in the stitches exceeded their capacity, there was an abrupt decrease in load as the all of the stitches fractured nearly simultaneously within the specimen. This behavior provided a very clear peak value, with the stress at the maximum load considered to be the flatwise tensile strength. Unlike the Type 2 material, the Type 4 core did not have as extensive a second region since the stitches failed fairly rapidly, although there was a slight degree of progressive failure prior to a complete loss in load carrying capacity. All of the Type 4 specimens experienced failure within the core material and not at the interface with the facesheets. Figure 2.24 is a photograph of the fracture that occurred at the peak load. The stiffness was again determined through the use of a linear regression analysis. A summary of the results for flatwise tensile strength and modulus for each specimen is presented in Table 2.8.

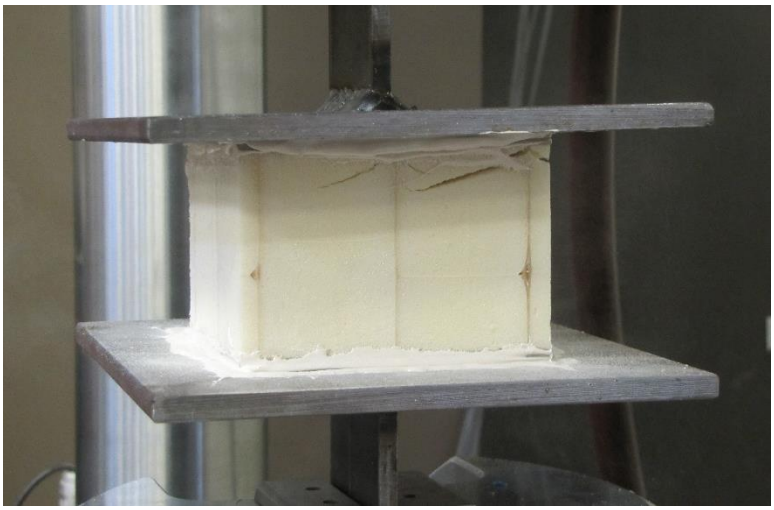

Figure 2.24: Damage at Failure for Flatwise Tension Testing of Type 4

Table 2.8: Flatwise Tension Testing Results for Type 4

Specimen	Flatwise Tensile Strength (psi)	Flatwise Tensile Modulus (psi)
4-1-T	97	4,150
4-2-T	86	3,870
4-3-T	82	3,700

2.4. SUMMARY AND RECOMMENDATIONS FOR NEXT PHASE

A summary of the results for the flatwise compression and tension testing are shown in Table 2.9. For the two plain foams, the Type 1 outperformed the Type 3 by more than a factor of two in terms of both strength and stiffness. This result is consistent with the higher density of the

Type 1 foam. In general, as the density of a structural foam increases, the strength and stiffness increases. In terms of the two reinforced foams, the Type 2 outperformed the Type 4, which is also as expected given that the FRP web reinforcement is much more extensive in the Type 2 foam.

Table 2.9: Summary of Flatwise Compressive and Tensile Testing

Core Type	Flatwise Compression (psi)		Flatwise Tension (psi)	
	Strength	Stiffness	Strength	Stiffness
Type 1 (PU RIGID)	151	5,317	114	6,850
Type 2 (WEB-CORE)	185	12,748	163	14,040
Type 3 (PRISMA FOAM)	59	2,153	47	2,330
Type 4 (PU STITCHED)	94	3,463	88	3,907

In comparing the Type 1 plain foam to the reinforced foams, the Type 1 foam performed very well, with strength and stiffness values falling between the two reinforced foams. In terms of strength, the Type 1 foam had compressive and tensile strengths equal to 82% and 70% of the Type 2 core, respectively. However, the stiffness of the Type 1 foam was only equal to 42% of the Type 2 foam in compression and 49% in tension. This lower stiffness performance will result in decreased efficiency of the sandwich panel. Nonetheless, the Type 1 plain foam outperformed the Type 4 stitched foam in terms of both strength and stiffness, and the plain foam offers a much more simplified manufacturing process compared to the stitched foam.

Based on their relative performances, the research team selected core Types 1, 2 and 3 for the next phase of testing. The Type 2 reinforced foam outperformed the other three materials in terms of both strength and, in particular, stiffness, with moduli values over twice that of the next performing material. The Type 1 plain foam was selected because it outperformed the Type 4 reinforced foam and offers a much more simplified manufacturing process. The Type 3 core was also chosen to move forward because the true value of this material is its use as a mold for the FRP layers that form a truss-type panel.

3. SMALL-SCALE PANEL TESTING

The next phase of the research study involved manufacturing and testing small-scale panels constructed with the Type 1 (PU RIGID), Type 2 (WEB-CORE), and Type 3 (PRISMA FOAM) cores selected from the component testing. This next phase focused on the flexural behavior of the specimens in terms of strength, stiffness, overall behavior, and modes of failure. The purpose of this phase of the research was to determine which FRP/PU foam combination to advance to the mid-scale panel testing program.

3.1. SANDWICH PANEL MANUFACTURING

The sandwich panels were manufactured using a process known as vacuum-assisted, resin transfer molding (VARTM). This process, shown schematically in Fig. 3.1, involves hand layup of the foam core and woven, biaxial, E-glass fabric followed by infusion of the resin through a vacuum-assisted process. Applying the vacuum also results in the outer atmospheric pressure compressing the fiber layers tight against the core. High permeability layers (distribution media) placed over the fibers reduces infusion time, and a standard peel ply prevents the resin from adhering to the vacuum bag. All specimens were post-cured for 1 hour at 160ºF and for 4 hours at 180ºF in a walk-in oven.

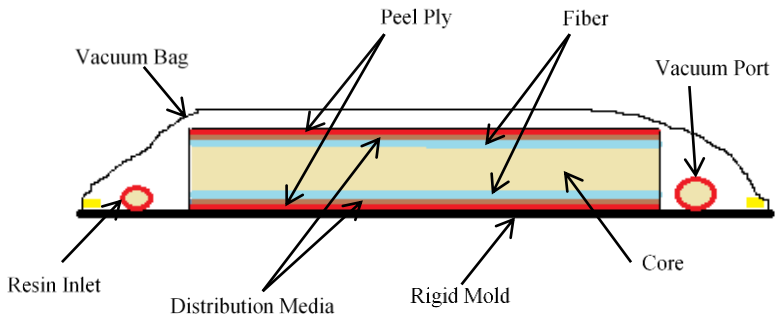

Figure 3.1: Schematic of VARTM Composite Manufacturing Process

For each of the three core types, the basic components were identical. The facesheets consisted of three plies of 0°/90°, biaxial, E-glass, plain weave, woven fabric (WR18/3010) manufactured by Owens Corning. The resin, manufactured by Bayer MaterialScience, was a two-part, thermoset polyurethane resin system with excellent thermal stability, good mechanical properties, and fewer environmental issues than vinyl ester or polyester resins. The differences between the sandwich panels involved the web reinforcement used in the Type 2 and Type 3 panels. For the Type 2 panels, the gridwork of web reinforcement consisted of a single ply of 0°/90°, biaxial, E-glass, plain weave, woven fabric. For the Type 3 panels, the diagonal web reinforcement, manufactured by VectorPly, consisted of two plies of +45°/-45°, double bias, E-glass, stitch bonded fabric (E-BXM1715) that was integrated with the facesheets.

3.2. THREE POINT FLEXURAL TESTING

In this test, relatively short beams were subjected to three-point bending in an effort to increase shear stresses and their impact on deformations while lessening the effects of bending moments and their associated stresses. Initially, the goal was to avoid local failure and cause shear failure in the core by using flat bars and rubber pads at the support and loading points in a an effort to decrease the effect of high pressure concentrations at these locations. However, it became evident that despite these efforts, the compressive stiffness and strength of the core materials in the flatwise direction was not high enough for shear failure to supersede localized failure under the concentrated load or local indentation. Nevertheless, these tests revealed conditions under which the different core types will fail locally, and they provided the load versus displacement response needed to estimate the flexural stiffness of the core materials. The procedure used for these tests, and the experimental results along with a short discussion of the results for each core type is presented in the following sections.

The test specimens had a nominal cross section of 3 in. x 2.25 in. However, the actual specimen depths varied slightly from the 2.25 in. nominal value for the different core types due to the standard foam sizes available. To compensate, as discussed later, the results were normalized in order to directly compare the performance of the three FRP/PU foam panel types.

3.2.1. Test Methodology. The three point tests were based on ASTM C393/C393M: Standard Test Method for Core Shear Properties of Sandwich Constructions by Beam Flexure (ASTM, 2011). This standard served as a guideline for the tests, however not all the details of the standard were strictly followed. Therefore, a detailed description of the specimen preparation, the test setup, and the test procedure is provided.

3.2.1.1. Specimen Preparation. The specimens for this experiment were produced by cutting small beams from a larger panel segment using a fine toothed band saw. The specimens were partitioned at random using a ruler and a square. After they were sectioned, a coarse grit belt sander was used to lightly sand away any imperfections and ensure the sides were adequately straight and orthogonal to the adjacent sides. Four specimens were cut for the Type 1 and Type 2 core configurations, and one specimen was cut for the Type 3 core configuration due to limited material availability for this sandwich panel type. A photograph of each specimen type is shown in Figs. 3.2, 3.3, and 3.4. These specimens were approximately 3 in. wide by 8 in. long, and had a depth equal to that of the associated sandwich construction (nominally 2.25 in.).

After the specimens were cut to size, strain gauges were applied to the center of the bottom facesheet of each specimen. The strain gauges were three-wire, 350 ohm, general purpose strain gauges that had a gauge length of 0.125 in. and a usable strain range of ± 3%. Specimen preparation for the strain gauge installation included light sanding of the facesheet followed by application of a two-part epoxy (AE-10) to provide a smooth surface for adhering the gauge. Once the epoxy cured, it was lightly sanded and cleaned with an adhesive catalyst. The gauge was then placed on the facesheet and adhered to the specimen with strain gauge adhesive (M-Bond 200). Peel ply tape and a slight amount of pressure was applied for 60 seconds to hold the strain gauge in place as the adhesive cured. The peel ply tape was removed and the lead wires were secured to the specimen to prevent any damage prior to testing.

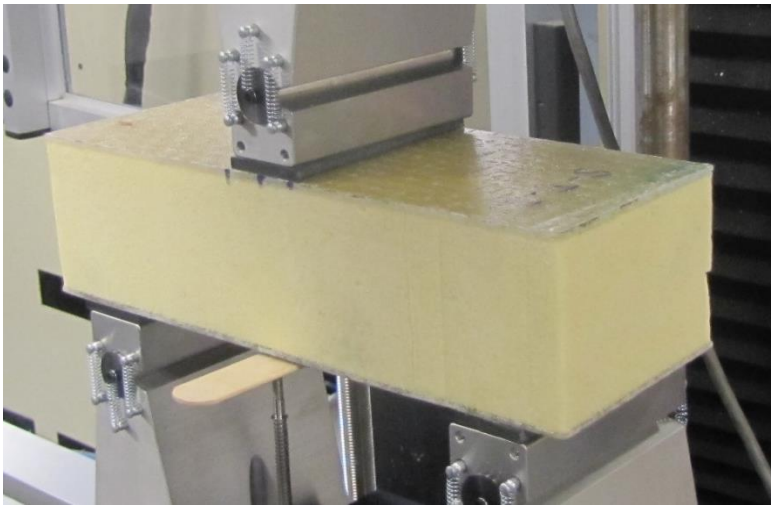

Figure 3.2: Type 1 (PU RIGID) Sandwich Panel Specimen

Figure 3.3: Type 2 (WEB-CORE) Sandwich Panel Specimen

3.2.1.2. Test Setup. The test setup used for the three point flexural experiment consisted of the Long Beam Flexure Test Fixture, manufactured by Wyoming Test Fixtures (Model No. CU-LF), modified and installed in an Instron 4469 Universal Testing Machine (UTM). For the three point loading tests, the supports were set up for a beam span of 6 in. and a single loading point positioned at mid-span. The loading pads at the supports and loading point were 1 in. wide flat bars that were free to pivot, and they were considered simple supports that imposed no concentrated moment on the specimen. Rubber pads with a Shore A hardness of 60 were inserted at the supports and loading point to help reduce and distribute the pressure concentrations under the loads. Linear potentiometers were mounted to the fixture to measure the deflection of the bottom face at mid-span, and since one was position on each side of the specimen, the average of

the two was recorded. The linear potentiometers had a metal spring assisted shaft with a 2 in. stroke length. A linear variable differential transducer (LVDT) with a spring assisted metal shaft and a 4 in. stroke length was mounted to the frame of the Instron 4469 UTM to measure the displacement of the crosshead. The load was measured through the 9 pin output of the Instron 4469 UTM. A photograph of the setup just prior to testing is presented in Fig. 3.5.

Figure 3.4: Type 3 (PRISMA FOAM) Sandwich Panel Specimen

Figure 3.5: Three Point Flexural Test Setup

3.2.1.3. Test Procedure. Specimens for the three point flexural tests were tested on multiple days under similar temperature and humidity conditions. Before testing, the width of each specimen was measured using digital or dial calipers to the nearest 0.001 in. A minimum of three measurements were taken and the average was reported. The height and facing thickness of

the specimens was measured from the original manufactured beams before partitioning any specimens. A minimum of 10 measurements were taken for each and the average was reported.

The supports were set to a span length of 6 in. and the loading point was set to mid-span using the markings on the test fixture and a ruler to verify the positions. The fixture was leveled, and the LVDT and linear potentiometers were then aligned parallel to the loading direction using a bubble level. The specimen was then placed into the fixture and the rubber pads were inserted at the support and loading points. The specimen was positioned with the strain gauge at mid-span using a ruler, and the overhang of the specimen was approximately 1 in. from the center of the support to the end of the specimen. Next, the crosshead was lowered until a small preload of 0-20 lb. was applied to the specimen. The deflection and strain readings were then zeroed. A video camera was used to videotape the tests for further review after the tests were complete. The method of loading the specimens involved displacement control at a rate of 0.1 in./min. The load, crosshead displacement, bottom face deflection at mid-span, and strain in the bottom facing at mid-span were recorded at a rate of 1-2 Hz. Finally, the test was ended once the crosshead displacement reached 30-70% of the depth of the specimen, which took 15-25 min. After failure, the specimen was promptly unloaded.

3.2.2. Test Results. For the three point flexural tests, the specimens displayed linear behavior prior to failure. However, as with the flatwise testing, there were false nonlinearities and discrepancies in the initial readings of the tests. The nonlinearities were caused by small gaps in the system and compression of the rubber pads. Also, at the beginning of test, the displacement was set to zero at a non-zero load. Both of these discrepancies lead to a false offset in the recorded data. This was corrected using the same methodology presented in Chapter 2, Section 2.2.2. Regression analysis was performed on multiple ranges of the data and the range with the highest correlation factor was chosen to be representative of the linear region. The genuine part of each curve was then offset by the x-axis intercept of the regression equation. Then, the false data at the beginning of each curve was replaced by a projection of the linear region that intersected the origin. This is graphically the same approach as shown in Fig. 2.6 in Chapter 2.

In the following sections, the results for the three point flexural testing are presented for each of the different sandwich constructions and their respective core types. The results and the observations made during the tests provided insights into the behavior of each sandwich construction and the reasons why they failed, and it allows for a qualitative discussion of the results as presented in Section 3.2.3. A more detailed analysis of the results is presented in Chapter 4 along with a comparison of the different core types based on stiffness and strength.

3.2.2.1. Results for Type 1. For the three point flexural tests, four specimens were prepared and successfully tested for the Type 1 sandwich construction. The false nonlinearities and offset were corrected for each of the data curves using the procedures mentioned previously. The bottom face deflection and the strain in the bottom facing at mid-span were then plotted as the dependent variable versus the load in Figs. 3.6 and 3.7, respectively. From these curves, several observations were made about the material behavior, and based on the observations made during the tests, a failure mode for the Type 1 specimens was determined.

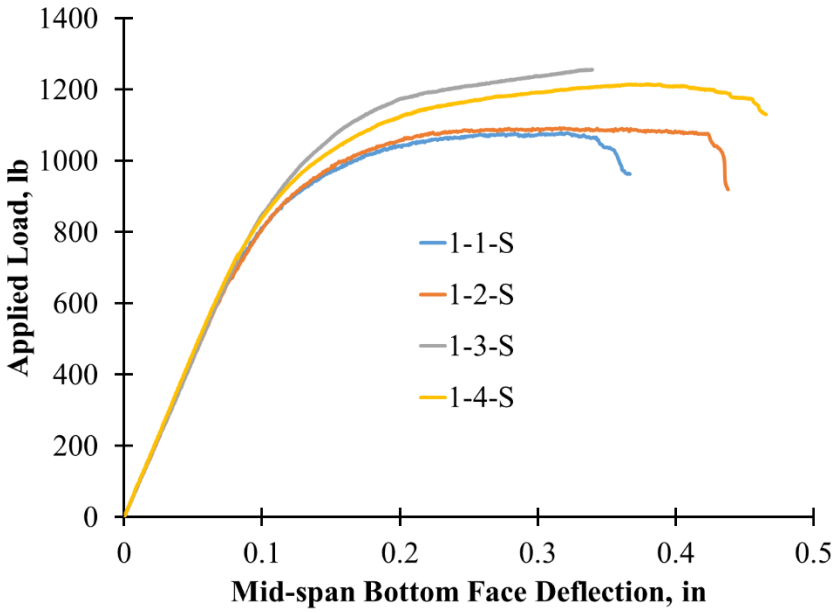

Figure 3.6: Applied Load vs. Mid-Span Bottom Face Deflection for Type 1

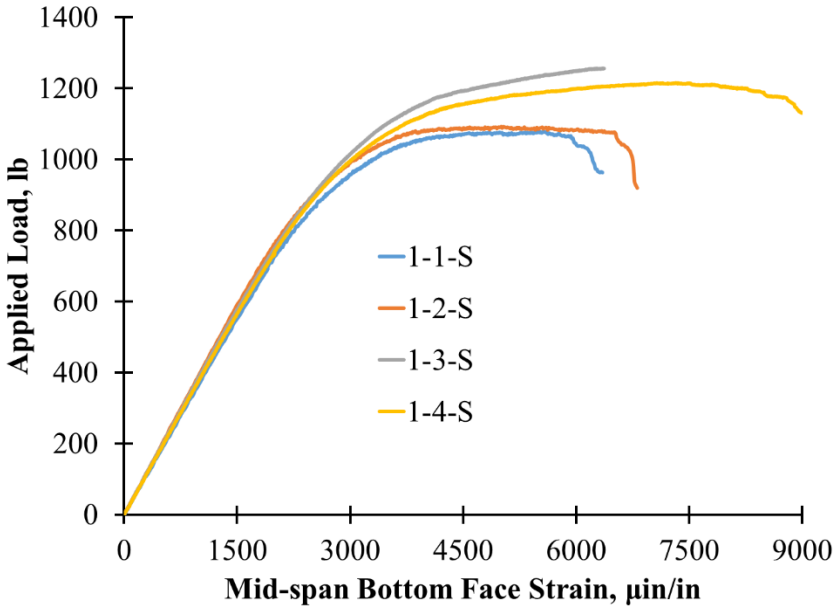

Figure 3.7: Applied Load vs. Mid-Span Bottom Face Strain for Type 1

All of the curves have a similar shape with two distinct regions. In the first region, the response was very linear, and this behavior can be attributed to the constituent materials. The sandwich construction consisted of a Type 1 core of rigid polyurethane foam with glass fiber

reinforced polyurethane facings. The initial response of the rigid polyurethane foam is linear elastic, which is evident in the results of the flatwise compression and tension tests detailed in the previous chapter. As for the glass reinforced polyurethane facings, polyurethane is not typically linear elastic but can often be approximated as linear elastic, and coupled with glass fibers, which are generally considered linear elastic, the composite has a behavior that is relatively linear elastic. As a result, the initial response in the first region is essentially linear elastic.

In the second region, the response became nonlinear, and this behavior is due to the crushable nature of the rigid polyurethane foam core and its relatively low stiffness. In the flatwise compression tests, the rigid polyurethane foam had nonlinear response that was characterized by an apparent yield point at its usable strength, at which point the foam could not carry any additional stress. During the three point flexural tests, the stress concentrations under the load became larger than the usable compressive strength in the foam, which lead to yielding of the foam under the load. Once the foam began to yield, the top facing had very little support, and the lack of stability coupled with the compressive stress in the top facing due to flexural stresses caused a buckle wave or wrinkle to form under the load. The buckle wave that formed had a wavelength proportional to the width of the loading bar. At this point, the top face began to deflect much more than the bottom face as foam under the load started to crush, which resulted in a permanent indentation in the top of the specimen. This failure mode is often referred to as local indentation. Then, the applied load continued to increase, but the rate at which it increased began to gradually decrease until it peaked, at which point a large portion of the foam under the load had yielded and the top facing had wrinkled excessively under the load. The load then began to decrease, and excessive deflection of the top facing eventually led to high stress concentrations under the edges of the loading bar that caused a facture in the facing and the core material underneath one edge of the loading bar. From this point on, the load began to decrease in an erratic stepped manor.

This type of failure occurred in Specimens 1-1-S, 1-2-S, and 1-4-S. As for Specimen 1-3-S, local indentation caused nonlinearity in the response, but before excessive local indentation could cause ultimate failure, a sudden facture occurred in the foam, which resulted in an abrupt drop in the load. The fracture appeared to originate in the foam near the top facing just under the load and propagated diagonally though the core until it reached the bottom facing, where it propagated through the foam along the interface between the core and the bottom facing, at which point a large portion of the core separated from the bottom facing. However, the failure occurred so quickly that the exact location where the fracture started is uncertain. This type of fracture is indicative of failure in the foam core due to shear stresses, but it is not entirely known why it only occurred in one of the specimens. One possibility could have been irregularities in the facing as the thickness of Specimen 1-3-S was not as uniform as the other specimens. The thickness of the top facing could have been larger under the point load than the average thickness, causing the facing to achieve a higher resistance to excessive local indentation.

In summary, the initial failure mode of all the Type 1 specimens was local indentation. The primary ultimate failure mode was excessive local indentation leading to a fracturing of the facing and core due to high stress concentrations at the edges of the loading bar. However, one

specimen ultimately failed due to shear stresses in the core. A photograph of the initial crushing of the foam where the response became nonlinear is shown in Fig. 3.8. Also, photographs of the ultimate failure due to excessive wrinkling of the facing, as well as shear failure in the foam, are shown in Figs. 3.9 and 3.10, respectively.

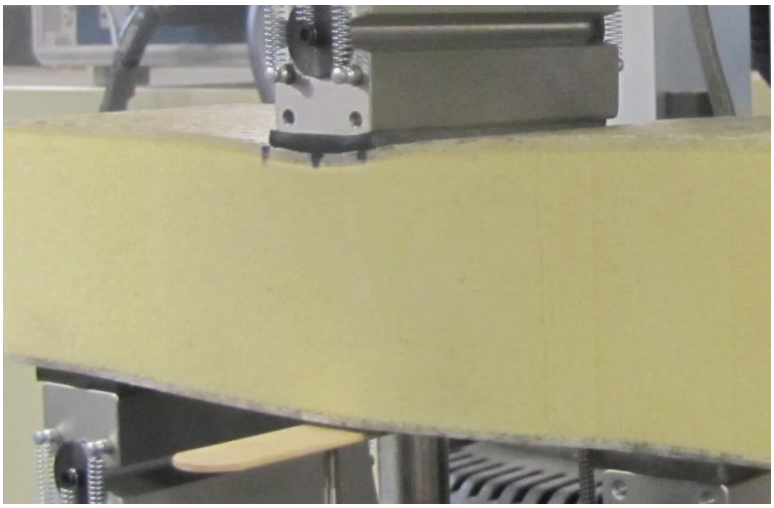

Figure 3.8: Initial Failure Due to Local Indentation for Type 1

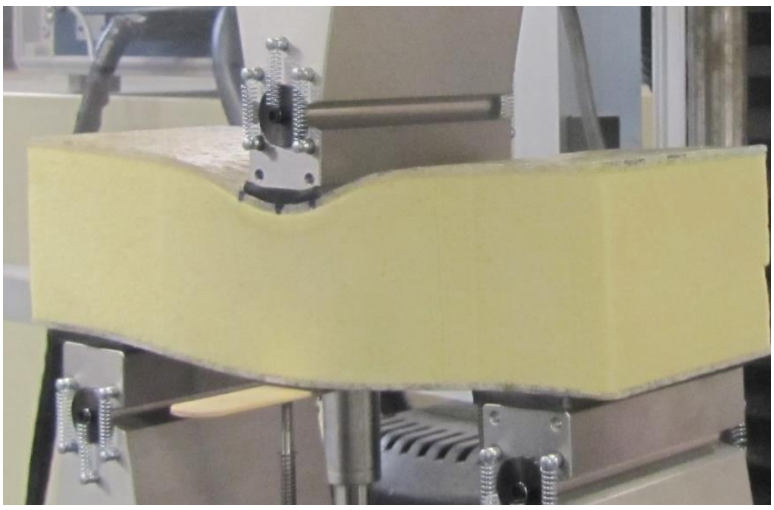

Figure 3.9: Ultimate Failure Due to Excessive Local Indentation for Type 1

3.2.2.2. Results for Type 2. For the three point flexural tests, four specimens were prepared and three were successfully tested for the Type 2 sandwich construction. Unfortunately, during testing, the data for the fourth specimen was lost due to a programing error, therefore the results for three of the specimens will be presented. Again, the false nonlinearities and offset were corrected for each of the data curves, and the corrected data was plotted. The bottom face

deflection and the strain in the bottom facing at mid-span were plotted as the dependent variable versus the load in Figs. 3.11 and 3.12, respectively. From these curves, several observations were made about the material behavior, and based on the observations made during the tests, a failure mode for the Type 2 specimens was determined.

Figure 3.10: Ultimate Failure Due to Shear Failure of the Core Material for Type 1

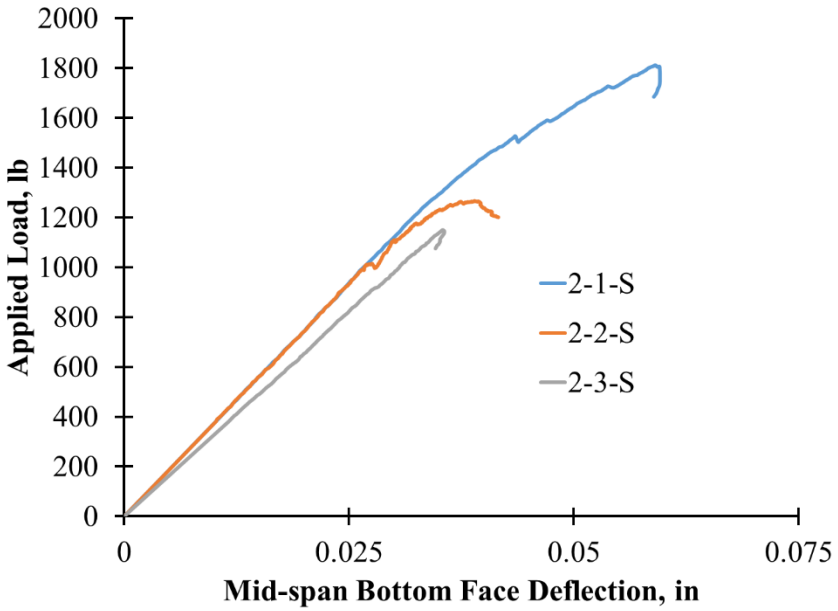

Figure 3.11: Applied Load vs. Mid-Span Bottom Face Deflection for Type 2

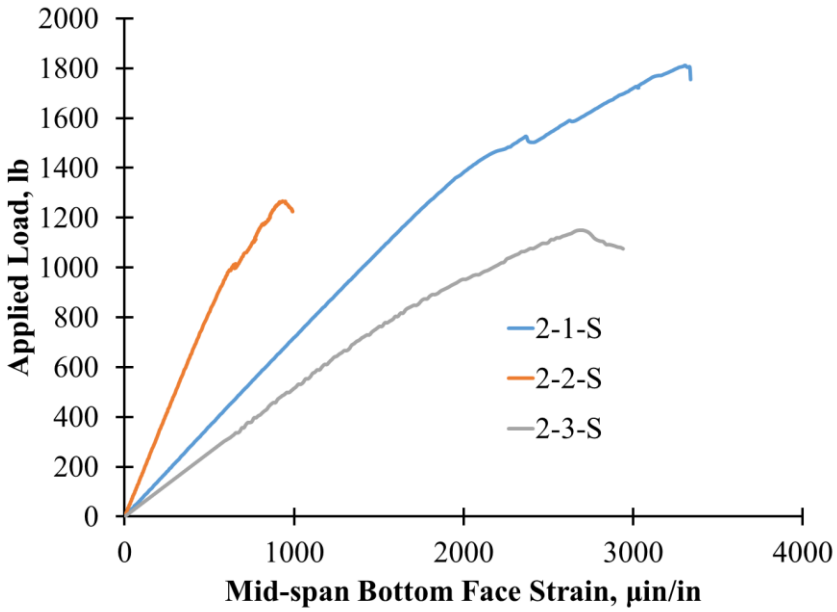

Figure 3.12: Applied Load vs. Mid-Span Bottom Face Strain for Type 2

Similar to the Type 1 specimens, all of the curves for the Type 2 specimens had a similar shape with two distinct regions. Initially, the response was linear, which can be attributed to the materials used in the construction. The sandwich construction consisted of a Type 2 core of flexible polyurethane foam with an FRP gridwork of web reinforcing, and the facings were made of the same glass fiber reinforced polyurethane used in the Type 1 construction. The results of the flatwise compression and tension tests presented in the previous chapter indicated that the Type 2 core can exhibit an apparent linear elastic response. Then, given the facings are the same as the Type 1 construction, the initial response is essentially linear elastic.

Inevitably, the response became nonlinear for the same reasons that the flatwise compression specimens exhibited nonlinear behavior. The reinforcing webs of the core supported the majority of the force from the loading point, and the flexible foam provides stability, but the reinforcing webs are very thin and hence prone to buckling. In the three point flexural specimens, the stress concentrations under the loading point caused the reinforcing webs under the load to buckle. At which point a wrinkle formed in the top facing under the load due to a lack of support from the core. As with the Type 1 specimens, the wrinkle wavelength was proportional to the width of the loading bar. Again, this failure mode is typically labeled as local indentation. The load continued to increase, but the rate of increase began to diminish as the top face began to deflect significantly more than the bottom face. At one point, the load peaked when the reinforcing webs beneath the load point began to fracture due to excessive buckling, and as a result, the top facing began to wrinkle excessively. Eventually, excessive wrinkling of the facing led to buckling and fracturing of the neighboring reinforcing webs that were not directly beneath the load, and fractures also formed in the top facing due to stress concentrations at the edges of the loading bar and at nearby transverse reinforcing webs. This response caused the load to

decrease erratically in a stepped manor as the loading bar crushed the core material and fractured the facings.

In conclusion, the initial failure mode for all three specimens was local indentation directly beneath the load initiated by buckling of the reinforcing webs. Then, the ultimate failure mode for each of the specimens was excessive local indentation caused by fracturing of the reinforcing webs. A photograph of the damage to the specimen when the response became nonlinear is presented in Fig. 3.13. A photograph of the damage at ultimate failure when the load reached its peak value is presented in Fig. 3.14.

Figure 3.13: Initial Failure Due to Buckling of the Reinforcing Webs and Local Indentation for Type 2

Figure 3.14: Ultimate Failure Due to Fracturing of Reinforcing Webs and Excessive Local Indentation for Type 2

3.2.2.3. Results for Type 3. For the three point flexural tests, one specimen was prepared and successfully tested for the Type 3 sandwich construction. Unfortunately, the foam blocks needed to manufacture the Type 3 panel for the small scale flexural tests were difficult to obtain in the size that was needed, and only one representative small scale beam could be manufactured in the time allowed for this stage of the project. Therefore, very few specimens could be produced from the single beam. After the test, the initial false nonlinearities and offset were corrected for each of the data curves, and the corrected data was plotted. The bottom face deflection and the strain in the bottom facing at mid-span were plotted as the dependent variable versus the load in Figs. 3.15 and 3.16, respectively. From these curves, several observations were made about the material behavior, and based on the observations made during the tests, a failure mode for the Type 3 specimens was determined.

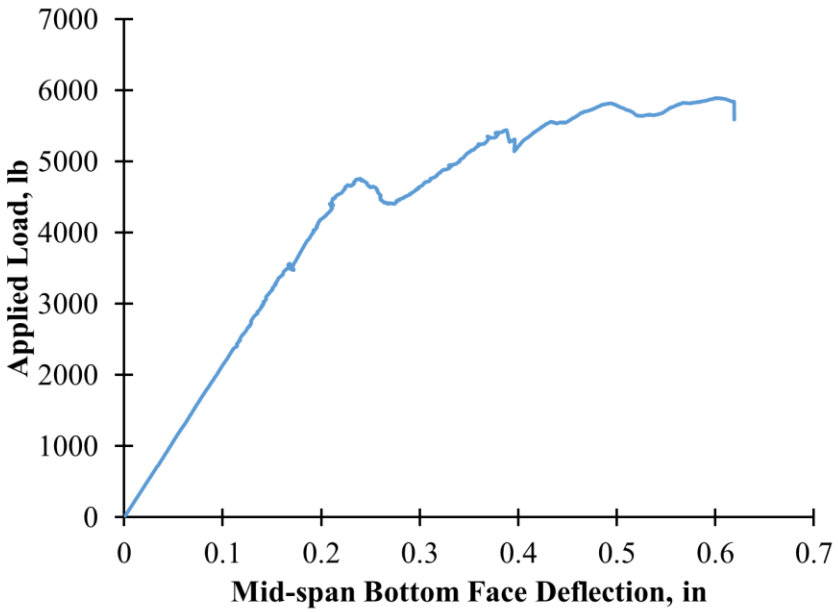

Figure 3.15: Applied Load vs. Mid-Span Bottom Face Deflection for Type 3

The curve for the Type 3 specimen had a similar shape to that for the Type 1 and Type 2 specimens, with two distinct regions. The initial response was linear, which, as with the other sandwich constructions, can be attributed to the materials used in the manufacture of the panel. The sandwich construction consisted of a Type 3 core of flexible polyurethane foam blocks in a trapezoidal shape that provided a mold for the truss-type panel. The diagonal web reinforcement was integrated with the facesheets, which were identical to the facesheets on the other two sandwich constructions. The flexible foam contributes very little to the behavior of the sandwich construction in the longitudinal direction, but it does provide extra stability to the facings and webs. In comparison to the facing layers, the diagonal web material differs with respect to the orientation of the fibers (±45° vs. ±90°), but overall the composite behavior should still be

generally linear elastic. Therefore, the apparent linear elastic response at the beginning of the test was as expected.

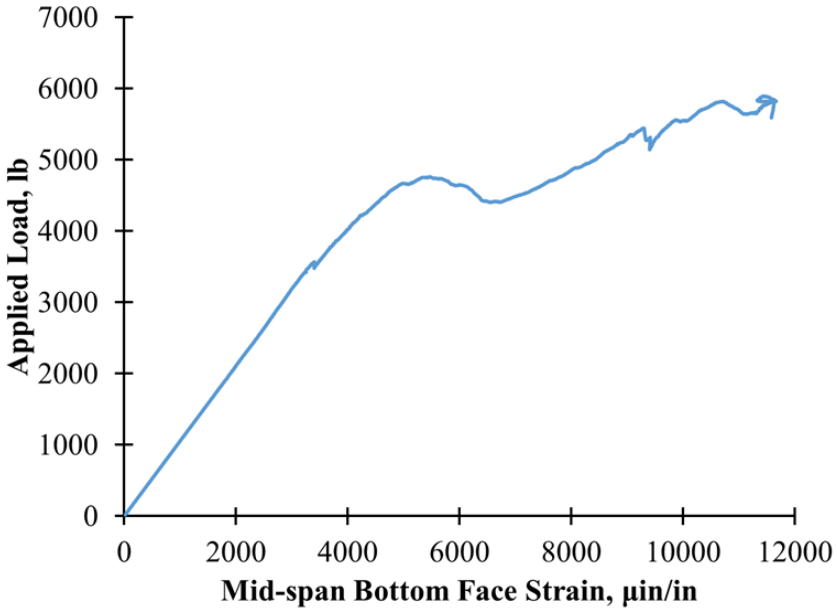

Figure 3.16: Applied Load vs. Mid-Span Bottom Face Strain for Type 3

The response then became nonlinear as the specimen began to show signs of damage. The first sign of damage was delamination (splitting) between the shear layers on one corner of the specimen near the bottom facing just above one of the supports, which caused a small but sudden drop in the load. Then, the load started to increase at nearly the same rate as the initial linear region. Eventually, a wrinkle in the top facing occurred just under the load point due to stress concentrations with a wavelength proportional to the width of the loading bar, which is indicative of local indentation failure, and the rate of increase in the load began to drop. At this point, the top face of the specimen began to deflect significantly more than the bottom face. The shear layers under the load point eventually began to deform and fracture between layers as the load peaked and then started to decrease in an erratic stepped manor. After significant damage, the shear layers began to bow outwards, which locally stabilized the specimen temporarily. This led to a slow increase in the load. However, the stress concentrations under the load eventually started to crush the deformed shear layers again, and as the layers gained and lost stability, the load continued to increase in general but in a very erratic fashion. At the end of the test, the load was still tending to increase, but the test was stopped as the top face had deflected more than half of the sandwich depth. Meanwhile, as local damage under the load kept intensifying, the initial split at the corner of the specimen continued to open and progressively increase in size. By the end the test, the split had caused significant unsymmetrical deformation at the end of the specimen where it occurred. The effects of this deformation are not immediately evident, but it is

certain that it significantly affected the response of the specimen by likely causing torsional forces in the specimen.

Summarizing the test, the initial failure mode involved splitting between the shear layers just above one of the supports, and the shear layer separation that formed became progressively larger throughout the remainder of the test, which likely had a significant effect on the response of the specimen. The ultimate failure mode was excessive local indentation, which led to crushing of the shear layers under the load point. A photograph of the splitting between shear layers at the beginning of the test that caused some nonlinearity in the response is shown in Fig. 3.17. The localized damage under the load point that caused erratic jumps in the applied load at the end of the test is shown in Fig. 3.18. Also, the severity of the unsymmetrical deformation caused by splitting of the shear layers by the end of the test is shown in Fig. 3.19.

Figure 3.17: Initial Failure Due to Splitting Between Shear Layers for Type 3

3.2.3. Discussion of Test Results. Based on the results of the three point flexural testing, several useful observations can be made about the three different core types and their associated sandwich constructions. All three panel types displayed some similar behaviors. The initial response of each of the constructions was essentially linear elastic. All three alternatives also showed nonlinear response prior to failure due to local strength and stability issues under the concentrated load. It was also apparent during that the test that, based on the displacement of the crosshead, the top face deflected noticeably more than the bottom face even at loads in the linear response range. These observations are consistent with the short span length and relatively low stiffness and strength of the core materials.

For the Type 1 specimens, the behavior of the rigid polyurethane foam governed the behavior of the specimens. The foam has a relatively low compressive strength and stiffness compared to the facing material, which led to local indentation failure. This mechanism was prevalent in all of the specimens and led to nonlinearity in the response. It also governed the

ultimate failure of all but one of the specimens. Specimen 1-3-S failed due to excessive shear stresses in the core at the ultimate load. This shear failure is inconsistent with the majority of Type 1 specimens, but it could have been influenced by inconsistencies in the thickness of the top facing in the specimen. However, overall, the Type 1 specimens showed very little variability with regard to the general deflection and strain response. This consistency in response can be attributed to the consistency in specimen construction, both dimensionally and materially.

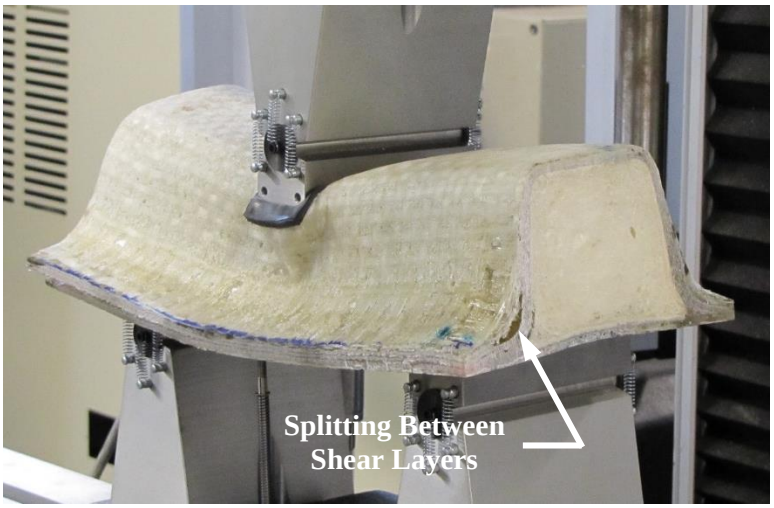

Figure 3.18: Ultimate Failure Due to Excessive Local Indentation and Splitting Between Shear Layers for Type 3

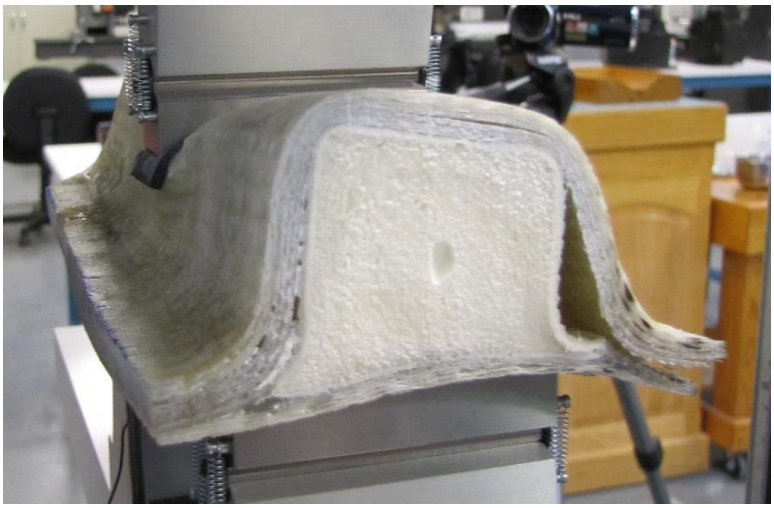

Figure 3.19: Unsymmetrical Deformation Caused by Splitting Between Shear Layers for Type 3

As for the Type 2 specimens, the behavior was governed by the reinforcing webs that were very thin relative to their width. Buckling of these webs under the load led to nonlinearity in the response, and eventually led to instability in the top facing, which led to local indention failure. This response was apparent in all of the specimens, and the mechanism eventually led to ultimate failure in all of the specimens due to fracturing of the reinforcing webs and local indentation. The variation in the results for the Type 2 specimens also highlights the importance of the distribution of the reinforcing webs. The width of all of the specimens was nearly the same, and the number and location of the longitudinal reinforcing webs was consistent between the three specimens as well. On the other hand, the distribution of the transverse reinforcing webs was inconsistent. The results seem to indicate that this distribution effected the deflection and strain response measured in the specimens. This is consistent with the fact that the first sign of failure was buckling in the transverse reinforcing webs.

The Type 3 specimen failed initially due to splitting between the shear layers at one corner or the specimen. This caused a small but noticeable drop in the load, but afterwards the load continued to increase at a rate comparable to the behavior prior to the fracture. The ultimate failure of the specimen was caused by local indentation, which eventually led to crushing of the shear layers beneath the load. It was noted that the fiber layers in the specimen were not completely saturated with polyurethane resin, and there were noticeable dislocations between the fibers and the foam at the ends of the specimen. Another troubling result was noticed when correcting the data. The slope of the load versus deflection curve was significantly less than what was expected based on the geometric stiffness of the fiber reinforce polyurethane. This indicates that the specimen most likely performed poorly due to manufacturing defects between the fiber layers that were not present in the specimens for the other two sandwich constructions, and it likely would have performed much better if the resin had fully saturated the fibers.

These observations provide significant insights into the behavior of the three sandwich constructions when used in short beams. The results of these tests show that localized effects under concentrated loads are the primary factor influencing the behavior of each of these panel types, resulting in failure in the specimens and the occurrence of nonlinear behavior prior to failure. The low strength and stiffness of the rigid foam core seems to dictate the behavior of the Type 1 sandwich construction. Furthermore, the instability of the thin reinforcing webs as well as the distribution of the webs seems to dictate the behavior of the Type 2 sandwich construction. As for the Type 3 sandwich construction, it is evident that the strength and quality of the bond between the fiber layers is important, as well as the stability of the top facing and the compressive strength of the diagonal webs. These tests also bring to light the ease of manufacturing of each of the different sandwich constructions. The excellent quality and results for the Type 1 and 2 specimens show that the manufacturing process for these two types has relatively fewer complications. The quality and results for the Type 3 specimen indicate that there are significantly more complications involved in the manufacturing process of the third sandwich construction. This result is consistent with the complexity of the sandwich construction for the Type 3 specimen, which requires significantly more steps in the manufacturing process. The resin infusion process is also more difficult for the Type 3 specimens. As the manufacturing

processes are performed more often and processes become more refined, these difficulties will become less influential on the quality and reproducibility of the Type 3 construction.

3.3. FOUR POINT FLEXURAL TESTING

The four point flexural experiments were initially intended to induce flexural failure in the facings by increasing the span length and the effects of bending moments while lessening the effects of shear forces. However, the high strength of the facing materials proved to be large enough that causing this type of failure would be difficult. Also, concerns over the stability of the thin facings for the Type 1 and 2 specimens indicated that local buckling in the facings due to compressive bending stresses would likely occur before the strength of the facings was reached. Therefore, the focus of the tests was directed towards the shear strength of the core materials. Using the results of the three point tests, the four point flexural tests were modified to try to induce shear failure in the specimens. The support span was increased, which increased the effects of bending stresses, and the loading bars were increased in width to reduce the localized effects near the loading and support points. These changes proved to be somewhat effective, but did not completely produce the desired results. Initial failure of the specimens was again influenced by localized effects under the concentrated load for some of the specimens, then for other specimens, initial failure was influenced by local buckling of the top facing between the two load points. However, the majority of the specimens ultimately failed due to reasons other than localized effects under the load points. Several of the specimens ultimately failed due to shear stresses in the core material, and a couple specimens had compressive failure in the top facing at the peak load. Nevertheless, several observations were made about the strength and behavior the different core types, and the load versus displacement response needed to estimate the flexural stiffness of the core materials was obtained. The procedure used for these tests, and the experimental results along with a short discussion of the results for each core type is presented in the following sections.

3.3.1. Test Methodology. The four point tests were based on ASTM C393/C393M: Standard Test Method for Core Shear Properties of Sandwich Constructions by Beam Flexure (ASTM, 2011). This standard served as a guideline for the tests, however not all the details of the standard were strictly followed. Therefore, a detailed description of the specimen preparation, the test setup, and the test procedure is provided.

3.3.1.1. Specimen Preparation. As with the three point tests, the specimens for this experiment were produced by cutting small beams from a larger panel segment using a fine toothed band saw. The specimens were partitioned using the same procedures as with the three point tests, and a coarse grit belt sander was again used to lightly sand away any imperfections and ensure the sides were adequately straight and orthogonal to the adjacent sides. Three specimens were cut for the Type 1 and Type 2 core configurations, and one specimen was cut for the Type 3 core configuration due to limited material availability for this sandwich panel type. A photograph of each core type is shown in Figs. 3.20, 3.21, and 3.22. These specimens were approximately 3.5-4.5 in. wide by 26 in. long, and had a depth equal to that of the associated sandwich construction (nominally 2.25 in.).

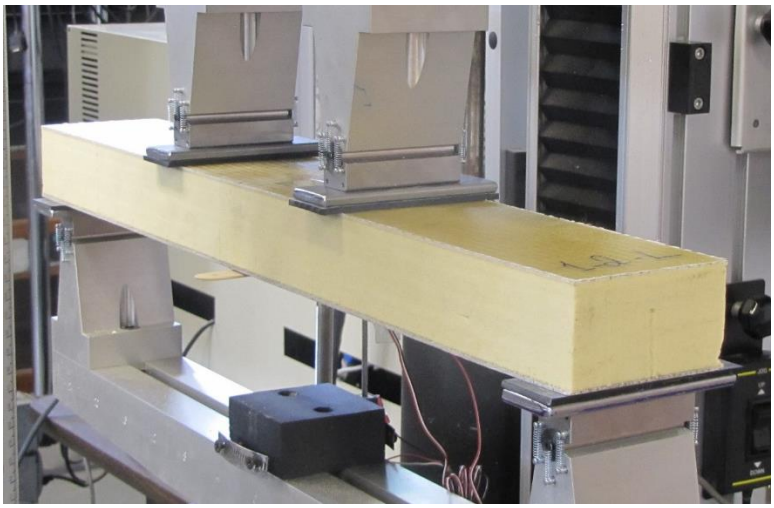

Figure 3.20: Type 1 (PU RIGID) Sandwich Panel Specimen

Figure 3.21: Type 2 (WEB-CORE) Sandwich Panel Specimen

Once the specimens were cut to the appropriate size, strain gauges were applied to the center of the top and bottom facesheet of each specimen. The strain gages were three-wire, 350 ohm, general purpose strain gauges that had a gauge length of 0.125 in. and usable strain range of ± 3%. The gauges were applied using the same procedure as that used for the three point test specimens. Preparation for the strain gauge installation included light sanding of the facesheets followed by application of a two-part epoxy (AE-10) to provide a smooth surface for adhering the gauge. Once the epoxy cured, it was lightly sanded and cleaned with an adhesive catalyst. The gauge was then placed on the facesheet and adhered to the specimen with strain gauge adhesive (M-Bond 200). Peel ply tape and a slight amount of pressure was applied for 60

seconds to hold the strain gauge in place as the adhesive cured. The peel ply tape was removed and the lead wires were secured to the specimen to prevent any damage prior to testing.

Figure 3.22: Type 3 (PRISMA FOAM) Sandwich Panel Specimen

3.3.1.2. Test Setup. The test setup used for the four point flexural experiment consisted of the same Long Beam Flexure Test Fixture, manufactured by Wyoming Test Fixtures (Model No. CU-LF), modified and installed in an Instron 4469 Universal Testing Machine (UTM). For the four point loading tests, the supports were set up for a beam span of 24 in. and the two loading points were positioned at the third points of the span. The loading pads at the supports and loading points were increased to 1.5 in. in width by placing ¼-in.-thick plates between the stock loading bars and the specimen. Rubber pads with a Shore A hardness of 60 were inserted at the supports and loading point to help reduce and distribute the pressure concentrations under the loads. Linear potentiometers were mounted to the fixture to measure the deflection of the bottom face at mid-span, and since one was position on each side of the specimen, the average of the two was recorded. The linear potentiometers had a metal spring assisted shaft with a 2 in. stroke length. A linear variable differential transducer (LVDT) with a spring assisted metal shaft and a 4 in. stroke length was mounted to the frame of the Instron 4469 UTM to measure the displacement of the crosshead. The load was measured through the 9 pin output of the Instron 4469 UTM. A photograph of the setup just prior to testing is presented in Fig. 3.23.

3.2.1.3. Test Procedure. Specimens for the three point flexural tests were tested on multiple days under similar temperature and humidity conditions and followed the same general procedure as that used for the three point flexural tests. Before testing, the width of each specimen was measured using digital or dial calipers to the nearest 0.001 in. A minimum of three measurements were taken and the average was reported. The height and facing thickness of the specimens was measured from the original manufactured beams before partitioning any specimens. A minimum of 10 measurements were taken for each and the average was reported.

Figure 3.23: Four Point Flexural Test Setup

The supports were set to a span length of 24 in. and the loading points were moved the third points of the span using the machined markings on the test fixture. The fixture was leveled, and the LVDT and linear potentiometers were then aligned parallel to the loading direction using a bubble level. The specimen was then placed into the fixture and the rubber pads along with the plates used to widen the loading area were inserted at the support and loading points. The specimen was positioned with the strain gauges at mid-span using a ruler, and the overhang of the specimen was approximately 1 in. from the center of the support to the end of the specimen. Next, the crosshead was lowered until a small preload of 0-20 lb. was applied to the specimen. The deflection and strain readings were then zeroed. A video camera was used to videotape the tests for further review after the tests were complete. The method of loading the specimens involved displacement control at a rate of 0.1 in./min. The load, the crosshead displacement, bottom face deflection at mid-span, and strain in the bottom and top facings at mid-span were recorded at a rate of 1-2 Hz. Finally, the test was ended once the crosshead displacement reached 30-60% of the depth of the specimen, which took 10-20 min with the exception of specimen 1-2-L, which was stopped at close to 160% of the specimen depth and took nearly 50 min. After failure, the specimen was promptly unloaded.

3.3.2. Test Results. Similar to the three point test specimens, the four point test specimens displayed linear behavior prior to failure. However, as with the three point testing, the same false nonlinearities and discrepancies appeared in the initial readings of the four point tests. Again, the nonlinearity was caused by gaps between the loading bars and the specimen as well as the compression of the rubber pads. Also, a false offset was created when the displacements and strains were zeroed at a non-zero load. This was corrected using the same methodology that is presented in Chapter 2, Section 2.2.2. Regression analysis of the linear portion of the curve was used to offset the data and replace the false data with a linear projection that intercepted the origin. A graphical representation of this process has been presented previously in Fig. 2.6 in Chapter 2.

In the following sections, the results for the four point flexural testing are presented for each of the different sandwich constructions and their respective core types. The results and the observations made during the tests provided insights into the behavior of each sandwich construction and the reasons why they failed, and it allows for a qualitative discussion of the results as presented in Section 3.3.3. A more detailed analysis of the results is presented in Chapter 4 along with a comparison of the different core types based on stiffness and strength.

3.3.2.1. Results for Type 1. For the four point flexural tests, four specimens were prepared and successfully tested for the Type 1 sandwich construction. The false nonlinearities and offset were corrected for each of the data curves using the procedures mentioned previously. The corrected bottom face deflection and the strain in the top and bottom facings at mid-span were then plotted as the dependent variable versus the load in Figs. 3.24, 3.25, and 3.26, respectively. From these curves, several observations were made about the material behavior, and based on the observations made during the tests, a failure mode for the Type 1 specimens was determined.

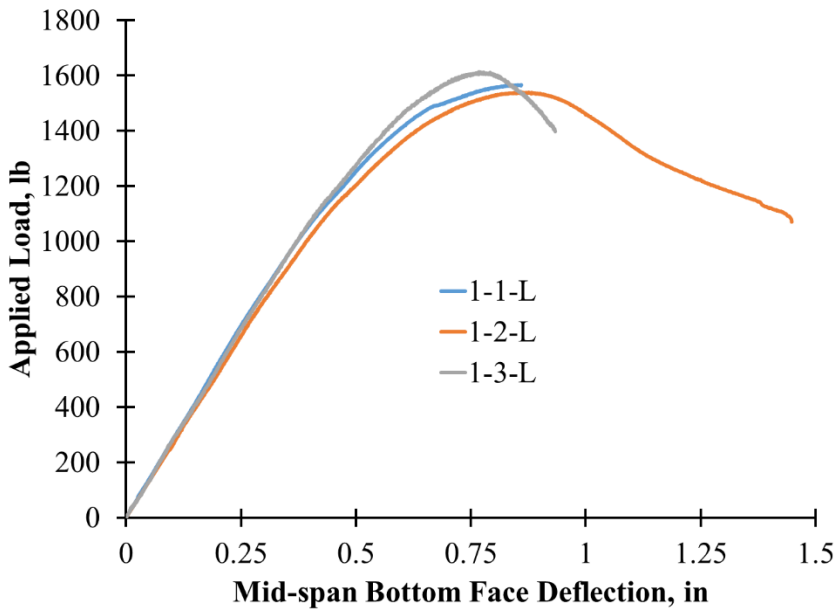

Figure 3.24: Applied Load vs. Mid-Span Bottom Face Deflection for Type 1

The behavior of the four point specimens was nearly the same as the behavior of the three point specimens. All of the curves had an initially linear region, and a nonlinear region that occurred just before ultimate failure. The Type 1 sandwich construction displayed the linear elastic behavior for the same reasons that the three point specimens displayed linear elastic behavior. The constituent materials of the sandwich construction, the rigid polyurethane foam core and the glass fiber reinforced polyurethane facings, display linear elastic tendencies. The rigid polyurethane foam core displayed an apparent linear elastic behavior in the initial results of the flatwise tests, and the glass fiber reinforced polyurethane is often considered to have a

composite response that is linear elastic. Therefore, the linear behavior was again expected for the four point flexural specimens.

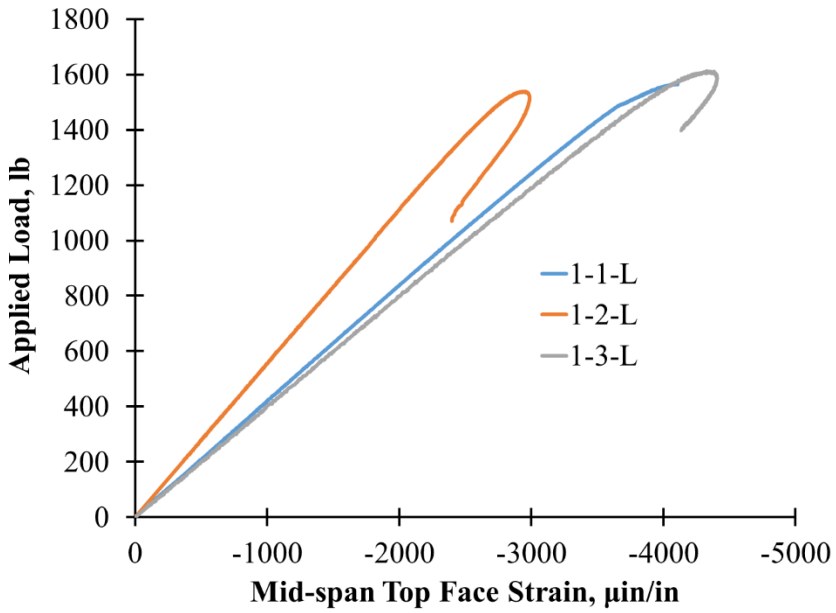

Figure 3.25: Applied Load vs. Mid-Span Top Face Strain for Type 1

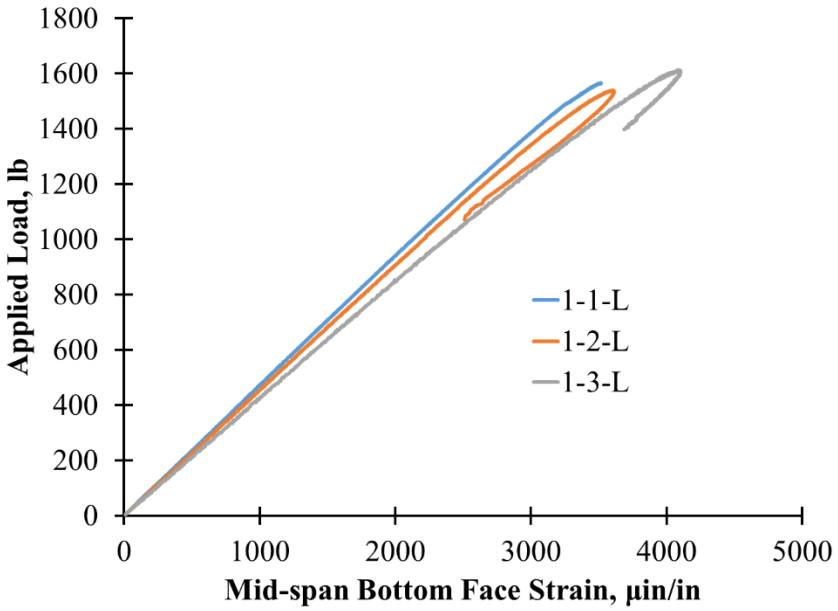

Figure 3.26: Applied Load vs. Mid-Span Bottom Face Strain for Type 1

As with the three point specimens, the nonlinear behavior was most likely due to the crushable nature of the rigid polyurethane foam core and its relatively low stiffness. The rigid polyurethane foam displayed nonlinear response in the flatwise compressive tests that occurred after the initial linear response and was characterized by an apparent yield point at its usable strength, at which point the foam could not support additional stress without significant damage and deformation. Amidst the four point flexural tests, the stress concentrations under the loading points became larger than the compressive strength in the foam, which lead to yielding of the foam under the load. Once the foam began to yield, the top facing lost stability and a wrinkle formed under the loading points, which had a wavelength proportional to the width of the loading bar. Again, this failure mode is typically designated as local indentation. At this point, the top face began to deflect much more than the bottom face as foam beneath the load began to crush, which permanently indented the top of the specimens. The applied load continued to increase, but the rate at which it increased began to gradually decrease. For Specimens 1-2-L and 1-3-L, the load peaked once the local indentation became too excessive. After this point, the load began to gradually decrease as the foam beneath the loading points crushed further. Specimen 1-2-L continued to lose load until excessive deformation led to concentrations of stress at the edges of the loading bars, which fractured the bottom side of the top facing in bending. At which point, the load dropped significantly. From this point on, the load began to decrease in an erratic stepped manor.

As for Specimen 1-3-L, the specimen lost capacity due to excessive local indentation, but before a bending fracture occurred in the top facing, the foam core suddenly fractured in a pattern indicative of shear failure in the core. The fracture appeared to start as a diagonal fracture in the core material on the support side of one of the loading points, and it propagated to the interfaces between the core and the top and bottom facings. Once the fracture reached this interface, it propagated through the foam along the interface until it reached the edge of the specimen, and a large segment of the core separated itself from the specimen. The fracture occurred so quickly that the location where the crack began is uncertain, but it appeared to originate within the diagonal crack in the core.

For Specimen 1-1-L, as the core yielded and the top facing began to wrinkle, but just before the deformation became excessive enough to cause the load to decrease, a shear fracture occurred that was similar to the three point test for Specimen 1-3-S. Both shear fractures in the four point tests occurred suddenly and were more energetic than the shear fracture that occurred in the three point test. The segments of the foam that separated from the specimens ejected out of the end of the specimens with substantial velocity and the remainder of the specimens ejected from the test fixture in the opposite direction. The reasons why each specimen behaved differently are not fully understood, but the differences are likely related to the different widths of the specimens and possible variations in the thickness of the top facings.

Reviewing the tests, the initial failure mode for all of the specimens was local indentation. The primary ultimate failure mode was excessive local indentation, which lead to bending fracture in the top facing or shear failure in the core. One specimen ultimately failed in shear before yielding and wrinkling could cause a loss in load. A photograph of the initial yielding of the foam where the response became nonlinear is shown in Fig. 3.27. Photographs of

the ultimate failure due to excessive wrinkling of the facing, as well as the fracture caused by shear failure in the foam, are shown in Figs. 3.28 and 3.29, respectively.

Figure 3.27: Initial Failure Due to Local Indentation for Type 1

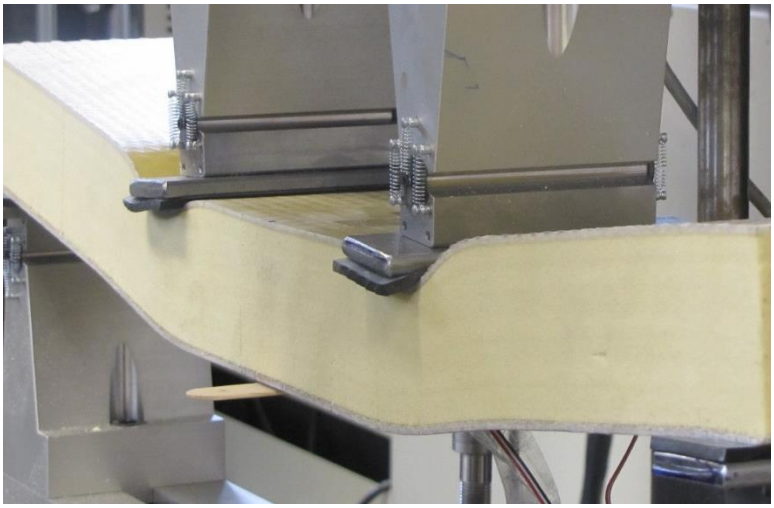

Figure 3.28: Ultimate Failure Due to Excessive Local Indentation for Type 1

3.3.2.2. Results for Type 2. For the four point flexural tests, three specimens were prepared and successfully tested for the Type 2 sandwich construction. Again, the false nonlinearities and offset were corrected for each of the data curves, and the corrected data was plotted. The bottom face deflection and the strain in the top and bottom facings at mid-span were then plotted as the dependent variable versus the load in Figs. 3.30, 3.31, and 3.32, respectively. From these curves, several observations were made about the material behavior, and based on the observations made during the tests, a failure mode for the Type 2 specimens was determined.

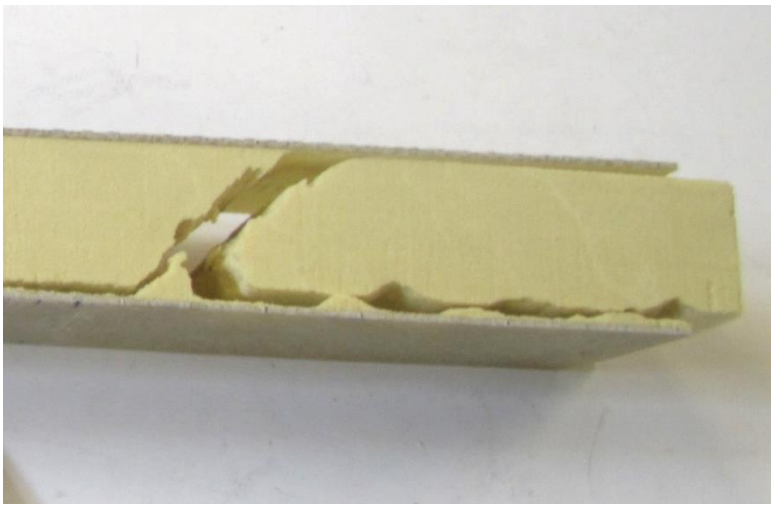

Figure 3.29: Ultimate Failure Due to Shear Failure of the Core Material for Type 1

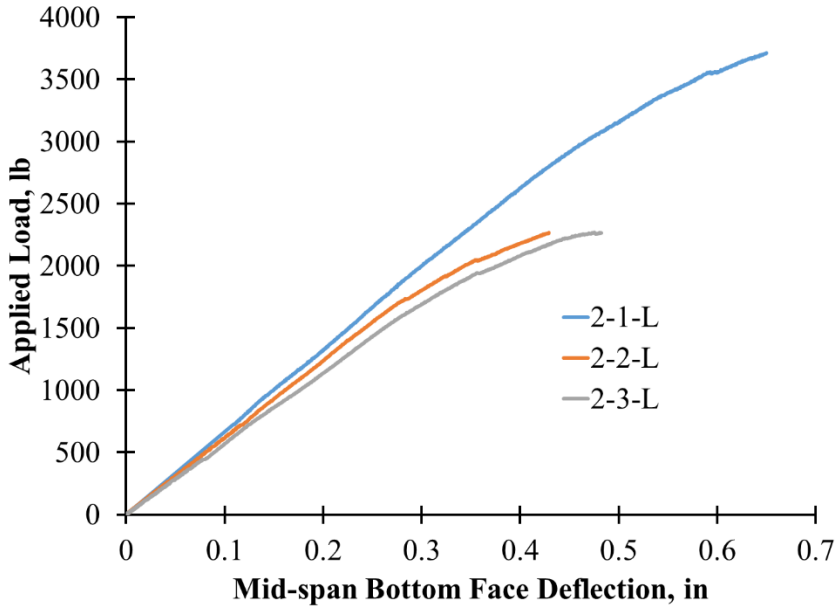

Figure 3.30: Applied Load vs. Mid-Span Bottom Face Deflection for Type 2

Similar to the Type 1 specimens, all of the curves for the Type 2 specimens had a similar shape with two distinct regions. Initially, the response was linear, which can be attributed to the materials used in the construction. The sandwich construction consisted of a Type 2 core of flexible polyurethane foam with an FRP gridwork of web reinforcing, and the facings were made of the same glass fiber reinforced polyurethane used in the Type 1 construction. The results of the flatwise compression and tension tests presented in the previous chapter indicated that the

Type 2 core can exhibit an apparent linear elastic response. Then, given the facings are the same as the Type 1 construction, the initial response is essentially linear elastic.

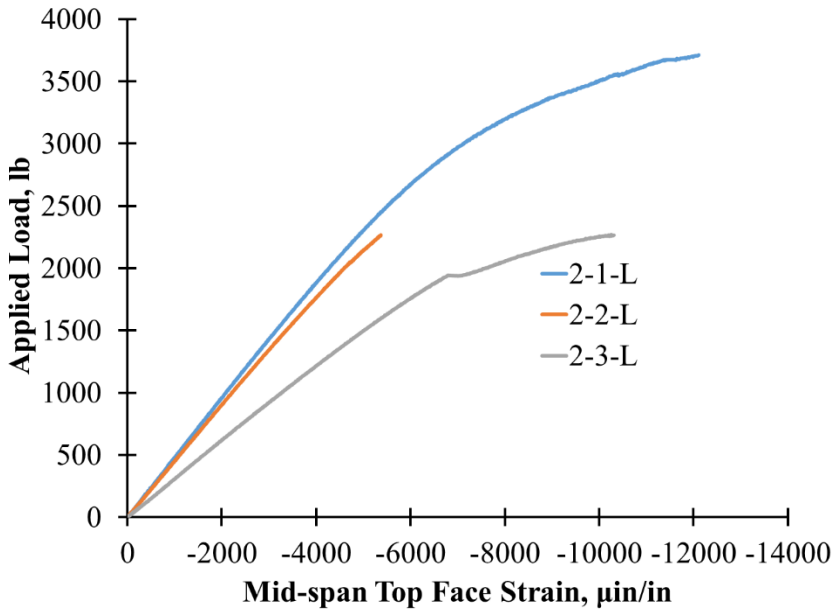

Figure 3.31: Applied Load vs. Mid-Span Top Face Strain for Type 2

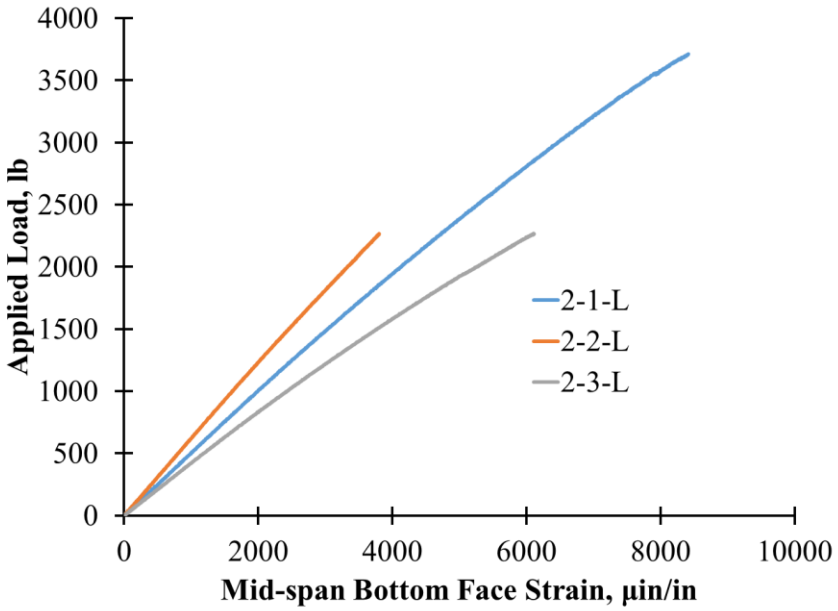

Figure 3.32: Applied Load vs. Mid-Span Bottom Face Strain for Type 2

The response became nonlinear for stability reasons that differ from the three point tests. The reinforcing webs of the core are thin and prone to buckling under compression, but no buckling of these webs under the load points was observed. However, the facings of the specimens were very thin relative to their width, and the top facing was prone to localized buckling between the cellular web gridwork, also known as intercellular dimpling/buckling. In the four point flexural tests, the compressive stress in the top facing became large enough between the load points that intercellular buckling occurred. This affect caused the load to become nonlinear as the stress was limited within the buckled sections and was forced to redistribute to more stable regions. The load continued to increase afterwards, but the rate of increase slowly diminished as more of the top face buckled locally between the load points. The load suddenly peaked and immediately dropped at the ultimate failure in all of the specimens but for two distinct reasons.

Specimen 2-1-L failed due to sudden compressive failure in the top facing in the form of a fracture under one of the load points. The other two specimens, 2-2-L and 2-3-L, failed due to a sudden fracture in the core near the supports that was indicative of shear failure. The shear fracture occurred diagonally through the core between the transverse webs and propagated to the interfaces between the core and the facings. At the interface, the fracture continued to slowly propagate through the core material as load was applied, but no part of the core completely separated from the specimen. These ultimate failures were energetic, but not quite as catastrophic as the Type 1 shear failures. The initial failure modes of all the specimens was intercellular buckling but the ultimate failure was different because of the different widths of the specimens and the different number of longitudinal reinforcing webs in the specimens. Specimen 2-1-L had three longitudinal reinforcing webs, while the other specimens only had two, which is why the first specimen carried substantially more load and failed ultimately due to compressive failure in the facings.

In conclusion, the initial failure mode was due to intercellular buckling in the top facing. The ultimate failure mode was shear failure in the core characterized by a diagonal fracture in the core material for Specimens 2-2-L and 2-3-L. For Specimen 2-1-L, the ultimate failure was caused by compressive failure of the top facing just beneath the load. A photograph of the initial intercellular dimpling is shown in Fig. 3.33. A photograph at ultimate failure due to excessive shear stress is shown in Fig. 3.34. Finally, the damage after compressive failure of the top facing in one of the specimens is shown in Fig. 3.35.

3.3.2.3. Results for Type 3. For the four point flexural tests, one specimen was prepared and successfully tested for the Type 3 sandwich construction. Again, supply and manufacturing issues due to the small scale of the specimens only allowed for one specimen to be constructed within the time allotted for this stage of the project. Therefore, the number of specimens was severely limited. Once the test was completed, the initial false nonlinearities and offset were corrected for each of the data curves, and the corrected data was plotted. The bottom face deflection and the strain in the top and bottom facings at mid-span were plotted as the dependent variable versus the load in Figs. 3.36, 3.37, and 3.38, respectively. From these curves, several observations were made about the material behavior, and based on the observations made during the tests, a failure mode for the Type 3 specimens was determined.

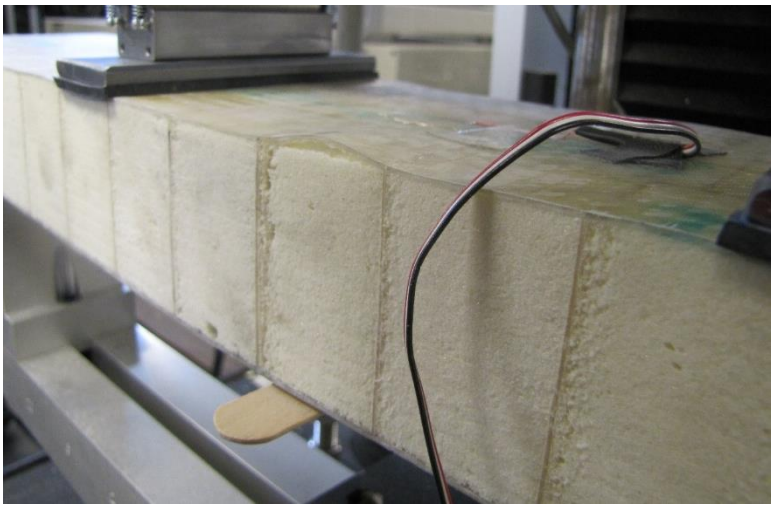

Figure 3.33: Initial Failure Due to Intercellular Buckling of the Top Facing for Type 2

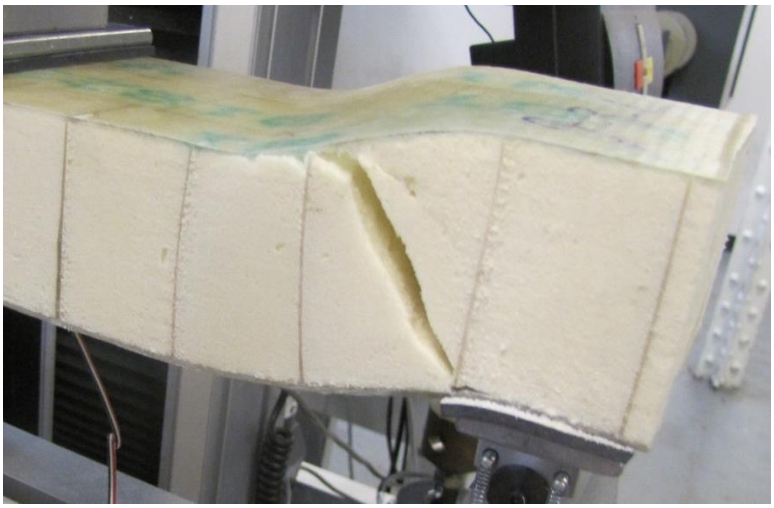

Figure 3.34: Ultimate Failure Due to Shear Failure of the Core Material for Type 2

The four point flexural response for the Type 3 specimen has a distinct linear region at the beginning of the test, and the behavior became nonlinear prior to ultimate failure. As with the other sandwich constructions, the initial linear response can be attributed to the materials used in the manufacture of the panel. The sandwich construction consisted of a Type 3 core of flexible polyurethane foam blocks in a trapezoidal shape that provided a mold for the truss-type panel. The diagonal web reinforcement was integrated with the facesheets, which were identical to the facesheets on the other two sandwich constructions. The flexible foam contributes very little to the behavior of the sandwich construction in the longitudinal direction, but it does provide extra

stability to the facings and webs. In comparison to the facing layers, the diagonal web material differs with respect to the orientation of the fibers (±45° vs. ±90°), but overall the composite behavior should still be generally linear elastic. Therefore, the apparent linear elastic response at the beginning of the test was as expected.

Figure 3.35: Ultimate Failure Due to Compressive Failure of the Top Facing for Type 2

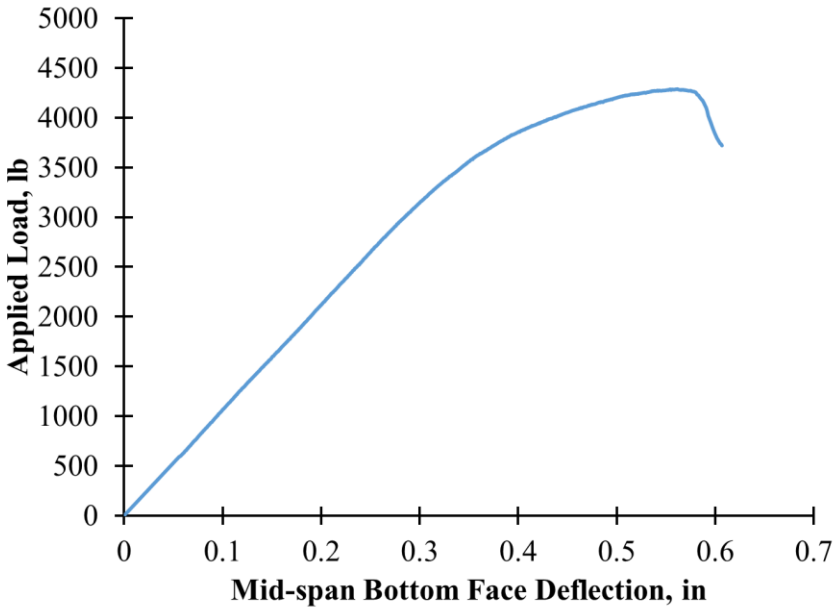

Figure 3.36: Applied Load vs. Mid-Span Bottom Face Deflection for Type 3

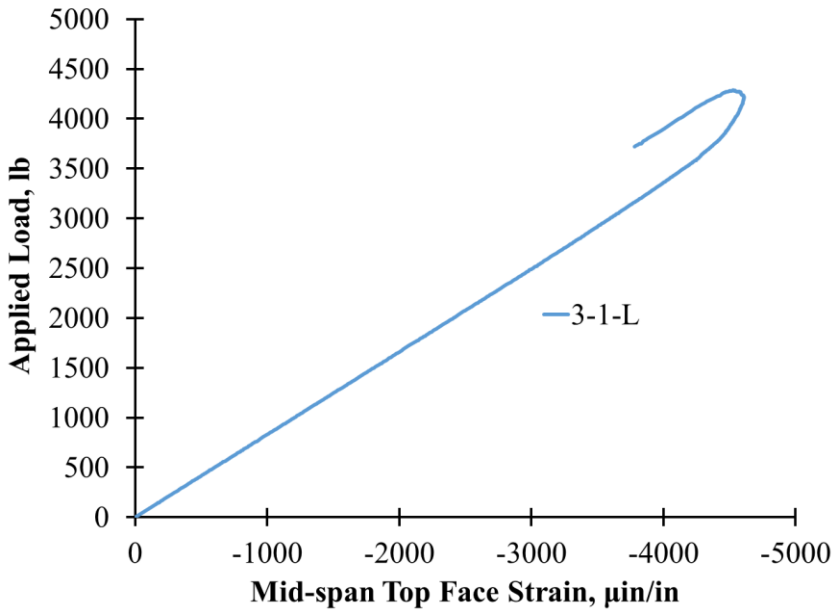

Figure 3.37: Applied Load vs. Mid-Span Top Face Strain for Type 3

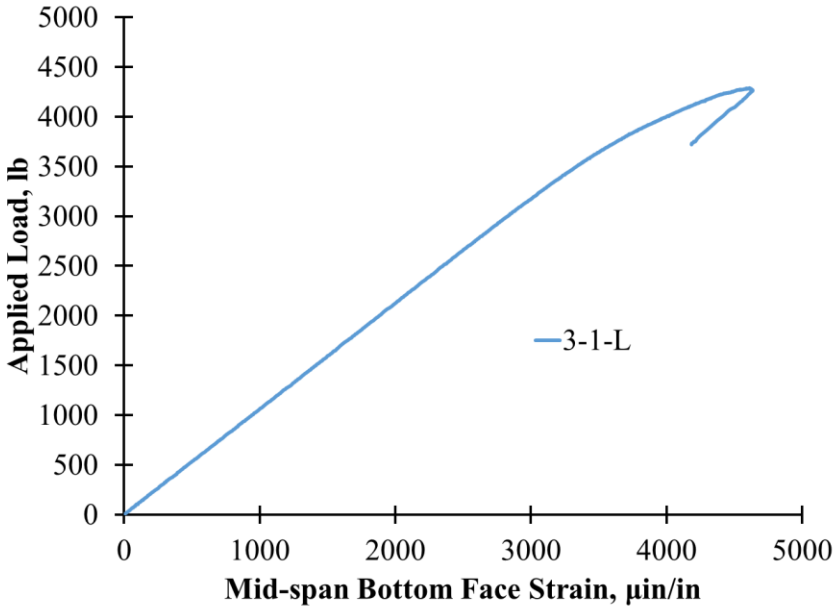

Figure 3.38: Applied Load vs. Mid-Span Bottom Face Strain for Type 3

The response eventually became nonlinear due to progressive compressive failure in the top facing under the load. The failure began at the outer layers and slowly progressed to the inner layers as the load increased. Due to the geometry of the specimen and the thickness of the top

facing, the failure could not occur as one immediate fracture similar to the failure previously discussed for Specimen 2-1-L. At this point, the load continued to increase, but the rate of increase slowed. As the compressive failure progressed through the top facing and into the diagonal webs, the load peaked as a hinge mechanism formed in the top facing. Then, as the shear layers in the diagonal webs started to fail in compression, the load dropped significantly and decreased in a stepped manor as the crushing progressed.

Summarizing the test, the failure mode was compressive failure under the load point in the top facing that caused initial nonlinearity. Then, as the compressive failure progressed into the diagonal webs of the specimen, ultimate failure occurred due to the formation of a hinge mechanism in the top facing. A photograph of the compressive failure for the Type 3 sandwich construction is shown in Fig. 3.39.

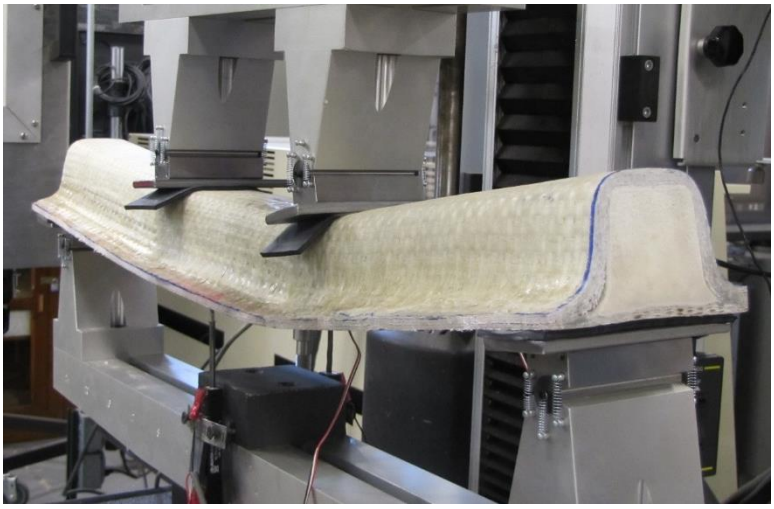

Figure 3.39: Ultimate Failure Due to Compressive Failure of the Top Facing for Type 3

3.3.3. Discussion of Test Results. Based on the results of the four point flexural testing, several useful observations can be made about the three different core types and their associated sandwich constructions. The initial response of each of the constructions was essentially linear elastic. As far as the nonlinear response is concerned, the observed mechanisms were different for each of the three types. However, this is expected considering the longer support span compared to the three point flexural test and the significant differences between the core types.

For the Type 1 specimens, the behavior of the rigid polyurethane foam continued to govern the behavior of the specimens. The low compressive strength and stiffness of the foam core led to local indentation in the four point specimens. This mechanism was again prevalent in all of the specimens and led to nonlinearity in the response. It also governed the ultimate failure of all but one of the specimens. Specimen 1-1-L failed ultimately due to shear stresses in the core. The variation in ultimate failure was likely due to reasons similar to that of the three point

specimens, with noticeable variations in the thickness of the facings. Also, the fact that the specimens had different widths likely contributed to the variations.

For the Type 2 specimens, the behavior was governed by the stability of the top facing. Localized buckling or intercellular dimpling in the top facing between the load points occurred in all three of the specimens. This led to nonlinearity in the response. The ultimate failure in the specimens was caused by two mechanisms. Specimen 2-1-L suffered sudden compressive failure in the top facing beneath the loading point. Specimens 2-2-L and 2-3-L ultimately failed due to shear fracture in the core material adjacent to the support. These variations were due to differences in the width and the number of longitudinal reinforcing webs in the specimens. The first specimen had three longitudinal reinforcing webs while the others had only two. This allowed compressive failure to dominate in the first specimen while shear failure dominated in the other two specimens.

For the Type 3 specimen, failure occurred due to compressive stresses in the top facing, and as the compressive failure progressed into the diagonal webs, a hinge mechanism formed in the top facing that resulted in ultimate failure. The poor resin saturation and dislocations between the fiber layers were also noticeable in the four point specimen, but no splitting failure occurred during the test. Also, the slope of the load versus deflection curve was of appropriate magnitude when considering the geometric stiffness of the cross-section. Therefore, the impact of the manufacturing defects appeared to be much less prevalent in the four point specimen. Nevertheless, performance would have improved if the defects were not present.

From these observations, it is evident that the Type 1 specimens still suffered from localized effects at the load points that caused initial nonlinearity in all of the specimens and ultimate failure in the majority of the specimens, while the other two sandwich constructions were not influenced significantly by these effects. Ultimate failure due to shear was an issue in one of the Type 1 specimens and occurred in the majority of the Type 2 specimens. Compressive failure of the top facing occurred in one of the Type 2 specimens and the Type 3 specimen. When considering ultimate failure, the Type 1 and Type 2 specimens predominately failed suddenly with fairly energetic fractures while the Type 3 specimen failed more gradually. Finally, the manufacturing issues were again present in the Type 3 specimen but seemed to have less of an effect on the results, yet they still hindered the performance of the sandwich construction.

4. STIFFNESS AND STRENGTH ANALYSIS OF SMALL-SCALE PANEL TESTS

The flexural behavior of the three different sandwich constructions can be quantitatively analyzed by fitting the experimental results to common theories and models. The low stiffness of the foam materials used in the cores coupled with the short spans that were used in the tests described previously often leads to complex behavior at the load and support points, and to get a truly accurate representation of the behavior, detailed models are needed. Higher order shear deformation theories and finite element models have often shown very good accuracy for sandwich constructions like the alternatives that were tested, but they take a significant amount of effort to develop and solve. Less exact but equally applicable theories such as Classical/Euler-Bernoulli Beam Theory (EBBT) and Timoshenko Beam Theory (TBT) are not nearly as detailed and are often conservative when estimating material properties, but when applied to beams, they can be solved analytically with relatively minimal effort using simple static equilibrium relationships and simplified support conditions. EBBT and TBT cannot predict nonlinear behavior or localized stress concentrations at concentrated loads. However, they can accurately predict global behavior when fitted to linear experimental results, and they can predict global equivalent stresses with sufficient accuracy.

Considering the scope of this study and the goals set forth, the primary goal at this stage was to compare the core types based on structural performance using the small scale experiments and recommend one sandwich construction to further develop into a bridge deck panel. EBBT and TBT will be sufficiently accurate to analyze the results and compare the different cores types to one another. The development of sophisticated models will be left to later stages of the project that focused on a single configuration. The assumptions and governing equations for both EBBT and TBT are readily available in the literature. The specific solutions used to estimate the stiffness and strength of each sandwich construction are presented in Sections 4.1 and 4.2, respectively.

4.1. ANALYSIS OF FLEXURAL STIFFNESS

The flexural stiffness of a beam is the combination of certain geometrical and material stiffness properties that relate the applied load to the resulting deflections. The prediction of deflection is a very important tool in designing sandwich panels, especially for their use in bridge decks. The deflection is often limited by certain serviceability criteria that are based on the intended use that the structural member will provide. For bridge decks, the deflection is limited severely to ensure the members do not cause unforeseen complications, and to ensure that people using them are comfortable as they drive over them. Therefore, the stiffness of each sandwich construction is an important comparison, if not the most important, considering this limit state controlled nearly all designs of the honeycomb sandwich panels that have been used in bridge decks in the past.

TBT will be used to estimate the flexural stiffness of the Type 1 and Type 2 sandwich constructions using a procedure similar to that presented in ASTM D7250/D7250M: Standard

Practice for Determining Sandwich Beam Flexural and Shear Stiffness (ASTM, 2012). The procedures in the ASTM were not directly used in this analysis, but they use a similar theory that produces the same analytical solutions. As for the Type 3 construction, EBBT will be used to estimate the flexural stiffness.

Considering the specific case used in the small-scale panel testing program, the governing equations can be solved by using static equilibrium and simple boundary conditions. The test conditions can be idealized as a simply supported beam with loading points that are equidistant from each support, which is statically determinant and has easily determined shear (*V*) and moment (*M*) distributions. The idealized conditions for the small-scale panel tests are represented in Fig. 4.1.

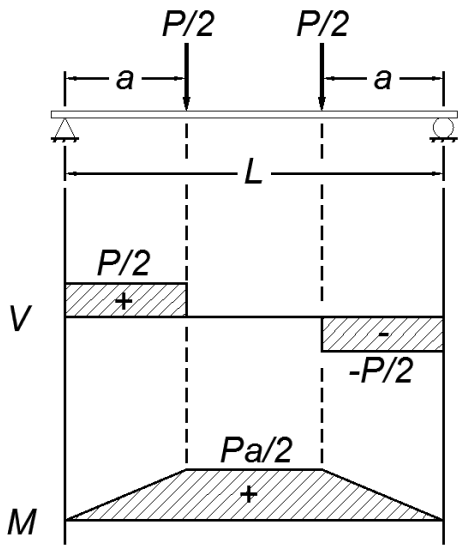

Figure 4.1: Idealized Support and Loading Conditions
for Small-Scale Panel Tests

The governing equations for both EBBT and TBT can then be solved using integration, and the integration constants can be solved by using the boundary conditions and the compatibility relationships. The boundary conditions include the curvature is equal to zero at mid-span and the deflection is equal to zero at the supports. Then, compatibility is maintained at $x = L/3$ where both the curvature and deflection must be equal on the left and right sides. From this, the solution is shown in Eqn. 4.1 for EBBT and Eqn. 4.2 for TBT, and these solutions are symmetric about the mid-span.

Where the deflection $w(x)$ is positive upwards. From these solutions, the deflections at mid-span for the three point loading case ($a = L/2$) and the four point loading case ($a = L/3$) can be determined. Applying EBBT, the solution for the three point loading case is presented in Eqn. 4.3, and the solution for the four point loading case is presented in Eqn. 4.4. Applying TBT, the

solution for the three point loading case is presented in Eqn. 4.5, and the solution for the four point loading case is presented in Eqn. 4.6.

$$w(x) = \frac{Px(x^2 + 3a^2 - 3aL)}{12EI}; 0 \le x \le a$$
$$w(x) = \frac{Pa(3x^2 - 3Lx + a^2)}{12EI}; a \le x \le \frac{L}{2} \quad (4.1)$$

$$w(x) = \frac{Px(x^2 + 3a^2 - 3aL)}{12EI} - \frac{Px}{2kAG}; 0 \le x \le a$$
$$w(x) = \frac{Pa(3x^2 - 3Lx + a^2)}{12EI} - \frac{Pa}{2kAG}; a \le x \le \frac{L}{2} \quad (4.2)$$

$$w_{1,max} = \frac{P_1 L_1^3}{48EI} \quad (4.3)$$

$$w_{2,max} = \frac{23P_2 L_2^3}{1296EI} \quad (4.4)$$

$$w_{1,max} = \frac{P_1 L_1^3}{48EI} + \frac{P_1 L_1}{4kAG} \quad (4.5)$$

$$w_{2,max} = \frac{23P_2 L_2^3}{1296EI} + \frac{P_2 L_2}{6kAG} \quad (4.6)$$

In these solutions, the sign of the deflection has been reversed so that the deflection *w(x)* is positive downwards, and the subscript "*1*" indicates the three point configuration (*a = L/2*) while "*2*" indicates the four point configuration (*a = L/3*). With these equations, the bending and shear stiffnesses of the sandwich constructions can be calculated based on the load versus deflection curves recorded during the tests. The following sections will show the variations of these equations used for each sandwich construction, and the results that the equations produced. Then, the results will be normalized to a "standard" size section with a 3 in. width and a 2 in. overall depth, which was chosen based on the geometric constraints of the specimens. The method of normalization will be applied to each construction while attempting to maintain key geometrical features. These concepts will be presented separately for each sandwich construction, and finally a comparison between the constructions is presented in Section 4.1.4, which will be based on common deflection limit states for bridge deck members.

4.1.1. Results for Type 1. In order to apply the TBT solutions discussed previously to the results for the Type 1 specimens, some observations are required along with some algebraic manipulation. For the Type 1 sandwich construction, an effective "*EI*" term can be found by summing the contributions of each part of the construction. The total quantity is then determined using Eqn. 4.7.

$$EI = E_f I_f + E_c I_c \tag{4.7}$$

Where the "*f*" subscript denotes the components from the facings and the "*c*" subscript denotes the components from the core. This relationship can be expanded using the dimensions of the sandwich construction presented in Fig. 4.2. The full expansion is presented in Eqn. 4.8.

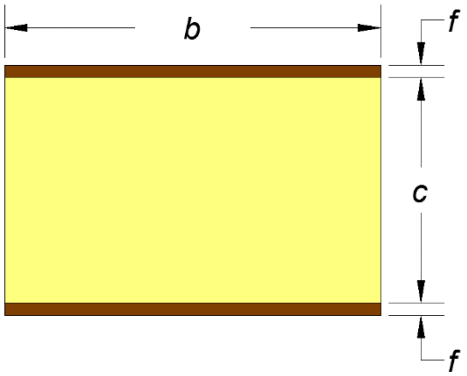

Figure 4.2: Dimensions of the Type 1 Sandwich Construction

$$EI = E_f \left(\frac{bf^3}{6} + \frac{bfd^2}{2}\right) + E_c \frac{bc^3}{12} \tag{4.8}$$

Where *d* is the sum of *c* and *f*, the moment arm between the centroids of the facings. From this expression, some terms can be eliminated because of their very small contribution. The first term in parentheses is the individual moment of inertias of the facings, and since it is proportional to "f^3", it is essentially zero given that the average facing thickness for the Type 1 construction was 0.095 in. Then, the last term, which is the contribution of the core, can be eliminated because the stiffness of the core is several magnitudes smaller than the stiffness of the facings. The resulting relationship is shown in Eqn. 4.9.

$$EI \approx \frac{E_f bfd^2}{2} \tag{4.9}$$

The shear stiffness of the Type 1 core can also be calculated based on the dimensions and material properties of the constituent materials. Typically, for this type of sandwich construction, it is assumed that the shear stresses are completely carried by the foam core. This is due to the small thickness of the facings, where the first moment of the area of the facings is so small that when the true shear stress predicted by elasticity theory is integrated over the area, the contribution of the facings is found to be negligible. Also, the shear stiffness of the core is low enough that the true shear stress predicted by elasticity theory will vary very little over the depth of the foam, and the shear correction factor can be considered to be nearly 1.0 for this type of core. Therefore, the shear stiffness becomes the expression in Eqn. 4.10.

$$kAG \approx G_c A_c = G_c bc \tag{4.10}$$

From these two expressions for the bending and shear stiffnesses, it is evident that they are both directly proportional to the width. Therefore, dividing these expressions by the width will provide a unit width quantity. These quantities are represented in Eqn. 4.11.

$$D = \frac{EI}{b}$$
$$U = \frac{kAG}{b} \tag{4.11}$$

Where *D* is the bending stiffness per unit width, and *U* is the shear stiffness per unit width. Given these new variables, the TBT solutions presented previously can be rewritten in the forms found in Eqns. 4.12 and 4.13.

$$w_{1,max} = \frac{P_1 L_1^3}{48 D b_1} + \frac{P_1 L_1}{4 U b_1} \tag{4.12}$$

$$w_{2,max} = \frac{23 P_2 L_2^3}{1296 D b_2} + \frac{P_2 L_2}{6 U b_2} \tag{4.13}$$

Where the subscripts designate which test setup to use for each of the parameters: "*1*" for the three point loading specimen and "*2*" for the four point loading specimen. The equations can then be further rearranged to extract *D* and *U* since they are independent of any geometrical expressions in the equations, so that the flexural test data can be used to solve for them as shown in Eqns. 4.14 and 4.15.

$$D\left(\frac{12}{L_1^2}\right) + U = \left(\frac{P}{w}\right)_1 \left(\frac{L_1}{4 b_1}\right) \tag{4.14}$$

$$D\left(\frac{216}{23L_2^2}\right) + U = \left(\frac{P}{w}\right)_2 \left(\frac{L_2}{6b_2}\right) \tag{4.15}$$

Where (*P/w*) is the slope of the linear region of the load versus mid-span bottom face deflection curve. These represent a system of equations that can be readily solved using matrix algebra and the recorded dimensions and slopes for a three point specimen and a four point specimen. Given that there were four specimens for the three point tests and three specimens for the four point tests, twelve possible iterations can be used to solve the equations. The average, standard deviation, and coefficient of variation for each stiffness calculated using all twelve iterations is presented in Table 4.1.

Table 4.1: Flexural Stiffness Results for Type 1

Flexural Stiffness	Average	Standard Deviation	Coefficient of Variation
Bending Stiffness per Unit Width, lb-in	397,600	51,180	12.9%
Shear Stiffness per Unit Width, lb/in	4,653	66	1.4%

The results must now be normalized to "standard" dimensions so a comparison can be made between the core types. The stiffness values need to be altered so that they are representative of a "standard" size section with a 3 in. width and a 2 in. overall depth that still maintains the primary features of the geometry. The primary feature that needs to be maintained is the thickness of the facings. Therefore, the only dimensions that need to change are the depth of the core and the width of the specimen for the Type 1 construction. This effects the bending stiffness by changing the width of the facings and the moment arm between the facings, and it effects the shear stiffness by change the width and height of the core material. In order to make the changes, the bending stiffness per unit width needs to be multiplied by the new width, and then it needs to be multiplied by the ratio of the normalized "d^2" term to that measured in the specimens. As for the shear stiffness per unit width, it needs to be multiplied by the new width also, then multiplied by the ratio of the normalized core height to the measured core height. A table of the normalized dimensions and the measured dimensions along with the bending and shear correction factors described above is presented in Table 4.2.

Using the correction factors, the total bending stiffness of the normalized cross-section becomes 1,042,000 lb-in.^{2}, and the total shear stiffness of the normalized section is 13,000 lb. Also, the stiffness results can be used to find effective properties of the constituent materials. The bending stiffness can be used to estimate the effective modulus of elasticity of the facing material using Eqn. 4.9, and the shear stiffness can be used to find the effective modulus of

rigidity of the core material using Eqn. 4.10. The effective modulus of elasticity of the facing was measured to be 2,024,000 psi and the effective modulus of rigidity of the core was measured to be 2,393 psi using the calculated stiffnesses.

Table 4.2: Dimensions and Stiffness Normalization Factors for Type 1

Dimensions	Normalized	Measured
Width, in	3.0	1.0
Total Depth, in	2.000	2.133
Facing Thickness, in	0.095	0.095
Core Thickness, in	1.811	1.944
Facing Moment Arm, in	1.905	2.039
Normalization Factors		
Bending Stiffness Factor, in	2.621	
Shear Stiffness Factor, in	2.795	

4.1.2. Results for Type 2. The same concepts and equations used for Type 1 specimens can be applied to the Type 2 specimens to calculate the bending and shear stiffnesses per unit width. The core material has reinforcing webs that could contribute to the bending stiffness of the sandwich construction, but since they are very thin and have a modulus of elasticity that is less than that of the facings, their contribution is negligible and can be neglected. The only significant effect this assumption can have on the calculations is that it could contribute a small amount to the bending stiffness, and eventually lead to a slight over estimation in the effective modulus of elasticity of the facing. Since there were three specimens for the three point tests and three specimens for the four point tests, nine possible iterations can be used to solve Eqns. 4.14 and 4.15 for the Type 2 specimens. The average, standard deviation, and coefficient of variation for each stiffness calculated using all nine iterations is presented in Table 4.3.

Table 4.3: Flexural Stiffness Results for Type 2

Flexural Stiffness	Average	Standard Deviation	Coefficient of Variation
Bending Stiffness per Unit Width, lb-in	528,100	81,790	15.5%
Shear Stiffness per Unit Width, lb/in	20,360	1,304	6.4%

The same normalization technique can be used to normalize the results to a "standard" size section with a 3 in. width and a 2 in. overall depth that still maintains the primary features of the geometry. The main features that needed to be maintained were the thickness of the facings and the reinforcing webs, and by using the same techniques as in the calculations for Type 1, these features are sufficiently preserved. A table of the normalized dimensions and the measured dimensions along with the bending and shear correction factors for the Type 2 sandwich construction is presented in Table 4.4.

Table 4.4: Dimensions and Stiffness Normalization Factors for Type 2

Dimensions	Normalized	Measured
Width, in	3.0	1.0
Total Depth, in	2.000	2.333
Facing Thickness, in	0.095	0.095
Core Thickness, in	1.811	2.143
Facing Moment Arm, in	1.905	2.238
Normalization Factors		
Bending Stiffness Factor, in	2.174	
Shear Stiffness Factor, in	2.534	

Applying the correction factors, the total bending stiffness of the normalized Type 2 cross-section becomes 1,148,000 lb-in.^{2}, and the total shear stiffness of the normalized section is 51,590 lb. The stiffness results were then used to find effective properties of the constituent materials. The bending stiffness was used to estimate the effective modulus of elasticity of the facing material using Eqn. 4.9, and the shear stiffness was used to find the effective modulus of rigidity of the core material using Eqn. 4.10. The effective modulus of elasticity of the facing was measured to be 2,227,000 psi and the effective modulus of rigidity of the core was measured to be 9,497 psi using the calculated stiffnesses for the Type 2 specimens.

4.1.3. Results for Type 3. For the Type 3 specimens, several simplifying assumptions can be made about the behavior of the cross-section. In flexure, the fiber reinforced shear layers and facings will carry the entire load, and the contribution of the foam is negligible. Then, the expression for the bending stiffness becomes Eqn. 4.16.

$$EI = E_f I_f + E_s I_s \tag{4.16}$$

Where the subscript "s" represents the shear layers. The modulus of elasticity of the facings is expected to be the same magnitude as the modulus of elasticity of the shear layers, but since the orientation of the shear layers does not align with the longitudinal direction of the beam, the modulus of elasticity of the shear layers is likely smaller than that of the facings. However, given the variability involved in the construction of these laboratory specimens combined with the fact that the modulus of elasticity is primarily a function of the resin, the same stiffness can be applied to the shear layers with minimal error. Therefore, the gross properties of the combination of facing layers and shear layers were used in the following calculations. With this simplification, Eqn. 4.16 becomes Eqn. 4.17.

$$EI = E_g I_g \tag{4.17}$$

Where "I_g" is the area moment of inertia of all the glass fiber reinforced polyurethane, and "E_g" is an effective modulus of elasticity of all the glass fiber reinforced polyurethane. As far as shear stiffness is concerned, the same concepts apply when considering the geometry of the Type 3 construction, and it is acceptable to consider the gross properties of the shear and facing layers combined. Therefore, the shear stiffness is represented by Eqn. 4.18.

$$kAG = k_g A_g G_g \tag{4.18}$$

Where again the terms representative of the shear and facing layers are combined as one gross material. When the geometry of the Type 3 cross-section is examined in detail, the expressions for the area moment of inertia and cross-sectional area are algebraically complicated, and a direct relationship to the width dimensions of the specimen is not possible. In fact, the width varies significantly throughout the cross-section because it is generally trapezoidal in shape, and an effective width of the glass reinforced polyurethane is difficult to define. Therefore, the equations must be used to solve for the total bending stiffness and shear stiffness, which will be represented by the variables in Eqn. 4.19.

$$\begin{aligned} D_t &= EI \\ U_t &= kAG \end{aligned} \tag{4.19}$$

Where "D_t" and "U_t" are the effective bending and shear stiffnesses for the total cross-section, respectively. Then, Eqns. 4.14 and 4.15 become Eqns. 4.20 and 4.21, respectively.

If these equations are evaluated using the flexural test results for the Type 3 specimens, there is only one iteration and, unfortunately, the solutions for the stiffnesses are non-rational. The calculated bending stiffness is negative and the calculated shear stiffness is relatively small

in magnitude. The expected result was high bending and shear stiffnesses based on the geometry of the specimens. This indicates that one or both of the flexural tests for the Type 3 specimens was misrepresentative of the sandwich construction. Based on the observations made during the tests, it is likely that the three point flexural test results were negatively affected by manufacturing defects present in the specimen before testing. These negative effects manifested as premature splitting between the shear layers, and a noticeable lack of stiffness in the load versus deflection response of the specimen. The defects were caused by poor resin saturation, and consisted of dislocations between the fiber layers at the interfaces between individual fiber layers and also at the interface between the shear layers and the flexible foam. The defects likely affected the four point test results as well, but the effects were far less apparent in the data recorded from the test. Therefore, an attempt to estimate the flexural stiffness using only the four point test result is presented in the following discussion.

$$D_t\left(\frac{12}{L_1^2}\right) + U_t = \left(\frac{P}{w}\right)_1\left(\frac{L_1}{4}\right) \tag{4.20}$$

$$D_t\left(\frac{216}{23L_2^2}\right) + U_t = \left(\frac{P}{w}\right)_2\left(\frac{L_2}{6}\right) \tag{4.21}$$

In order to solve for any of the stiffness values, the theory must be reduced to one equation and one unknown. Since the magnitude of the shear stiffness of the Type 3 core (the FRP diagonals) is very large compared to that for Types 1 and 2, the shear deformations in the four point specimen are a relatively small percentage of the total deflection, and EBBT can be used to solve for the bending stiffness.

Therefore, using Eqn. 4.4 and applying the bending stiffness definition previously described, the solution for the mid-span deflection in the four point tests becomes Eqn. 4.22.

$$w_{2,max} = \frac{23P_2L_2^3}{1296D_t} \tag{4.22}$$

With this result, the total bending stiffness can be estimated by rearranging Eqn. 4.22 into Eqn. 4.23.

$$D_t = \left(\frac{P}{w}\right)_2\left(\frac{23L_2^3}{1296}\right) \tag{4.23}$$

Using Eqn. 4.23 and the four point flexural test results, the total bending stiffness of the Type 3 construction was determined as 2,597,000 lb-in.^{2}. Considering the short span to depth ratio (~10) used in the four point experiments, the bending stiffness found with Eqn. 4.23 will be a conservative estimate because the shear deformations were neglected. However, the deflections

that can be predicted using Eqn. 4.23 and the bending stiffness found using the experimental results will still be sufficient in the linear region of the response. Unfortunately, a sufficient estimate of shear stiffness cannot be found using the experimental data.

Now the cross section needs to be normalized to maintain its key features, and fit the gross dimensions of the "standard" specimen, which has a 3 in. width and a 2 in. overall depth. In order to accomplish this, the dimensions of the Type 3 cross section were measured in detail, and a drawing of the cross section was completed in a CAD software program. From this, the area moment of inertia of the glass reinforced polyurethane can be readily determined. Then, the length and height dimensions of the cross section were reduced without changing any of the facing and web thicknesses or the angular orientation of the webs in order to have a total height of 2 in. and a total cross-sectional area of 6 in.^{2}, which now fits the "standard" specimen definition. From this standard section, the transformed area moment of inertia of the glass reinforced polyurethane was calculated. Then, to normalize the bending stiffness calculated earlier, the value was multiplied by the ratio of the transformed area moment of inertia to measured area moment of inertia of the glass reinforced polyurethane. The dimensions of the measured cross section and the transformed cross section are presented in Figs. 4.3 and 4.4, respectively.

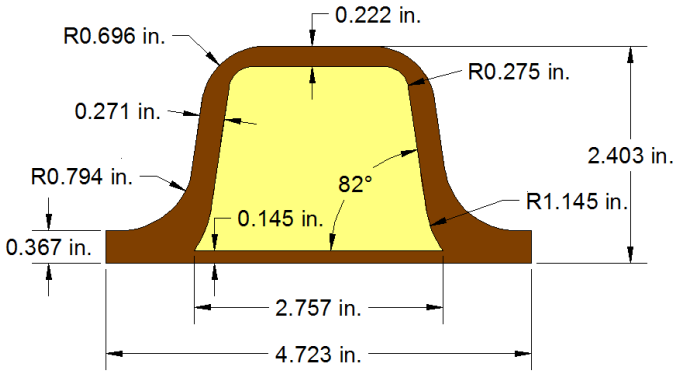

Figure 4.3: Measured Dimensions of the Type 3 Cross Section

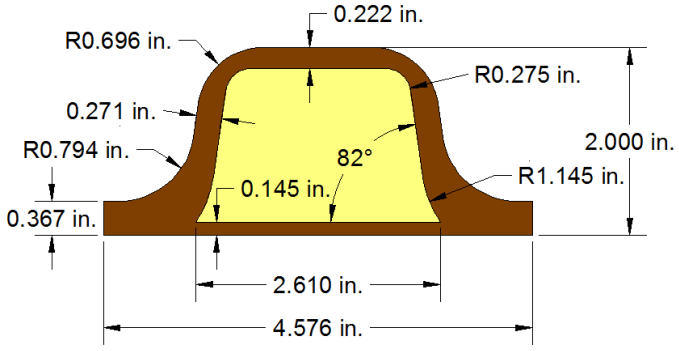

Figure 4.4: Normalized Dimensions of the Type 3 Cross Section

The area moment of inertia of the fiber reinforced polyurethane was 1.913 $in.^4$ for the actual cross section, and the normalized cross section had an area moment of inertia or 1.174 $in.^4$. Therefore, the normalization factor for the bending stiffness was calculated as the ratio of these two values, 0.614. This process results in a normalized bending stiffness of 1,594,000 $lb\text{-}in.^2$, and using Eqn. 4.19, the effective modulus of elasticity for all the fiber reinforced polyurethane layers combined is estimated to be 1,358,000 psi. Again, this estimation of the modulus of elasticity is conservative for two reasons. The contribution of shear deformations was not considered in the theory used for the Type 3 specimens, and the shear layers were considered to have the same modulus of elasticity as the facing layers, when in reality they likely have a slightly lower modulus of elasticity because the shear layers were not oriented in the same direction as the facing layers, which should lead to the effective modulus of elasticity being lower.

4.1.4. Discussion of Stiffness Analysis Results. The analysis of flexural stiffness clearly shows that the Type 3 construction has the highest flexural stiffness despite flaws due to poor resin saturation. The Type 2 construction had the second best performance, while the Type 1 construction performed the poorest with regard to flexural stiffness. This result is consistent with the geometric stiffness of each construction and the fact that the materials used in each construction were very similar, if not exactly the same in most cases. The Type 3 construction had the largest geometric stiffness, while the Type 2 construction had the second largest, and the Type 1 construction had the lowest geometric stiffness. Table 4.5 summarizes the results for each construction after normalizing each cross section to a depth of 2 in. and a total cross-sectional area to 6 $in.^2$.

Table 4.5: Summary of Estimated Flexural Stiffnesses for Each Panel Type

Construction Type	Normalized Total Bending Stiffness ($lb\text{-}in.^2$)	Normalized Total Shear Stiffness (lb)
1	1,042,000	13,000
2	1,148,000	51,590
3	1,594,000	-

From the stiffness analysis, the material properties for each sandwich construction were also measured. This includes the effective modulus of elasticity of the facing material and the effective shear modulus of the core for each construction when subjected the bending moments and shear forces in the configurations used in the experiments. Also, the effective modulus of elasticity in bending of the Type 3 configuration was estimated, but standard bending theory was used and the facing was a combination of outer facing layers and shear layers. Both of these simplifications can lead to an under estimation of the modulus of elasticity of the facing layers alone, and this is reflected in the results presented in Table 4.6.

Table 4.6: Summary of Estimated Material Properties for Each Panel Type

Construction Type	Effective Modulus of Elasticity of Facings (psi)	Effective Shear Modulus of the Core (psi)
1	2,024,000	2,393
2	2,227,000	9,497
3	1,358,000	-

The facings of both Types 1 and 2 were essentially the same material, which is why the effective modulus of elasticity is nearly the same for each. The effective modulus of elasticity for the Type 3 construction is noticeably less than that for Types 1 and 2 but of the same order of magnitude. Again, this is likely due to the simplifications discussed previously. However, the geometric stiffness of the Type 3 construction was much larger, which resulted in the largest bending stiffness. As for shear modulus, the Type 1 core is nearly one-fourth of the shear modulus recorded for the Type 2 core, which indicates that the reinforcing webs are more effective than an increase in foam density.

These results are important for evaluating serviceability limit states. All structural elements have deflection limits that are intended to ensure the element functions properly and does not cause discomfort to individuals using the structure. For bridge deck elements, the deflection limits are relatively high, and typically they are dictated as the span length of the element divided by eight hundred (*L/800*). If this limit state is applied using the normalized stiffness values for each construction and the four point testing configuration with a 24 in. span, a load limit can be determined, and the results are shown in Table 4.7. For theses load limits, it is evident that the Type 3 construction has a much higher capacity when considering this serviceability limit state. Also, the load limits are quite small, especially when considering the potential strength capacity of these constructions.

Table 4.7: Serviceability Load Limits for Each Normalized Construction Type

Construction Type	Serviceability Load Limit (lb)
1	55
2	103
3	195

4.2. ANALYSIS OF FLEXURAL STRENGTH

The flexural strength of a sandwich panel is dependent on many factors that are related to the stresses present in each component of the construction. These stresses are used to predict the limiting failure mode and ultimately the capacity of the sandwich construction, which is beneficial to design. Failure can occur in each of the different components with a variety of different mechanisms causing the failure. The primary failure modes encountered in the small-scale panel tests included local indentation, delamination, shear failure of the core, intercellular buckling, and compressive failure of the facing. Also, failure generally occurred in two phases. The first phase consisting of initial failure characterized by non-linearity in the response and noticeable damage to the specimen, which caused a decrease in the rate of increase in the load but did not cause a loss in load carrying capacity. The second phase was ultimate failure that occurred during the non-linear response, which was characterized by excessive damage to the specimen and a peak in the load after which the load decreased and never recovered.

The ultimate failure load was very easy to define considering that it occurred at the peak load, but the initial failure was much more difficult to define. It occurred at the transition between linear and non-linear response, which is challenging to quantify in a precise manor, particularly for complex composite constructions such as those used for the sandwich panels. In order to estimate this initial failure load, an offset of the linear response region was used to intercept the data at a point near the transition. Figure 4.5 graphically depicts this methodology. The offset was chosen to minimize the amount of non-linear behavior before the offset line intercepted the corrected data curve, in effect limiting the overestimation of the initial failure load. The offset also had to be large enough that the noise in the data did not cause the offset to prematurely intercept the corrected data curve, which would cause an underestimation of the initial failure load. Therefore, a 0.01% offset was chosen as a percentage of the span length to meet these criteria.

Once the offset was chosen and the initial failure loads were estimated, the global stresses and other useful quantities could be calculated using EBBT and TBT, as well as other physical relationships. The specific solutions used to calculate these quantities are presented in the following sections along with the results of an analysis using the experimental results of the small-scale panel tests. These concepts will be presented separately for each sandwich construction, and finally a comparison between the constructions is presented in Section 4.2.4.

Bending stresses are often the limiting factor for facing failure modes like intercellular buckling and compressive failure of the facing. Shear stresses are the limiting factor for shear failure in the core, and they are related to peeling stresses that cause delamination failures. EBBT and TBT can be adapted to predict bending and shear stresses. The assumptions and governing equations for both EBBT and TBT are readily available in the literature. Considering the specific loading cases used in the small-scale panel tests, the equations for bending stress and average shear stress can be solved using static equilibrium and the same idealized loading and support conditions presented in Fig. 4.1. The solution for maximum bending stress is presented as Eqn. 4.24, and the equation for maximum average shear stress is presented as Eqn. 4.25.

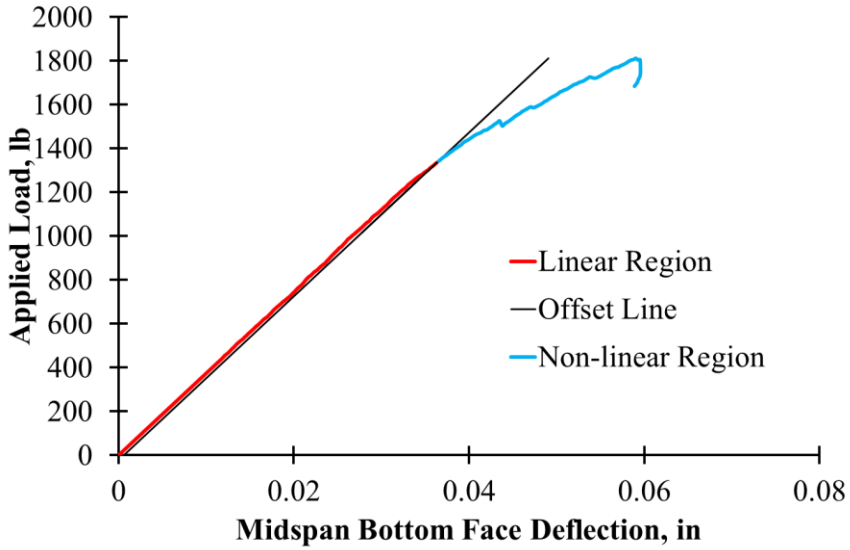

Figure 4.5: Estimate of Initial Failure Load Using Offset Method

$$\sigma = \pm \frac{Paz}{2I} \tag{4.24}$$

$$\tau_{avg} = \frac{P}{2A} \tag{4.25}$$

Where "σ" in the axial bending stress in the x-direction, with a negative sign indicating compressive stress and a positive sign indicating tensile stress. Then, "P" is the total applied load, "a" is the distance from the support to the load, "z" is the distance from the neutral axis to the extreme fibers in the z-direction, "I" is the area moment of inertia about the y-axis, and "A" is the cross-sectional area in shear. From this solution, the stresses can be solved for the three point loading case ($a = L/2$) and the four point loading case ($a = L/3$). The solution for the three point loading case is present in Eqns. 4.26 and 4.27, and the solution for the four point loading case is presented in Eqns. 4.28 and 4.29.

$$\sigma = \pm \frac{P_1 L_1 z_1}{4I_1} \tag{4.26}$$

$$\tau_{avg} = \frac{P_1}{2A_1} \tag{4.27}$$

$$\sigma = \pm \frac{P_2 L_2 z_2}{6 I_2} \tag{4.28}$$

$$\tau_{avg} = \frac{P_2}{2 A_2} \tag{4.29}$$

In these solutions, "*1*" indicates the three point loading configuration (*a = L/2*) while "*2*" indicates the four point loading configuration (*a = L/3*). From these equations, the bending and shear stresses in the sandwich constructions were calculated based on the dimensions and failure loads recorded for each test.

For local indentation, there are several factors that effect this failure mode. These factors include the geometric and material stiffness of the facing and core, as well as the strength of the core. Initially, local indentation is dependent on the strength of the core material and the out of plane compressive stress in the core. These out of plane stresses are proportional to the pressure imposed by the point loads acting on the beam, and in design, the pressures are often limited to the compressive strength of the foam. However, in practice, this proves to be conservative in some cases and not conservative in other cases. Nonetheless, the pressure imposed by the point loads is a good indicator of failure due to local indentation. Then, once the initial failure begins, the facing loses stability, allowing bending stresses to wrinkle the facing at the load point, which causes a significant loss in load carrying capacity. The pressure imposed by the point load is estimated using Eqn. 4.30 since rectangular loading bars were used.

$$p_{pad} = \frac{P}{N A_{pad}} \tag{4.30}$$

Where "p_{pad}" is the average pressure imposed by the point load, "*P*" is the applied load, "A_{pad}" is contact area between the load point and the specimen, and "*N*" is the number of loading points, *N = 1* for three point loading and *N = 2* for four point loading. The following sections will indicate how these equations for stress and pressure were adapted to each of the sandwich constructions. These concepts will be presented separately for each sandwich construction, and finally a discussion and comparison between the constructions will be presented in Section 4.2.4, also the load at each failure point will be compared to the serviceability load discussed in Section 4.1.4.

4.2.1. Results for Type 1. In order to evaluate the flexural strength of the Type 1 core, it is necessary to examine the sandwich panel construction in order to determine the appropriate values for the previously derived equations. For the Type 1 sandwich construction, bending stresses are carried primarily by the facings, and using the dimensions previously presented in Fig. 4.2, the effective moment of inertia is as shown by Eqn. 4.31.

$$I \approx \frac{bf^3}{6} + \frac{bfd^2}{2} \tag{4.31}$$

From this expression, the first term can be eliminated since it is proportional to "f^3" and is essentially zero given that the average facing thickness for the Type 1 construction was 0.095 in. This simplification results in Eqn. 4.32.

$$I \approx \frac{bfd^2}{2} \tag{4.32}$$

Then, the "*z*" term needed to calculate the bending stresses is equal to half the height of the cross section. This allows Eqns. 4.26 and 4.28 for the three point and four point loading configurations, respectively, to be rewritten as Eqns. 4.33 and 4.34 for the Type 1 sandwich construction.

$$\sigma = \pm \frac{P_1 L_1 h_1}{4 b_1 f_1 d_1^2} \tag{4.33}$$

$$\sigma = \pm \frac{P_2 L_2 h_2}{6 b_2 f_2 d_2^2} \tag{4.34}$$

Where "*h*" is the height of the cross-section, and for simplification the magnitude of the stress will be the only thing considered since the bending stresses in the facings will be equal in magnitude and opposite in direction.

Next, the shear stress can be calculated based on the dimensions of the Type 1 core. Typically, for this type of sandwich construction, it is assumed that the shear stresses are completely carried by the foam core. This assumption is due to the small thicknesses of the facings, as the first moment of the area of the facings is so small that when the true shear stress predicted by elasticity theory is integrated over the area, the contribution of the facings is found to be negligible. Also, the shear stiffness of the core is low enough that the true shear stress predicted by elasticity theory will vary very little over the depth of the core, causing the average shear stress to be nearly equal to the true shear stress in the core. Therefore, the area of the core can be used in the shear stress Eqns. 4.27 and 4.29 for the three point and four point loading configurations, respectively, resulting in Eqns. 4.35 and 4.36.

$$\tau_{avg} = \frac{P_1}{2 b_1 c_1} \tag{4.35}$$

$$\tau_{avg} = \frac{P_2}{2 b_2 c_2} \tag{4.36}$$

For the Type 1 sandwich construction, Eqn. 4.30 for pressure under the load is not effected by the geometry of the construction. The "A_{pad}" term is simply the width to the loading pad multiplied by the width of the specimen.

All of the strength concepts presented previously can now be applied to the initial failure loads of the Type 1 specimens while minimizing the error. These concepts can also be applied to the ultimate failure load. However, due to localized damage and changes in the cross-sectional geometry that result in the non-linear portion of the response, the stresses calculated by these equations become less accurate representations at the ultimate failure load condition. Nevertheless, these stress terms are still valuable tools when comparing the different core types. Tables 4.8 and 4.9 summarize the strength analysis for each Type 1 specimen.

Table 4.8: Summary of Initial Failure Analysis for Type 1

Specimen	Initial Failure Condition				
	Failure Mode*	Applied Load (lb)	Avg. Pressure Under the Load (psi)	Max. Bending Stress in the Facings (psi)	Max. Avg. Shear Stress in the Core (psi)
1-1-S	1	589	198	1,611	51
1-2-S	1	627	210	1,713	54
1-3-S	1	714	237	1,931	61
1-4-S	1	601	199	1,621	51
1-1-L	1	794	67	4,392	52
1-2-L	1	823	72	4,718	56
1-3-L	1	984	75	5,524	58
*Failure Mode Codes: (1) Local Indentation, (2) Shear Failure in the Core, (3) Delamination, (4) Intercellular Buckling, (5) Compression Failure of the Facing.					

From these results, it is evident that the initial failure mode for all of the Type 1 specimens was local indentation. The average pressure under the load point varied considerably from the three point test results to the four point test results for both the initial and ultimate failure. It is evident that the three point specimens failed at significantly higher pressures that the four point specimens. This result is most likely due to the nature of the test setup. The three point setup promotes a symmetrical distribution of pressure beneath the point load, while in the four point setup, an unsymmetrical distribution of pressure beneath the point loads may occur, which could lead to much higher stresses on the outer edges of the loading bars. The loading bars were fabricated to rotate freely during the test in an effort to prevent this localized stress concentration, but it did not allow the pressure to distribute as evenly as expected. Also, the bending stresses in the facings were much larger in the four point specimens, which could have contributed to premature local indentation due to stress interaction. It is also interesting to note that when these pressures are compared to the flatwise compression strength values established in Chapter 2, there is no immediate correlation. If flatwise compressive strength was used to

estimate local indentation failure, it would be conservative for the three point specimens and unconservative for the four point specimens.

Table 4.9: Summary of Ultimate Failure Analysis for Type 1

Specimen	Ultimate Failure Condition				
	Failure Mode*	Applied Load (lb)	Avg. Pressure Under the Load (psi)	Max. Bending Stress in the Facings (psi)	Max. Avg. Shear Stress in the Core (psi)
1-1-S	1	1,078	362	2,948	93
1-2-S	1	1,092	367	2,985	94
1-3-S	2	1,257	417	3,397	107
1-4-S	1	1,215	403	3,278	104
1-1-L	2	1,566	133	8,668	103
1-2-L	1	1,539	136	8,827	105
1-3-L	1	1,613	123	9,054	95
*Failure Mode Codes: (1) Local Indentation, (2) Shear Failure in the Core, (3) Delamination, (4) Intercellular Buckling, (5) Compression Failure of the Facing.					

Two of the specimens, 1-3-S and 1-1-L, had an ultimate failure other than excessive local indentation. These two specimens failed ultimately due to shear fractures in the core. This occurred at average shear stresses of 107 psi and 103 psi for Specimens 1-3-S and 1-1-L, respectively, which is inconsistent with Specimens 1-4-S and 1-2-L, which had average shear stresses of 104 psi and 105 at ultimate failure, respectively, but did not fail due to shear fracture in the core. This result is likely due to variations in the thickness of the facings and variations in the material properties of the constituent materials in the Type 1 construction, which are a result of their heterogeneous nature at smaller size scales. Also, at ultimate failure, the core of each specimen had undergone significant damage, which caused inaccuracies in the calculations. In order to better understand the failure mechanisms, more detailed analysis is required, such as higher order and finite element analyses.

4.2.2. Results for Type 2. The same concepts and equations used for the Type 1 specimens can be applied to the Type 2 specimens to calculate the bending and shear stresses as well as the pressures under the load points. The core material contains reinforcing webs that will contribute to the bending stiffness of the sandwich construction, but since they are very thin and have a modulus of elasticity that is less than that of the facings, their contribution can be neglected. The only significant effect this assumption may have on the calculations is that it could contribute a small amount to the bending stress, and eventually lead to a slight over estimation in the strength of the facing. Tables 4.10 and 4.11 summarize the strength analysis for each Type 2 specimen.

Table 4.10: Summary of Initial Failure Analysis for Type 2

Specimen	Initial Failure Condition				
	Failure Mode*	Applied Load (lb)	Avg. Pressure Under the Load (psi)	Max. Bending Stress in the Facings (psi)	Max. Avg. Shear Stress in the Core (psi)
2-1-S	1	1,344	450	3,316	105
2-2-S	1	1,015	336	2,479	78
2-3-S	1	1,150	387	2,853	90
2-1-L	4	2,299	176	10,405	123
2-2-L	4	1,713	153	9,047	107
2-3-L	4	1,666	127	7,494	89
*Failure Mode Codes: (1) Local Indentation, (2) Shear Failure in the Core, (3) Delamination, (4) Intercellular Buckling, (5) Compression Failure of the Facing.					

Table 4.11: Summary of Ultimate Failure Analysis for Type 2

Specimen	Ultimate Failure Condition				
	Failure Mode*	Applied Load (lb)	Avg. Pressure Under the Load (psi)	Max. Bending Stress in the Facings (psi)	Max. Avg. Shear Stress in the Core (psi)
2-1-S	1	1,812	606	4,471	141
2-2-S	1	1,267	420	3,095	98
2-3-S	1	1,150	387	2,853	90
2-1-L	5	3,712	285	16,802	199
2-2-L	2	2,267	203	11,972	142
2-3-L	2	2,269	173	10,209	121
*Failure Mode Codes: (1) Local Indentation, (2) Shear Failure in the Core, (3) Delamination, (4) Intercellular Buckling, (5) Compression Failure of the Facing.					

From these results, it is evident that the initial and ultimate failure mode for all of the Type 2 specimens in the three point test was local indentation. Also, it is evident that if the flatwise compressive strength estimated in Chapter 2 was used to predict local indentation failure in these specimens, it would have been very conservative. The four point specimens did not fail due to local indentation, but it is evident that the same would hold true with respect to using the results from Chapter 2 to predict local indentation failure.

The four point tests all initially failed due to intercellular buckling, which is caused by stability issues in the top facing of the sandwich panel. The bending stress at which this occurred varied significantly between specimens due to the variation in the distribution of reinforcing webs in the core. It was noted during the tests that for Specimens 2-2-L and 2-3-L, the dimple

wave occurred at the free edges of the cells in the top facing because the specimens were sectioned with two longitudinal rows of webs centralized in the width of the specimens, which led to a lack of support from the webs at the edges of the top facing. Specimen 2-1-L had three longitudinal rows of reinforcing webs, two of which supported the edges of the top facing, and this led to a significant difference in the behavior of this specimen. The intercellular buckling for Specimen 2-1-L occurred in the interior cells, and as a result, the non-linear response in this specimen was less pronounced, and compression failure in the facing was the ultimate failure mode. The bending stress at ultimate failure is an estimate of the compressive strength of the facing material, but it should be noted that the intercellular buckling causes a non-linear distribution of bending stress in the top facing, which results in this value serving as a conservative estimate (*i.e.*, the full section modulus was used to calculate the stress at ultimate, but the portion of the compression flange that buckled prior to ultimate failure supports a smaller stress than the unbuckled portions).

As for the other two specimens, 2-2-L and 2-3-L, the ultimate failure mode involved shear failure in the core material, and the average shear stress at this point is an estimate of the shear strength of the Type 2 core. However, due to the large variation in the distribution of longitudinal reinforcing webs, this is a conservative estimate because Specimen 2-3-L had the same number of longitudinal webs as Specimen 2-2-L, but the cross-sectional area was larger, which resulted in a lower average shear stress. Also, Specimen 2-1-L withstood a greater amount of shear stress at failure because it had three longitudinal rows of reinforcing webs, compared to two rows for Specimens 2-2-L and 2-3-L. This result verifies that the average shear stresses in Specimens 2-2-L and 2-3-L are near the lower bound of the true range of shear strength displayed by the Type 2 core.

4.2.3. Results for Type 3. Several simplifying assumptions can be made about the behavior of the Type 3 sandwich construction. In flexure about the major axis, the fiber reinforced shear layers and facings will support the entire load, and the contribution of the foam is negligible. The expressions for the bending stress described in Eqns. 4.26 and 4.28 then become Eqns. 4.37 and 4.38.

$$\sigma = \pm \frac{P_1 L_1 z_1}{4 I_{frp}} \tag{4.37}$$

$$\sigma = \pm \frac{P_2 L_2 z_2}{6 I_{frp}} \tag{4.38}$$

Where "I_{frp}" is the area moment of inertia of the fiber reinforced polyurethane (FRP) layers, which is the same for both the three point and four point specimens. It should be noted the FRP facing layers and shear layers consist of two different glass fiber orientations, which means that the any strength values calculated using this equation are effective properties that are conservative when compared to the properties of the facing layers alone.

As for the shear stress, it will also be carried entirely by the FRP, but to compare the Type 3 construction to the other two constructions, the shear stress will be averaged across the entire cross-section to calculate the average shear stress in a manner that is more representative of the method used for the previous two types. This method is a conservative representation of the true shear stresses in the material, but it is a more representative comparison tool, especially considering that similar behavior occurs in the core of the Type 2 sandwich construction, albeit to a lesser extent. Therefore, in the calculations, Eqns. 4.27 and 4.29 will be used with the area of the entire cross section as the shear area.

The calculation for the pressure under the load for the Type 3 construction uses Eqn. 4.30 where "A_{pad}" is equal to the width of the loading pad multiplied by the width of the specimen in contact with the loading pad, which was determined using the measurements taken of the cross section prior to the tests. Tables 4.12 and 4.13 summarize the strength analysis for each Type 3 specimen.

Table 4.12: Summary of Initial Failure Analysis for Type 3

Specimen	Initial Failure Condition				
	Failure Mode*	Applied Load (lb)	Avg. Pressure Under the Load (psi)	Max. Bending Stress in the Facings (psi)	Max. Avg. Shear Stress in the Core (psi)
3-1-S	3	3,479	2,885	4,084	239
3-1-L	5	3,097	856	9,693	212
*Failure Mode Codes: (1) Local Indentation, (2) Shear Failure in the Core, (3) Delamination, (4) Intercellular Buckling, (5) Compression Failure of the Facing.					

Table 4.13: Summary of Ultimate Failure Analysis for Type 3

Specimen	Ultimate Failure Condition				
	Failure Mode*	Applied Load (lb)	Avg. Pressure Under the Load (psi)	Max. Bending Stress in the Facings (psi)	Max. Avg. Shear Stress in the Core (psi)
3-1-S	1	5,895	4,888	6,920	404
3-1-L	5	4,288	1,185	13,423	294
*Failure Mode Codes: (1) Local Indentation, (2) Shear Failure in the Core, (3) Delamination, (4) Intercellular Buckling, (5) Compression Failure of the Facing.					

These results indicate the areas of concern for the Type 3 construction. The three point specimen failed initially due to splitting (delamination) that occurred between the shear layers, and it ultimately failed due to excessive local indentation. The initial splitting failure was due to dislocations between the shear layers that formed due to poor resin saturation during

manufacturing, which severely limited performance of the specimen. However, despite this defect, the effects on strength were fairly small when compared to the effects on stiffness previously discussed. Unfortunately, the three point results do not really allow for accurate estimations of material strength due to the manufacturing defect, but the results do provide some general indications that can be used in comparison to the other two types. The four point specimen failed both initially and ultimately due to compressive failure in the top facing, which allows for a good estimate of the effective properties of the FRP materials. However, to reiterate, the poor resin saturation likely had a negative effect on the capacity of the specimen. In addition, incorporation of the shear layers into the calculations will lead to a strength in the facing that is expected to be less than the strength of the facings measured in the other two construction types.

4.2.4. Discussion of Strength Analysis Results. Utilizing the results of the strength analysis, the core types can be compared based on the observed failure modes and the stresses and loading pressures that were calculated. For the Type 1 sandwich construction, the primary failure mode was local indentation, which occurred in all of the specimens as the initial failure mode and was the ultimate failure mode for 5 of the 7 specimens (71%). The remaining two failed ultimately due to shear fracture in the core. From this, the pressure under the load that caused local indentation failure can be analyzed, and it is evident that the beam configuration had a significant effect on the pressure at failure, both the initial and ultimate failure mode. Table 4.14 summarizes the local indentation data for the Type 1 panel.

Table 4.14: Summary of Local Indentation Failure Stresses for Type 1

Specimens	Average Pressure Beneath Load Point (psi)	
	Initial Failure	Ultimate Failure
Three Point Loading	211	377
Four Point Loading	72	129

The ultimate shear strength of the Type 1 core can be estimated based on the average shear stress in the two specimens that ultimately failed due to shear fracture. The estimated average shear strength is 105 psi, which is a conservative estimate considering the circumstances of the tests discussed previously.

As for the Type 2 specimens, local indentation occurred only in the three point specimens at an average pressure under the load of 391 psi at initial failure and 471 psi at ultimate failure. The four point specimens failed initially due to intercellular buckling, which occurred in the top facing at an average bending stress of 8,980 psi. Then, the specimens failed ultimately due to compressive failure in the facing (one specimen) or shear failure in the core (two specimens).

The estimated ultimate compressive strength of the facing was 16,800 psi and the estimated ultimate shear strength of the core was 132 psi, but both of these estimates are conservative for the reasons discussed previously.

The Type 3 specimens had a variety of failure modes occur during the flexural tests. For the three point specimen, initially failure occurred due to splitting (delamination) between the shear layers at an average shear stress of 239 psi. Then, ultimate failure occurred due to excessive local indentation at a pressure under the load of 4,890 psi. As for the four point specimen, both initial and ultimate failure were cause by compressive failure in the top facing at an initial bending stress of 9,690 psi and an ultimate bending stress of 13,400 psi. As with the other two sandwich construction types, theses quantities are conservative estimates for reasons discussed previously.

From these results, it is apparent that the Type 1 construction had the lowest performance. The facing strength should have been comparable to the other two types due to the similar construction. However, the effectiveness of the facings is directly influenced by the ability of the core to utilize the full capacity of the facing material. In comparison to the other two construction types, the lower stiffness of the Type 1 core significantly reduced the effectiveness of the facings to support the imposed bending stresses. The Type 1 core material also supported the lowest bearing pressures beneath the loading points and experienced shear failure at the lowest shear stress.

The Type 2 core was the next highest in terms of strength performance. With regard to the strength of the facings, the Type 2 had the second best utilization of flexural modulus through the use of reinforcing webs in a flexible foam, which improved the effective moment of inertia while remaining very light in weight. Unfortunately, this construction also had stability issues in the facing that limited the capacity due to intercellular buckling. The Type 2 construction was also second highest in terms of the ability of the core material to withstand higher pressures beneath the loading points. Finally, the estimated shear strength for the Type 2 construction was also significantly greater than that for the Type 1 core but not as high as the shear stresses withstood by the Type 3 core.

The Type 3 core had the highest performance with regard to strength. The addition of the diagonal shear layers between the flexible foam blocks proved to be the most effective utilization of the cross section. However, this modification also significantly increased the weight and complexity, which lead to several manufacturing issues that limited the performance of the Type 3 construction. Despite these issues, the Type 3 core displayed the highest potential material strength by withstanding far greater pressures beneath the loading point than the other two cores, as well as withstanding the highest shear stresses.

4.3. SUMMARY AND RECOMMENDATIONS FOR NEXT PHASE

The analysis of flexural stiffness clearly shows that the Type 3 construction has the highest flexural stiffness despite flaws due to poor resin saturation. The Type 2 construction had the second best performance, while the Type 1 construction performed the poorest with regard to flexural stiffness. This result is consistent with the geometric stiffness of each construction and

the fact that the materials used in each construction were very similar, if not exactly the same in most cases. The Type 3 construction had the largest geometric stiffness, while the Type 2 construction had the second largest, and the Type 1 construction had the lowest geometric stiffness.

The relative stiffness performance of the different panel types was very critical in determining which sandwich construction to move forward to the next phase of the research. All structural elements have deflection limits that are intended to ensure the element functions properly and does not cause discomfort to individuals using the structure. For composite bridge deck elements, the deflection limits are relatively high, and typically they are dictated as the span length of the element divided by eight hundred (*L/800*). If this limit state is applied using the normalized stiffness values for each construction and the four point testing configuration with a 24 in. span, a load limit can be determined, and the results are shown in Table 4.15. For theses load limits, it is evident that the Type 3 construction has a much higher capacity when considering this serviceability limit state.

Table 4.15: Serviceability Load Limits for Each Normalized Construction Type

Construction Type	Serviceability Load Limit (lb)
1	55
2	103
3	195

The analysis of flexural strength also clearly shows that the Type 3 construction has the highest performance despite flaws due to poor resin saturation. The Type 2 construction had the second best performance, while the Type 1 construction performed the poorest with regard to flexural strength. For the Type 3 sandwich construction, the addition of the diagonal shear layers between the flexible foam blocks proved to be the most effective utilization of the cross section. However, this modification also noticeably increased the weight and complexity, which lead to several manufacturing issues that limited the performance of the Type 3 panel. Despite these issues, the Type 3 core also withstood far greater pressures beneath the loading point than the other two cores, as well as withstanding the highest shear stresses.

As a result of the stiffness and strength evaluation of the three types of sandwich construction, the research team selected the Type 3 panel for the next phase of the research project. The research team felt that the poor resin saturation that plagued the Type 3 specimens was more a function of the nonstandard PRISMA FOAM thicknesses used for the small-scale specimens. To fabricate the test specimens, the research team had to cut the foam sections from standard PRISMA FOAM material, which resulted in a lack of uniformity in the core used to form the small-scale Type 3 specimens. The next phase of the research involved mid-scale

panels that could employ standard foam sections, and it was believed that the poor resin saturation issue would thus be either eliminated or significantly reduced.

5. MID-SCALE PANEL TESTING AND ANALYSIS

The next phase of the research study involved manufacturing, testing, and evaluating mid-scale panels constructed with the Type 3 (PRISMA FOAM) core selected from the small-scale testing and analysis phase. This next phase included static and fatigue flexural testing as well as durability testing in order to evaluate strength, stiffness, overall behavior, and modes of failure of the Type 3 sandwich construction. These mid-scale panels used standard PRISMA FOAM segments, had a nominal thickness of 4 in., and were manufactured through the VARTM process discussed in detail in Chapter 3. The purpose of this phase of the research was to verify the performance of the Type 3 sandwich construction in order to determine whether it truly represented a viable bridge deck alternative to reinforced concrete.

5.1. PANEL DESCRIPTION AND MANUFACTURING

A schematic of the Type 3 mid-scale panel cross section is shown in Fig. 5.1. The top and bottom facesheets were constructed with three plies of 0°/90°, biaxial, E-glass, plain weave, woven fabric (WR18/3010) manufactured by Owens Corning. The diagonal webs, manufactured by VectorPly, consisted of three plies of +45°/-45°, double bias, E-glass, stitch bonded fabric (E-BXM1715) that was integrated with the facesheets. To enhance bonding to the foam core and between plies, the foam was matted with two plies of +45°/-45°, E-glass, knitted fabric.

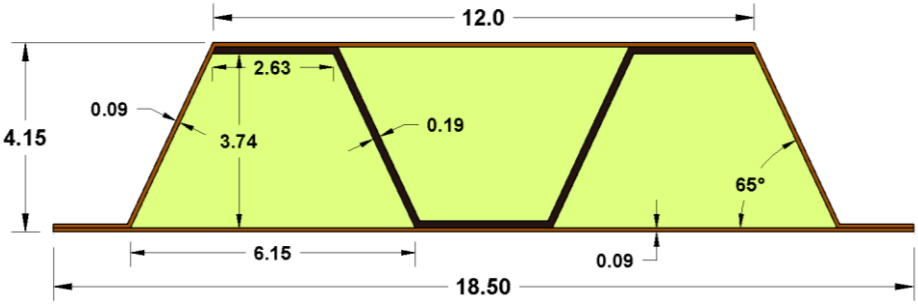

Figure 5.1: Schematic of Type 3 Mid-Scale Panel Cross Section (dimensions in inches)

The specimens were manufactured using the VARTM process discussed in detail in Chapter 3. The mid-scale panels used the same resin as that used to fabricate the small-scale panels, a two-part, thermoset polyurethane resin system manufactured by Bayer MaterialScience. A photograph of one of the panels undergoing the VARTM manufacturing process is shown in Fig. 5.2. The specimens were post-cured for 1 hour at 160ºF and for 4 hours at 180ºF in a walk-in oven. A total of nine mid-scale panels were manufactured with the cross section shown in Fig. 5.1 and an overall length of 48 in. A photograph of four of the completed Type 3 mid-scale panels is shown in Fig. 5.3.

Figure 5.2: VARTM Manufacturing Process for Type 3 Mid-Scale Panels

Figure 5.3: Type 3 Mid-Scale Panel Test Specimens

5.2. FRP COUPON TESTING

The in-place compressive and tensile properties of the panel facings and webs were determined through coupon testing. The coupons were cut from one of the Type 3 mid-scale specimens randomly selected for this purpose. A total of 12 coupon specimens were removed from the panel, 6 from the facings and 6 from the diagonal webs. Each tension or compression series consisted of 3 coupons. The tension tests were performed in accordance with ASTM D3039/D3039M: Standard Test Method for Tensile Properties of Polymer Matrix Composite Materials (ASTM, 2008), and the compression tests were performed in accordance with ASTM

D3410/D3410M: Standard Test Method for Compressive Properties of Polymer Matrix Composite Materials with Unsupported Gage Section by Shear Loading (ASTM, 2008). A summary of the test results is shown in Table 5.1, and a photograph of one of the facing tension tests is shown in Fig. 5.4.

Table 5.1: Summary of FRP Coupon Tension and Compression Testing

Component	Tension (ksi)		Compression (ksi)	
	Ultimate Strength	Modulus	Ultimate Strength	Modulus
Facing	38.4	2,027	14.9	1,920
Web	25.5	1,712	18.6	1,053

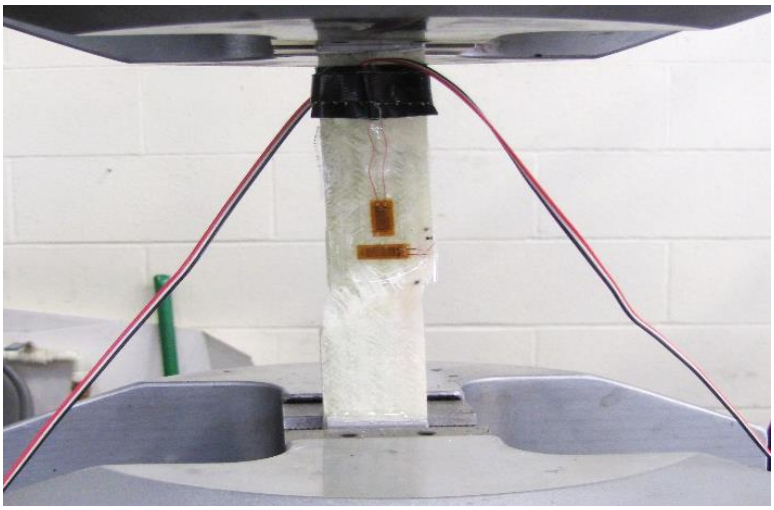

Figure 5.4: Facing Coupon Failure During Tension Test

The results indicate that both the facings and webs are stronger in tension than in compression. Furthermore, the facings are much stronger than the webs in tension (51% higher), but the webs are stronger than the facings in compression (25% higher). However, the facings have a higher modulus of elasticity in both tension and compression compared to the webs, and the material for the webs also had a slightly nonlinear response due to fiber reorientation (the fibers were at a 45° angle relative to the direction of the applied load on the coupon).

5.3. STATIC FLEXURAL TESTING

The static flexural testing program had two objectives. The first objective was to evaluate the strength, stiffness, overall behavior, and modes of failure of the Type 3 sandwich panel under

loading conditions similar to that which a bridge deck would be exposed (i.e., shear, flexure, bearing). The second objective was to serve as a control point for the fatigue flexural testing and durability studies.

5.3.1. Test Setup and Methodology. The test setup and methodology for the static flexural testing was based on ASTM C393/C393M: Standard Test Method for Core Shear Properties of Sandwich Constructions by Beam Flexure (ASTM, 2011). This standard served as a guideline for the tests. The span length for the panels measured 43 in. with two equal point loads applied at a distance of 15.5 in. from each support as shown in Fig. 5.5. This setup provided a section of uniform moment within the panel (uniform flexural stresses) as well as reasonable shear spans for the given specimen depth.

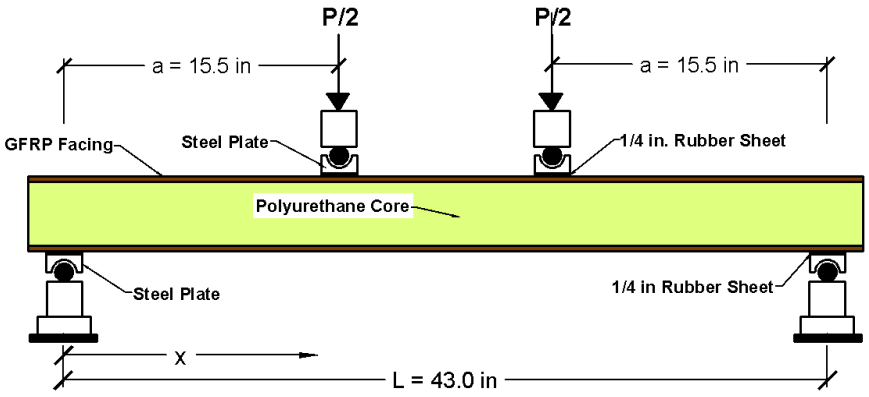

Figure 5.5: Schematic of Mid-Scale Panel Test Setup

Testing was performed using the MTS-880 Universal Testing Machine (UTM) located in the structural engineering lab. The test fixture, shown in Fig. 5.6, was constructed from HSS4x8x1/4 sections for both the supporting base and the loading head. A steel plate/roller system was used to apply the loads and provide support at each end. High durometer neoprene pads were placed between the FRP panels and the steel plate/roller system. The test fixture base was anchored to the MTS using a 1/2-in.-thick steel plate and 3/8-in. bolts, while the loading head was secured in the hydraulic grips of the MTS machine. The completed test setup is shown in Fig. 5.7. Each mid-scale test specimen was loaded to failure at a displacement-control rate of 0.05 in./min.

5.3.2. Specimen Instrumentation. Specimen instrumentation consisted of high-precision strain gauges, direct current variable transformers (DCVTs), and linear variable differential transformers (LVDTs). A total of eight strain gauges were mounted to each test specimen near mid-span, with two placed on both facesheets and four installed vertically on one of the diagonal webs. The DCVTs and LVDTs measured vertical displacement of the panel specimens, with the DCVTs installed along the length of the specimen, four on each side, while one LVDT was placed along the panel top surface immediately above both supports.

Figure 5.6: Fabricated Steel Test Fixture for Mid-Scale Panel Testing

Figure 5.7: Mid-Scale Panel Test Setup

The strain gauges were three-wire, 350 ohm, general purpose strain gauges that had a gauge length of 0.125 in. and a usable strain range of ± 3%. Specimen preparation for the strain gauge installation included light sanding of the facesheet or diagonal web followed by application of a two-part epoxy (AE-10) to provide a smooth surface for adhering the gauge. Once the epoxy cured, it was lightly sanded and cleaned with an adhesive catalyst. The gauge was then placed on the facesheet and adhered to the specimen with strain gauge adhesive (M-Bond 200). Peel ply tape and a slight amount of pressure was applied for 60 seconds to hold the strain gauge in place as the adhesive cured. The peel ply tape was removed and the lead wires were secured to the specimen to prevent any damage prior to testing. Photographs of the strain gauges installed on the top facesheet and web are shown in Figs. 5.8 and 5.9, respectively.

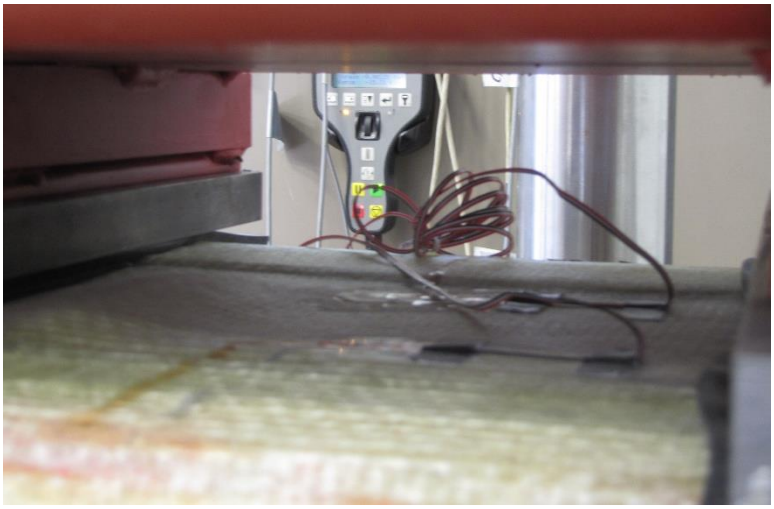

Figure 5.8: Strain Gauges Installed Along Top Facesheet at Mid-Span

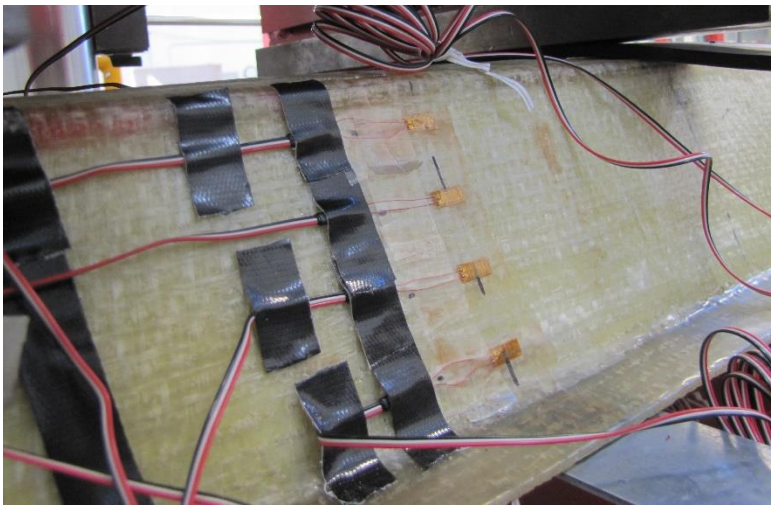

Figure 5.9: Strain Gauges Installed Along Diagonal Web at Mid-Span

5.3.3. Test Results and Discussion. Static flexural testing was performed on two of the Type 3 mid-scale panels, subsequently referred to as CP-1 and CP-2, where the "CP" designation stands for "control panel". The load-deflection curves for the two panels are shown in Fig. 5.10. Both specimens displayed an essentially linear response throughout the loading except for a slight reduction in stiffness immediately prior to failure. The strain gauge readings verified the linear response throughout loading and throughout the depth of the specimens (plane sections remained plane). A summary of the test results is shown in Table 5.2, which includes the maximum load at failure, corresponding maximum mid-span deflection, and the calculated bending stresses in the facesheets at failure. During the test, both specimens experienced a loud "popping" sound at a load of approximately 12.8 kips and deflection of 0.75 in. Examination of

the specimens revealed that a portion of the top facesheet (compression flange) debonded from the foam core and buckled upward, also referred to as dimpling, as shown in Fig. 5.11. At failure, both specimens experienced a second loud "popping" sound. Examination of the specimens revealed a compression failure of the top facesheet beneath one of the loading points, as shown in Fig. 5.12, which was accompanied by an outward buckling of the diagonal web as shown in Fig. 5.13.

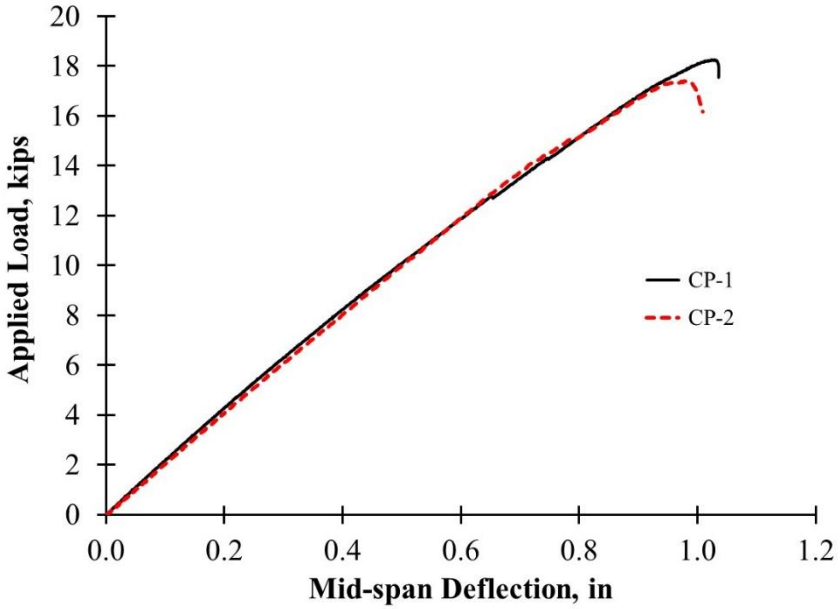

Figure 5.10: Applied Load vs. Mid-Span Deflection for Type 3

Table 5.2: Summary of Static Flexural Testing

Specimen	Max. Applied Load (kips)	Max. Deflection (in)	Facesheet Bending Stress at Failure (ksi)	
			Tension	Compression
CP-1	18.26	1.04	15.28	11.14
CP-2	17.40	0.98	14.56	10.62
Average	17.83	1.01	14.92	10.88

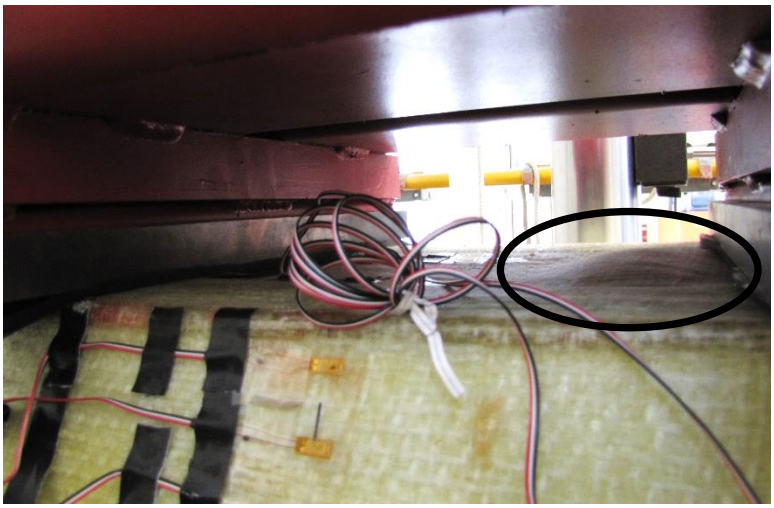

Figure 5.11: Top Facesheet Buckling (Dimpling) During Testing

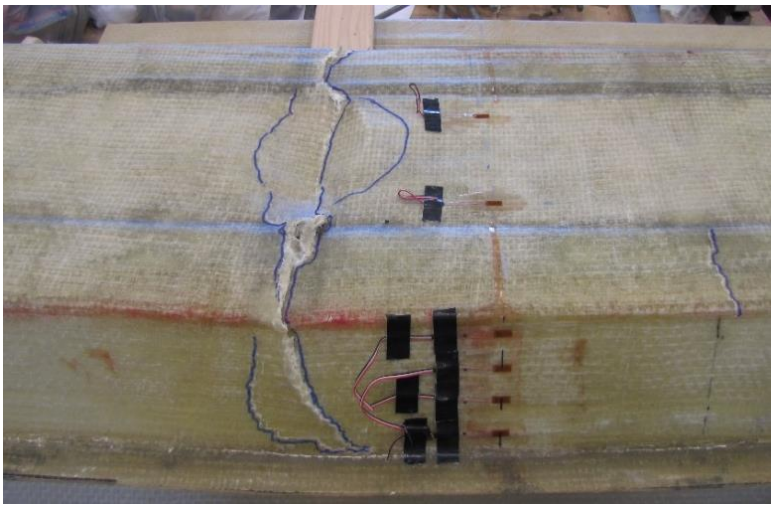

Figure 5.12: Compression Failure of Top Facesheet

5.4. FATIGUE FLEXURAL TESTING

The objective of the fatigue flexural testing program was to evaluate the resistance of the Type 3 panel to cyclic loading. The fatigue testing used the same setup as that used for the static testing (see Fig. 5.7), while the protocol involved two stages, fatigue loading under the specified stress range and number of cycles (Stage 1) followed by static loading to failure (Stage 2). The instrumentation used for the fatigue flexural testing was the same as that used for the static flexural testing, but the instrumentation was installed between the two stages to prevent damage during the cyclic loading.

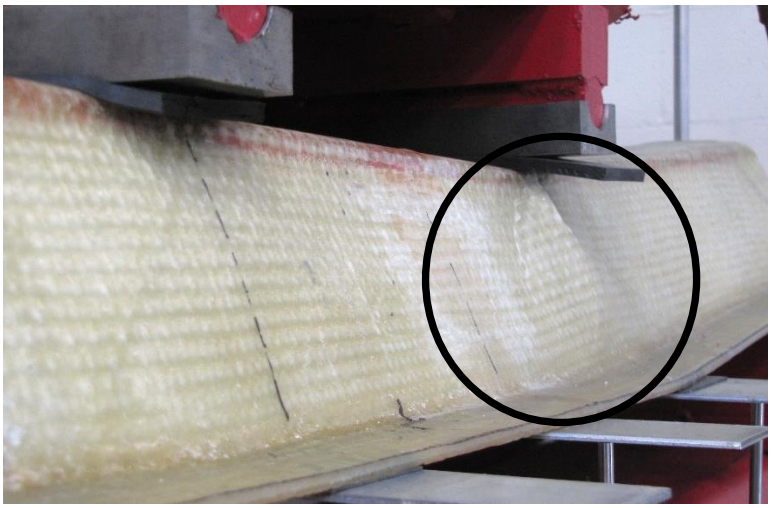

Figure 5.13: Buckling of Diagonal Web at Failure

The fatigue testing included two stress ranges and two limits on the number of cycles based on a combination of several references. A peak cyclic stress of 20 percent of the ultimate load capacity was adopted based on recommendations in ACI 440.2R: Guide for the Design and Construction of Externally Bonded FRP Systems for Strengthening Concrete Structures (ACI, 2008). A value of 2 million cycles was adopted based on requirements for steel bridge components in the *AASHTO LRFD Bridge Design Specifications* (AASHTO, 2013). The research team also included a fatigue test based on a peak cyclic stress of 45 percent of the ultimate load capacity in order to evaluate a higher serviceability rating. The average of the results from the static flexural testing program was used to establish the fatigue specimen ultimate load capacity in order to determine the upper and lower bound values for the cyclic loading. A 5 percent threshold was used as the lower bound of the cyclic loading in order to maintain stability of the specimens within the test setup.

A total of three, Type 3, mid-scale panels were tested under the fatigue testing protocol. After the required number of fatigue cycles, the panels were removed from the test setup, thoroughly inspected for signs of damage, instrumented with strain gauges, and then placed back into the test setup for static loading to failure. None of the fatigue specimens showed any signs of damage as a result of the cyclic loading stage, and all three specimens outperformed the control panels in terms of both strength and stiffness during the static loading stage (residual capacities greater than one). The results are summarized in Table 5.3, and all specimens failed in the same manner as the control panels, compression failure of the top facesheet beneath one of the loading points. The specimen designation, such as Specimen FP-20-2 for example, indicates a fatigue panel (FP) with the first number referring to the peak cyclic stress as a percentage of the ultimate load capacity (20 percent for this specimen), and the second number indicating the number of cycles in millions (2 million for this specimen).

Although the fatigue panels indicated ultimate static strength capacities from 14 to 34 percent higher than the control panels, it is important to note that there was a fair amount of

variability in the panel construction as a result of the manufacturing limitations of the Composites Manufacturing Laboratory at Missouri S&T. However, even accounting for those variations, it is apparent that the fatigue loading did not result in any degradation in strength for the Type 3 sandwich panel. The fatigue specimens also exceeded the control panels in terms of stiffness, with values from 5 to 14 percent higher. This increased stiffness may be the result of the manufacturing variations, or it may be the result of reorganization of the polymer linkages during the fatigue loading, which enhances the performance of the FRP and has been reported by other researchers. Either way, it appears that no degradation in stiffness occurred for the Type 3 sandwich panels as a result of the cyclic loading.

Table 5.3: Summary of Fatigue Flexural Testing

Specimen	Max. Static Applied Load (kips)	Max. Static Deflection (in)	Residual Capacity*	
			Strength	Stiffness
FP-20-1	23.37	1.25	1.32	1.05
FP-20-2	20.35	0.95	1.14	1.15
FP-45-2	23.89	1.20	1.34	1.14
*Residual Capacity: Ratio of static response of fatigue panel to static response of control panels.				

5.5. DURABILITY TESTING

Bridge decks are exposed to severe environmental conditions, and although composites eliminate the corrosion concerns normally associated with reinforced concrete, there is a potential for both freeze-thaw and hygrothermal damage to decks constructed with FRP materials. As a result, the objective of the durability testing was to evaluate whether exposure to the severe environment of a bridge deck would reduce the effectiveness of the Type 3 panel. The durability testing involved two stages, exposure to a variety of accelerated environmental conditions (Stage 1) followed by static loading to failure (Stage 2). The test setup and instrumentation used for the static loading portion of the durability evaluation was identical to that used for the static flexural testing (see Section 5.3). However, the instrumentation was installed between the two stages to prevent damage during the environmental exposure.

The particular sequence used to cycle both temperature and humidity was based on weather data accumulated in Missouri over the previous 30 years. This sequence included freeze-thaw cycling, high temperature cycling with constant relative humidity, and relative humidity cycling with three different constant temperatures. The sequences consisted of the following:

- Sequence No. 1 (Freeze-Thaw): 50°F to -4°F at 20% RH.

- Sequence No. 2 (High Temperature): 68°F to 122°F at 40% RH
- Sequence No. 3 (High Humidity No. 1): 60 to 100% RH at 68°F
- Sequence No. 4 (High Humidity No. 2): 60 to 100% RH at 77°F
- Sequence No. 5 (High Humidity No. 3): 60 to 100% RH at 104°F

A single environmental exposure progression consisted of 10 cycles of Sequence No. 1, followed by 30 cycles of Sequence No. 2, followed by 10 cycles each of Sequence Nos. 3, 4, and 5, which totaled 70 cycles. This progression was repeated 5 times for a total of 350 cycles. Each cycle was held constant for 2 hours and had a 30 to 50 minute ramp up and ramp down time, resulting in a total duration of approximately 52 days. However, due to the complexity of the environmental exposure combined with minor mechanical difficulties with the test chamber, the environmental exposure lasted for a total of 73 days.

Two, Type 3, mid-scale panels were tested under the durability testing protocol. Prior to their exposure in the environmental chamber, the specimens were prepared by protecting their ends with a supplemental epoxy coating and waterproof tape, as shown in Fig. 5.14. This step was necessary since the actual bridge deck panels would completely encapsulate the PRISMA FOAM core. The panels were also elevated within the environmental chamber to allow air circulation on all sides (see Fig. 5.14). After the required number of days within the chamber, shown in Fig. 5.15, the panels were removed, thoroughly inspected for signs of damage, instrumented with strain gauges, and then placed into the static loading test setup. The only change in the specimens due to the environmental exposure involved a noticeable yellowing of the PRISMA FOAM core. During the static loading stage, all of the durability panels failed in the same manner as the control panels, compression failure of the top facesheet beneath one of the loading points. However, the data indicated a noticeable decrease in static flexural strength for the durability panels, with the results summarized in Table 5.4.

The durability panels suffered a noticeable drop in ultimate strength due to the environmental exposure, with a decrease of approximately 25 percent compared to the control panels. This reduction is consistent with the FHWA guidelines on composite deck design, which recommends an environmental durability factor of 0.65 to account for degradation of properties over time and represents a 35 percent decrease in strength. However, the durability panels did show a slightly higher stiffness than the control panels, 8 to 14 percent, which is likely due to extended curing of the polyurethane resin during the high temperature sequences.

5.6. SUMMARY

The purpose of this phase of the research was to verify the performance of the Type 3 sandwich construction in order to determine whether it truly represented a viable bridge deck alternative to reinforced concrete. The evaluation included static and fatigue flexural testing as well as durability testing in order to evaluate strength, stiffness, overall behavior, and modes of failure of the Type 3 sandwich construction. Results of this phase indicated the following:

- The panels displayed linear-elastic behavior throughout the majority of their response during the static flexural testing, with only a slight decrease in stiffness near failure.

- The panels failed at a bending stress of 10.88 ksi in the facesheet under compression while the compression coupon tests failed at a stress of 14.9 ksi. The lower stress at failure for the panel was likely the result of the local buckling (dimpling) that occurred in a portion of the top facesheet, which caused a redistribution of load and higher stresses in the remaining portion of the cross section than those calculated assuming a fully effective cross section.
- The fatigue loading did not result in any degradation to either strength or stiffness, and the panels failed under the subsequent static loading in the same manner as the control panels, compression failure of the top facesheet beneath one of the loading points.
- The environmental exposure resulted in a 25 percent degradation in ultimate strength but a slight increase in stiffness. Failure of the environmental panels under the subsequent static loading occurred in the same manner as the control panels.

Figure 5.14: Durability Specimens within Environmental Chamber

Table 5.4: Summary of Durability Testing

Specimen	Max. Static Applied Load (kips)	Max. Static Deflection (in)	Residual Capacity*	
			Strength	Stiffness
DP-1	13.61	0.70	0.76	1.14
DP-2	13.40	0.67	0.75	1.08
*Residual Capacity: Ratio of static response of durability panel to static response of control panels.				

Figure 5.15: Environmental Chamber

6. FULL-SCALE PANEL CONSTRUCTION AND TESTING

The purpose of this phase of the research was to construct and load test a full-scale deck panel using the Type 3 sandwich construction. The research team worked with Structural Composites, Inc., the manufacturer of the PRISMA FOAM core material, to design and fabricate a full-scale deck panel measuring five feet wide by eight feet long with a nominal thickness of eight inches. This phase served as a proof-of-concept for the FRP deck by taking the research out of the lab and producing an actual, full-scale deck panel.

The design of the panel was based on the standard AASHTO Truck or Tandem (2013), whichever controlled a particular aspect. In accordance with FHWA guidelines, panel stresses were limited to 20% of the ultimate strength but did not include the durability factor of 0.65 as the panel did not undergo any environmental exposure prior to testing. As with most FRP deck panels, deflection controlled the panel design and was based on AASHTO and FHWA guidelines of 1/800 of the supporting span length. No wearing surface was applied to the panel.

The manufacturing process used a modified VARTM infusion process to facilitate full wetting of the reinforcing fabric. The cross section of the panel used two rows of 4-in.-thick PRISMA FOAM panels, which resulted in a mid-depth horizontal FRP sheet in addition to the top and bottom facesheets. The top and bottom facesheets were constructed with eight plies of 0°/90°, biaxial, E-glass, plain weave, woven fabric (WR18/3010) manufactured by Owens Corning. The mid-depth horizontal sheet contained four plies of the same E-glass fabric. The diagonal webs, manufactured by VectorPly, consisted of four plies of +45°/-45°, double bias, E-glass, stitch bonded fabric (E-BXM1715) that was integrated with the facesheets. To enhance bonding to the foam core and between plies, the foam was matted with two plies of +45°/-45°, E-glass, knitted fabric.

After manufacturing, the research team thoroughly inspected the full-scale prototype deck panel for signs of any fabrication defects. This inspection included drilling access holes and inserting a borescope to examine the deck. Ultrasonic testing was also used to search for voids, delaminations, resin variations, broken fibers, and other subsurface defects. The results of the inspection found some minor voids near the end of the deck opposite to the resin infusion ports.

As part of the proof-of-concept, the research team subjected the prototype full-scale panel to a load test at a specialized facility for testing road surfaces. The load test, shown in Fig. 6.1, consisted of placing the panel in a trench and driving a road surface test machine over the panel. The test machine applied an 18 kip wheel load to the center of the eight foot span of the panel during each pass. This wheel load was applied through two standard, semi-trailer truck tires arranged 24 in. on center. The test machine drove over the panel a total of 100 times, with the panel visually inspected after each series of 10 passes. The panel did not show any signs of damage and remained level and plumb after each test series.

The next step in evaluating the full-scale prototype panel involved fatigue testing of the panel under a service loading condition. The fatigue loading used hydraulic actuators to apply a 40 kip concentrated load at midspan of the panel. The load was applied over an area of two

square feet and cycled between 5 kips and 40 kips over 2 million cycles. After the required number of fatigue cycles, the research team inspected the panel, which did not show any signs of damage and remained level and plumb at the end of testing. Subsequent forensic examination of the panel did not reveal any damage, although the team did observe several voids at the end of the panel opposite to the resin infusion ports.

Figure 6.1: Load Test of Full-Scale Prototype Panel

7. SUMMARY AND RECOMMENDATIONS

The objective of this research was to develop, test, and evaluate fiber-reinforced, polyurethane (PU) foams to replace the costly honeycomb construction currently used to manufacture FRP bridge deck panels. Initially, the effort focused on developing an FRP sandwich panel to replace the precast, stay-in-place forms currently used to construct reinforced concrete bridge decks. However, during the course of the project, the research effort expanded to include full-depth bridge deck panels as well.

The research plan involved investigating alternative PU foam formulations and configurations; performing component testing to evaluate the different PU foam alternatives; and manufacturing, testing, and evaluating small-scale, mid-scale, and full-scale FRP/PU foam sandwich panels. Initially, the research team investigated four different types of PU foam. From those, three were selected to move forward to the next phase of the research – manufacturing, testing, and evaluating small-scale FRP/PU foam sandwich panels. The results of the small-scale testing and analysis phase lead to selection of a single FRP/PU foam sandwich panel to move forward to the next phase – manufacturing, testing, and evaluating mid-scale sandwich panels. Finally, as a proof-of-concept, the researchers manufactured and tested a full-scale deck panel. This final chapter contains a summary of this study and presents recommendations based on the results.

7.1. SUMMARY OF ALTERNATIVE FOAMS AND COMPONENT TESTING

The research team selected four PU foams to serve as potential candidates for the core of the FRP sandwich panels. These foams represented the full range of infill types currently available and included the following:

- Type 1: High density foam (PU RIGID)
- Type 2: Low density foam with FRP webs (WEB-CORE)
- Type 3: Trapezoidal, low-density foam with mat reinforcement (PRISMA FOAM)
- Type 4: Low density stitched foam (PU STITCHED)

Based on their relative performances during the flatwise tension and compression testing portion of the study, the research team selected core Types 1, 2 and 3 for the small-scale panel testing and evaluation phase. The Type 2 reinforced foam outperformed the other three materials in terms of both strength and, in particular, stiffness, with moduli values over twice that of the next performing material. The Type 1 plain foam was selected because it outperformed the Type 4 reinforced foam and offers a much more simplified manufacturing process. The Type 3 core was also chosen to move forward because the true value of this material is its use as a mold for the FRP layers that form a truss-type panel.

7.2. SUMMARY OF SMALL-SCALE PANEL TESTING AND ANALYSIS

The small-scale panel phase of the research involved manufacturing panels using the three types of foam selected from the previous phase followed by testing and analysis to determine which FRP/PU foam combination to advance to the mid-scale panel testing program. The testing and analysis focused on the flexural behavior of the specimens in terms of strength, stiffness, overall behavior, and modes of failure.

The small-scale sandwich panels were manufactured using a process known as vacuum-assisted, resin transfer molding (VARTM). This process involves hand layup of the foam core and woven, biaxial, E-glass fabric followed by infusion of the resin through a vacuum-assisted process. Applying the vacuum also results in the outer atmospheric pressure compressing the fiber layers tight against the core. High permeability layers (distribution media) placed over the fibers reduces infusion time, and a standard peel ply prevents the resin from adhering to the vacuum bag. All specimens were post-cured for 1 hour at 160ºF and for 4 hours at 180ºF in a walk-in oven.

For each of the three core types, the basic components were identical. The facesheets consisted of three plies of 0°/90°, biaxial, E-glass, plain weave, woven fabric (WR18/3010) manufactured by Owens Corning. The resin, manufactured by Bayer MaterialScience, was a two-part, thermoset polyurethane resin system with excellent thermal stability, good mechanical properties, and fewer environmental issues than vinyl ester or polyester resins. The differences between the sandwich panels involved the web reinforcement used in the Type 2 and Type 3 panels. For the Type 2 panels, the gridwork of web reinforcement consisted of a single ply of 0°/90°, biaxial, E-glass, plain weave, woven fabric. For the Type 3 panels, the diagonal web reinforcement, manufactured by VectorPly, consisted of two plies of +45°/-45°, double bias, E-glass, stitch bonded fabric (E-BXM1715) that was integrated with the facesheets.

The analysis of flexural stiffness clearly showed that the Type 3 construction has the highest flexural stiffness despite flaws due to poor resin saturation. The Type 2 construction had the second best performance, while the Type 1 construction performed the poorest with regard to flexural stiffness. This result is consistent with the geometric stiffness of each construction and the fact that the materials used in each construction were very similar, if not exactly the same in most cases. The Type 3 construction had the largest geometric stiffness, while the Type 2 construction had the second largest, and the Type 1 construction had the lowest geometric stiffness.

The analysis of flexural strength also clearly shows that the Type 3 construction has the highest performance despite flaws due to poor resin saturation. The Type 2 construction had the second best performance, while the Type 1 construction performed the poorest with regard to flexural strength. For the Type 3 sandwich construction, the addition of the diagonal shear layers between the flexible foam blocks proved to be the most effective utilization of the cross section. However, this modification also noticeably increased the weight and complexity, which lead to several manufacturing issues that limited the performance of the Type 3 panel. Despite these issues, the Type 3 core also withstood far greater pressures beneath the loading point than the other two cores, as well as withstanding the highest shear stresses.

As a result of the stiffness and strength evaluation of the three types of sandwich construction, the research team selected the Type 3 panel for the next phase of the research project. The research team felt that the poor resin saturation that plagued the Type 3 specimens was more a function of the nonstandard PRISMA FOAM thicknesses used for the small-scale specimens. To fabricate the test specimens, the research team had to cut the foam sections from standard PRISMA FOAM material, which resulted in a lack of uniformity in the core used to form the small-scale Type 3 specimens. The next phase of the research involved mid-scale panels that could employ standard foam sections, and it was believed that the poor resin saturation issue would thus be either eliminated or significantly reduced.

7.3. SUMMARY OF MID-SCALE PANEL TESTING AND ANALYSIS

The mid-scale panel phase of the research involved manufacturing, testing, and evaluating mid-scale panels constructed with the Type 3 (PRISMA FOAM) core selected from the small-scale testing and analysis phase. This next phase included static and fatigue flexural testing as well as durability testing in order to evaluate strength, stiffness, overall behavior, and modes of failure of the Type 3 sandwich construction. These mid-scale panels used standard PRISMA FOAM segments, had a nominal thickness of 4 in., and were manufactured through the VARTM process discussed previously. The purpose of this phase of the research was to verify the performance of the Type 3 sandwich construction in order to determine whether it truly represented a viable bridge deck alternative to reinforced concrete.

The mid-scale panels used the same components as those used to manufacture the small-scale Type 3 panels although with an increase in the number of reinforcing fabric plies. The top and bottom facesheets were constructed with three plies of 0°/90°, biaxial, E-glass, plain weave, woven fabric (WR18/3010) manufactured by Owens Corning. The diagonal webs, manufactured by VectorPly, consisted of three plies of +45°/-45°, double bias, E-glass, stitch bonded fabric (E-BXM1715) that was integrated with the facesheets. To enhance bonding to the foam core and between plies, the foam was matted with two plies of +45°/-45°, E-glass, knitted fabric.

The mid-scale panel phase included static and fatigue flexural testing as well as durability testing in order to evaluate strength, stiffness, overall behavior, and modes of failure of the Type 3 sandwich construction. Results of this phase indicated the following:

- The panels displayed linear-elastic behavior throughout the majority of their response during the static flexural testing, with only a slight decrease in stiffness near failure.
- The panels failed at a bending stress of 10.9 ksi in the facesheet under compression while the compression coupon tests failed at a stress of 14.9 ksi. The lower stress at failure for the panel was likely the result of the local buckling (dimpling) that occurred in a portion of the top facesheet, which caused a redistribution of load and higher stresses in the remaining portion of the cross section than those calculated assuming a fully effective cross section.
- The fatigue loading did not result in any degradation to either strength or stiffness, and the panels failed under the subsequent static loading in the same manner as the

control panels, compression failure of the top facesheet beneath one of the loading points.

- The environmental exposure resulted in a 25 percent degradation in ultimate strength but a slight increase in stiffness. Failure of the environmental panels under the subsequent static loading occurred in the same manner as the control panels.

7.4. SUMMARY OF FULL-SCALE PANEL CONSTRUCTION AND TESTING

The purpose of this phase of the research was to construct and load test a full scale deck panel using the Type 3 sandwich construction. The research team worked with Structural Composites, Inc., the manufacturer of the PRISMA FOAM core material, to design and fabricate a full scale deck panel measuring five feet wide by eight feet long with a nominal thickness of eight inches. This phase served as a proof-of-concept for the FRP deck by taking the research out of the lab and producing an actual, full-scale deck panel.

The prototype panel underwent a detailed inspection, load testing at a specialized facility, fatigue testing in the laboratory, and a thorough forensic examination. The deck performed extremely well under both the load test truck, which applied an 18 kip wheel load at midspan of the panel, and the fatigue loading, which applied a load of 40 kips at midspan of the panel for a total of 2 million cycles. The initial detailed inspection revealed some minor voids near the end of the deck opposite the resin infusion ports. The forensic examination, performed after completion of the fatigue testing, revealed several voids at the end of the panel opposite the resin infusion ports. However, the inspection did not reveal any damage as a result of the load testing and fatigue testing.

7.5. RECOMMENDATIONS

Based on the results of this study, the research team recommends proceeding with the Type 3 (PRISMA FOAM) sandwich panel as a viable alternative to reinforced concrete bridge decks. To facilitate this implementation, additional work is required in order to develop the design methodology and construction details necessary to implement FRP deck panels on an actual bridge, addressing issues such as panel-to-panel connections, panel-to-girder connections, bridge skew, roadway crown, bridge rail attachment, and deck drainage.

8. SUPPLEMENTARY INFORMATION

FRP bridge decks offer several advantages over traditional reinforced concrete decks or steel grating systems. These advantages include significantly lower weight, rapid installation, ease of installation, fatigue resistance, corrosion resistance, chemical resistance, high quality control during manufacturing, minimal maintenance, and a long service life.

However, all materials have both advantages and disadvantages, and the previous sections of this report detailed the investigation of a novel approach to FRP bridge decks aimed at reducing or eliminating one of the major impediments to their adoption throughout North America, namely first cost considerations. This section of the report addresses some other common concerns and questions involving FRP bridge decks and this research study.

8.1. UV RESISTANCE

The matrix material for the FRP deck in this study consisted of a two-part, thermoset, polyurethane resin manufactured by Bayer MaterialScience. The "A" component of the resin was an Isocyanate NB#840859 ISO, Diphenylmethane Diisocyanate (MDI-Aromatic), while the "B" component was a low viscosity (350 cP) Polyol (RTM NB#840871). The components react rapidly after mixing to form a highly cross-linked thermoset polymer with excellent thermal stability and mechanical properties. Thermoset polyurethanes also possess very good resistance to UV degradation, but as part of the product development process, Bayer MaterialScience performed testing of the polyurethane to determine its inherent UV resistance.

The test protocol consisted of exposing resin coupons to UV radiation and comparing both tensile and compressive properties to control specimens. The UV exposure was conducted for 2,000 hours in accordance with ASTM D4329: Standard Practice for Fluorescent Ultraviolet (UV) Lamp Apparatus Exposure of Plastics (ASTM, 2013). The tension tests were performed in accordance with ASTM D3039/D3039M: Standard Test Method for Tensile Properties of Polymer Matrix Composite Materials (ASTM, 2008), and the compression tests were performed in accordance with ASTM D3410/D3410M: Standard Test Method for Compressive Properties of Polymer Matrix Composite Materials with Unsupported Gage Section by Shear Loading (ASTM, 2008). Results of the testing indicated a degradation of less than 2% in the material properties, both strength and stiffness.

Furthermore, if necessary, there are also several relatively simple ways to enhance the UV resistance of polymers through additives in the form of stabilizers, absorbers, or blockers. The least expensive solution involves the addition of carbon black at dosages of 1 to 2%, which provides protection through the blocking process. Other possibilities include titanium dioxide, which also protects through blocking, as well as benzophenones and benzotriazoles, which absorb the UV radiation and re-emit it at a less harmful wavelength, mainly as heat. The final solution typically involves a combination of additives and, in general, is a relatively simple modification to the resin system.

8.2. FIRE RESISTANCE

In general, thermoset resins are either naturally fire retardant or contain additives to prevent combustion. However, polymers will tend to suffer a decrease in material strength at temperatures far lower than steel or concrete. FRP materials start to lose strength when their temperatures reach what is referred to as the glass transition temperature, typically around 220°F for most polymers. At temperatures of approximately 680°F, most FRP materials have lost 50% of their load carrying capacity, with a 90% loss in strength at around 1100°F. In comparison, the corresponding temperatures for structural steel are 550°F, 1100°F, and 1700°F and are much higher for reinforced concrete depending on the amount of cover.

As a result, fires present a more serious problem for FRP bridges, either complete structures or FRP decks on traditional steel and concrete girders. With regard to overpasses where a burning car or truck below will expose the underside of the FRP deck to fire, one option is to install insulation. This approach has been used successfully in buildings that have undergone FRP repairs to reinforced concrete columns, beams, and slabs (Benichou, et al., 2010). This approach would also be necessary for overpasses that have undergone FRP repairs to prestressed and reinforced concrete elements. With regard to fires occurring on top of the bridge, in general, most car and truck fires direct the majority of their heat upward and away from the deck, which will also be partially insulated by the polymer-concrete wearing surface. However, the decks are susceptible to prolonged fires due to the burning of large oil spills, although these are relatively rare occurrences (Alnahhal, et al., 2006).

8.3. QUALITY CONTROL

One issue that occurred during the small-scale, mid-scale, and full-scale Type 3 specimen testing was the occurrence of manufacturing defects (incomplete resin saturation and dislocations between fiber layers) and variability between specimens. These defects were most evident in the small-scale specimens, which was partially attributed to the process of modifying the standard PRISMA FOAM sections in order to construct the necessary panel thicknesses. There was a noticeable improvement in the mid-scale Type 3 specimens, although some defects still existed. For the full-scale panel specimen, the manufacturing defects were relatively minor and consisted of several voids at the end of the panel opposite to the resin infusion ports. Nonetheless, the occurrence of these defects raises the issue of quality control and, more important, inspection methods to insure the performance of FRP bridge deck panels.

With regard to the manufacturing defects, the quality of the panels improved as the specimens moved from small-scale to mid-scale to full-scale construction. Part of this was due to the use of standard PRISMA FOAM sections for the mid-scale and full-scale deck specimens. Improvements also occurred due to the learning curve associated with constructing the specimens in the Missouri S&T Composites Lab. The full-scale panels had the fewest defects as these were constructed by a composites manufacturing company. The prototype nature of this first full-scale panel was likely the cause of the slight voids detected in the panel, which would be significantly reduced during production runs.

However, to maintain quality control of the panels, the research team recommends that inspection methods be written into the specifications for FRP deck panels. Typical inspection methods already used in the composites industry include visual inspection, tapping, acoustic emission, thermography, ultrasound, and x-ray radiography (GangaRao and Vijay, 2010). The research team also recommends load testing of all FRP deck installations prior to acceptance, which has been performed in previous FRP deck projects throughout North America.

8.4. HIGH WATER EVENTS

Another concern for FRP decks involves the behavior of these types of bridges during a high water event. Specifically, what concerns arise due to the fact that a sealed FRP deck panel will float? FRP decks weigh, on average, about 25 psf. With a typical deck thickness of 8-1/2 in. including the wearing surface, when submerged, a buoyancy force of 20 psf is generated. Assuming an AASTHO Type 4 girder with an 8 ft. girder spacing, there is a factor of safety of 1.5 on developing any net uplift forces on the connection of the superstructure to the piers and abutments. Assuming one connection at each panel corner, the resulting 20 psf buoyancy force acting on a standard 5 ft. x 8 ft. panel would require that the connections to the girders resist an uplift force of 200 lb. each, which is a relatively modest amount. As the FRP panels are typically symmetrical about a horizontal plane, the panel capacity will far exceed the 20 psf upward force generated while the panels are submerged.

8.5. OVERLAY

FRP bridge decks require an overlay to provide both skid resistance and wear resistance. These overlays typically consist of asphalt, epoxy-modified asphalt, polymer concrete (epoxy, polyester, methacrylate, polyurethane), and polymer-modified concrete (synthetic latexes such as styrene-butadiene, polychloroprene, polyacrylic ester, styrene acrylic, vinyl acetate copolymers, polyvinyl acetate). In general, polymer concrete overlays have shown the best performance in terms of wear resistance, durability, and compatibility with the underlying FRP deck and are usually installed with a thickness of 1/2 in. or 5/8 in (Aboutaha, et al., 2012; Barquist, et al., 2005). In addition to providing skid resistance, the overlay protects the top FRP facesheet from highly localized concentrated forces.

8.6. ECONOMICS

In general, FRP decks are two to three times the initial cost of traditional reinforced concrete decks, which has severely limited their use. However, on a life cycle basis, FRP decks are cost effective alternatives, more so once indirect costs are included as a part of deck repair costs or complete re-decking projects. FRP decks are also cost effective for re-decking projects where the bridge has required posting, as the significant decrease in dead load may allow re-rating to the original design capacity. Nonetheless, deterioration of our nation's infrastructure combined with decreased funding for state departments of transportation often lead to decisions made on the basis of first cost alone.

The objective of this research study was to develop alternative manufacturing techniques for the purpose of reducing FRP deck initial costs. Based on the Type 3 (PRISMA FOAM) system, the resulting cost of the prototype full-scale deck panel was less than one half the cost of a comparable honeycomb FRP deck construction. Furthermore, on a production run for an actual bridge, the manufacturer estimates a further decrease in unit costs of 40% to 50%, bringing the FRP deck alternative in line with reinforced concrete deck initial costs. The exact costs will be a function of several factors including bridge complexity, skew angle, cross-slope, railings, drainage, size, etc., but it appears that the Type 3 system will be competitive with conventional reinforced concrete on a first cost basis.

8.7. PARTIAL-DEPTH VS. FULL-DEPTH PANELS

The objective of the research was to develop, test, and evaluate fiber-reinforced, polyurethane (PU) foams to replace the costly honeycomb construction currently used to manufacture FRP bridge deck panels. Initially, the effort focused on developing an FRP sandwich panel to replace the precast, stay-in-place forms currently used to construct reinforced concrete bridge decks. However, during the course of the project, the research effort expanded to include full-depth bridge deck panels as well.

All of the development and test results from the study are equally applicable to both partial-depth and full-depth FRP deck panels. These results indicate that a 3-in.-thick, Type 3, partial-depth FRP panel will support the construction weight of the subsequent reinforced concrete deck. More structurally efficient thicker panels will reduce the unit costs, while thinner panels will increase the unit costs due to the need for additional FRP layers. Composite action with the subsequent reinforced concrete deck requires a mechanical connection (shear keys, T-upstands) combined with a layer of adhesive. The mechanical connections add complexity to the panel manufacturing process that will increase production costs of the partial-depth panel. Further testing with alternative adhesives might allow removal of the mechanical connections and result in a simpler, and thus less costly, partial-depth panel.

REFERENCES

American Association of State Highway Transportation Officials (AASHTO). (2013). *AASHTO LRFD Bridge Design Specifications*, 6th Edition, 2013 Interim Revisions, Washington, D.C.

Aboutaha, R.S., Lui, E., Martin, G., Petrina, P., Phoenix, L., and Giannelis, E. (2012). *Investigation of Durability of Wearing Surfaces for FRP Bridge Decks*, Transportation Infrastructure Research Consortium/New York State Department of Transportation, Project No. C-01-50, 397 pp.

ACI 440.2R (2008). Guide for the Design and Construction of Externally Bonded FRP Systems for Strengthening Concrete Structures. American Concrete Institute, Farmington Hills, MI.

Alnahhal, W.I., Chiewanichakorn, M., Aref, A.J., and Alampalli, S. (2006). *Temporal Thermal Behavior of Damage Simulations of FRP Deck*, Journal of Bridge Engineering, American Society of Civil Engineers, V. 11, No. 4, pp. 452-464.

ASTM C297/C297M (2010). Standard Test Method for Flatwise Tensile Strength of Sandwich Constructions. American Society for Testing and Materials, West Conshohocken, PA.

ASTM C365/C365M (2011). Standard Test Method for Flatwise Compressive Properties of Sandwich Cores. American Society for Testing and Materials, West Conshohocken, PA.

ASTM C393/C393M (2011). Standard Test Method for Core Shear Properties of Sandwich Constructions by Beam Flexure (2011). American Society for Testing and Materials, West Conshohocken, PA.

ASTM D3039/D3039M (2008). Standard Test Method for Tensile Properties of Polymer Matrix Composite Materials. American Society for Testing and Materials, West Conshohocken, PA.

ASTM D3410/D3410M (2008). Standard Test Method for Compressive Properties of Polymer Matrix Composite Materials with Unsupported Gage Section by Shear Loading. American Society for Testing and Materials, West Conshohocken, PA.

ASTM D4329 (2013). Standard Practice for Fluorescent Ultraviolet (UV) Lamp Apparatus Exposure of Plastics. American Society for Testing and Materials, West Conshohocken, PA.

ASTM D7250/D7250M (2012). Standard Practice for Determining Sandwich Beam Flexural and Shear Stiffness. American Society for Testing and Materials, West Conshohocken, PA.

Barquist, G., Lovejoy, S., Nelson, S., and Soltesz, S. (2005). *Evaluation of Wearing Surface Materials for FRP Bridge Decks*, Oregon Department of Transportation/Federal Highway Administration, Salem, OR, Report No. OR-DF-06-02, 34 pp.

Benichou, N., Kodur, V.K.R., Green, M.F., and Bisby, L.A. (2010). *Fire Performance of Fibre-Reinforced Polymer Systems Used for the Repair of Concrete Buildings*, National Research Council, Canada, Construction Technology Update No. 74.

GangaRao, H.V.S. and Vijay, P.V. (2010). *Feasibility Review of FRP Materials for Structural Applications*, Constructed Facilities Center, Department of Civil & Environmental Engineering, West Virginia University, Morgantown, WV, Submitted to the U.S. Army Corps of Engineers, 116 pp.

Koch, G.H., Brongers, M.P.H., Thompson, N.G., Virmani, Y.P., and Payer, J.H. (2002). *Corrosion Costs and Preventive Strategies in the United States*, U.S. Department of Transportation, Federal Highway Administration, Washington, D.C., Publication No. FHWA-RD-01-156.